UNIVERSITY OF LONDON THESIS

Degree PhD Year 2007 Name of Author MURTAGH, Daniel James

Positron Impact Ionization Phenomena

Daniel James Murtagh

A thesis submitted to the University of London for the degree of

Doctor of Philosophy

November 30, 2007

Department of Physics and Astronomy

University College London

ProQuest LLC
789 East Eisenhower Parkway
P.O. Box 1346
Ann Arbor, MI 48106-1346

The work presented in this thesis is my own work

Signed

Daniel James Murtagh

ABSTRACT

In the present work, a beam of positrons, obtained from a radioactive source (^{22}Na) in conjunction with a W moderator and guided by a magnetic field, has been used to investigate low energy positron-impact ionization phenomena from atomic and molecular targets.

For He below threshold, the investigation discovered vacuum contaminants increased with gas load and hence concluded that the high γ-ray/ion signal observed by Szluinska and Laricchia (2004a) in Ne could not be safely attributed to annihilation. A detailed measurement of the total ionization cross-section for He has been performed from below threshold for Ps formation to high energy. Combined with previously measured data and previously measured direct ionization cross-sections (Moxom *et al* 1996, Ashley *et al* 1996), a new determination of the positronium formation cross-section has been achieved and compared to other available experimental measurements and theoretical calculations.

Measurements of the excited state ($n > 1$) positronium formation cross-section for He and Ar have been performed and compared to available theoretical calculations. This work has been motivated both for a direct comparison with theory and to test the hypothesis that structure observed in the total (all n) positronium formation cross-sections for the heavier noble gases, is due to excited state positronium formation (Laricchia *et al* 2002). The present study is unable to verify fully this hypothesis due to the experimental methods insensitivity to positronium

formation in to the 2S or $n > 2$ states. However, the present results are close to the most sophisticated theoretical calculation of positronium formation into the 2P state (Campbell *et al* 1998).

CONTENTS

LIST OF FIGURES

LIST OF TABLES

ACKNOWLEDGMENTS

Firstly, I would like to thank my supervisor Prof Nella Laricchia, for inviting me to join her group and secondly for all her support, help and advice over the years of my PhD. I would also like to thank Dr Marta Szluinska for all her help in teaching me the "black art" of running the "old beam". Dr Peter Van Reeth for his valuable assistance proof reading this work. Dr Simon Armitage for proof reading, useful discussions and hydration. Dr Zoran Pesic and Dr Akos Kover for their assistance and teaching me some of their own "unique methods" in the lab. I thank, John Dumper, Ted Oldfield and Rafid Jawa for all their technical assistance, without their help this work would not have been possible. Last but not least all those I have shared an office and or lab with: Dr Dawn Leslie, Dr Cristiana Arcidiacono, Simon Brawly, Dave Cooke and Dumpy the lab koala.

I'd also like to thank my family for all their support over the years, letting me get on with it even though they never really understood why. All my friends who have been there for me over the period of this work, names are too numerous to mention but you know who you are, thanks.....

1. INTRODUCTION

The positron, the anti-particle of the electron, was first predicted by Dirac (1930a), who realized that the negative energy solutions to his new relativistically-invariant wave-equation were physically significant. The suggested interpretation (the so called "hole theory") supposes that the sea of energy levels from $-mc^2$ to $-\infty$ are normally filled by electrons in accordance with the Pauli exclusion principle. A vacancy (or a hole) in one of these state would appear as a positively charged particle with positive mass. Initially, Dirac assumed this particle would be a proton; however, it was shown by Weyl (1931) that the masses associated with the positive energy states (particle) and negative energy states (antiparticle) were equal.

The prediction of Dirac (1930a) and Weyl (1931) that a particle with the same mass as the electron but with a positive charge exists was verified when the particle was observed by Anderson (1932a, 1932b, 1933) in a cloud chamber from cosmic rays, followed by Blackett and Occhialini (1933) who confirmed that the charge to mass ratio was the same as for the electron.

After the discovery of the positron, Mohorovicic (1934) predicted the existence of a bound state which consisted of an electron and a positron. The spectroscopic structure of this state, called positronium (Ps), was calculated by Ruark (1945), and its binding energy and lifetime by Wheeler (1946). The first experimental observation of positronium was made by Deutsch (1951) using measurements of positron lifetimes in gases.

1.1 Properties of the positron and Ps

The positron is a stable particle in vacuum (lifetime $> 4 \times 10^{23}$ years (Aharonov *et al* 1995)) with a mass of 9.109×10^{-31} kg (Beier *et al* 2002), a spin of one-half and an equal but opposite charge (and hence opposite magnetic moment to that of the electron).

A positron in normal matter will, after a short time, annihilate with an electron. The lifetime of a positron in matter is inversely proportional to the electron density. The total rest-mass energy of an electron positron pair is 1.022 MeV which, after annihilation, will be distributed between a number of photons. The number of these is determined by charge parity (P_c) conservation. For a photon the charge parity is $P_c = -1$, hence the charge parity for n photons is :

$$P_c = (-1)^n \tag{1.1}$$

and the charge parity for an electron positron system is given by (Yang 1950):

$$P_c = (-1)^{L+S} \tag{1.2}$$

where $L + S$ is the total angular momentum for the system. The annihilation probability is proportional to α^m, where α is the fine structure constant and m the number of photon interactions (or of vertices on a Feynman diagram) in a given decay mode. Feynman diagrams for the one, two, three and four γ-ray decay modes are shown in 1.1; in the one γ-ray decay mode z represents any third body.

In the non-relativistic limit the 2-γ-ray annihilation cross-section of an electron and positron in a singlet state found by Dirac (1930b) is :

$$Q_{2\gamma} = \frac{\pi r_0^2 c}{v} \tag{1.3}$$

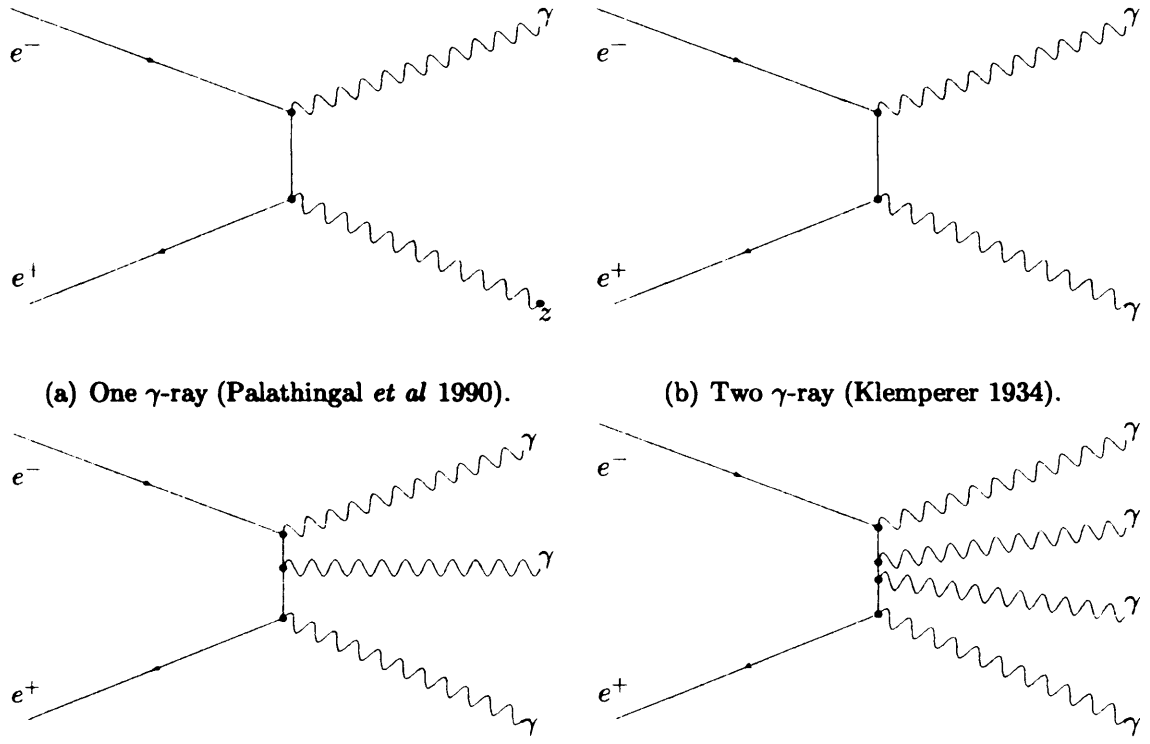

(a) One γ-ray (Palathingal *et al* 1990).

(b) Two γ-ray (Klemperer 1934).

(c) Three γ-ray (Chang *et al* 1982).

(d) Four γ-ray (Adachi *et al* 1990).

Fig. 1.1: Feynman diagrams for observed annihilation modes.

where v is the positron velocity with respect to the electron and $r_0 = e^2/4\pi\epsilon_0 m_0 c^2$ is the 'classical' electron radius in which m_0 is the mass of the electron . The annihilation rate is given by

$$\lambda = \pi r_0^2 c n_e \tag{1.4}$$

where n_e is the number of free electrons. If the electrons available for annihilation are bound to atoms or molecules, this is expressed as :

$$\lambda = \pi r_0^2 c n Z \tag{1.5}$$

where n is the number of atoms or molecules each having Z electrons. As the positron will influence the charge density around it, the term Z is usually replaced with Z_{eff}, interpreted as the effective number of electrons available to the positron for annihilation. The 2-γ annihilation cross-section thus becomes :

$$Q_{2\gamma} = \frac{\pi r_0^2 c Z_{eff}}{v} \tag{1.6}$$

As stated above, positronium is a quasi-stable bound-state of an electron and positron. Its lifetime against annihilation in its ground-singlet state (para-positronium) is 125 ps, and 142 ns in its triplet state (ortho-positronium). As shown above, $(-1)^n = (-1)^{L+S}$, hence positronium in its singlet state can only annihilate to an even number of photons and in its triplet state to an odd number of photons. The formation ratio of ortho-positronium to para-positronium is ~3:1 hence, positronium self-annihilation is dominated by the 3-γ mode in the ground state, as long as there is no significant quenching of Ortho-Ps (Charlton and Humberston 2001). The lowest order contributions for 2-γ and 3-γ annihilation rates of positronium in a state n are given by (Ore and Powell 1949):

$$\Gamma_{2\gamma}(n_{Ps},{}^1S_0) = \frac{1}{2}\frac{mc^2}{\hbar}\frac{\alpha^5}{n_{Ps}^3} \tag{1.7}$$

and

$$\Gamma_{3\gamma}(n_{Ps},{}^3S_1) = \frac{2}{9\pi}(\pi^2 - 9)\frac{mc^2}{\hbar}\frac{\alpha^6}{n_{Ps}^3} \tag{1.8}$$

respectively, where α is the fine structure constant. Due to their relative reduced mass as $\mu_H \sim 2\mu_{Ps}$ the energy levels of positronium are half those of hydrogen, so its ground state binding energy is 6.8 eV. An energy level diagram for positronium is shown in figure 1.2. The 2S state is metastable with a lifetime of order days against de-excitation and 1.1 μs against annihilation. The Lyman-α transition has a lifetime against spontaneous transition of 3.2 ns and a wavelength of 243 nm. Due to the large magnetic moment of the positron (as opposed to the proton), the magnitude of the magnetic spin-spin and spin-orbit interactions are similar, hence there is no hyperfine structure.

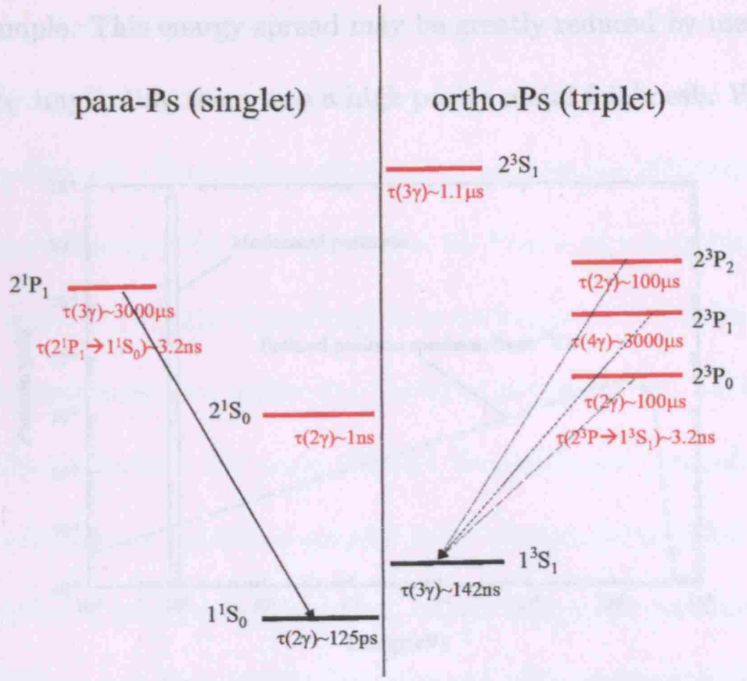

Fig. 1.2: Energy level diagram for positronium identifying Lyman-α transitions (Rich 1981).

1.2 Low energy positron sources for atomic physics

Low energy positrons for atomic scattering experiments are typically produced by moderating high energy positrons (β^+) emitted during nuclear decay of radio isotopes (e.g. ^{22}Na). The properties of some β^+ emitting isotopes are shown in table 1.1. β^+ particles are emitted from a source with a large energy spread; see figure

Isotope	β^+ Branching ratio	Endpoint energy (MeV)	Half-life
^{22}Na	0.91	0.54	2.6 yr
^{58}Co	0.15	0.47	70.8 d
^{64}Cu	0.19	0.65	12.7 h
^{11}C	0.99	0.96	20.4 min

Tab. 1.1: Properties of some radioisotopes used to produce low energy positrons.

1.3 for an example. This energy spread may be greatly reduced by moderating the β^+ particles by implanting them into a high purity metal foil/mesh. When fast β^+

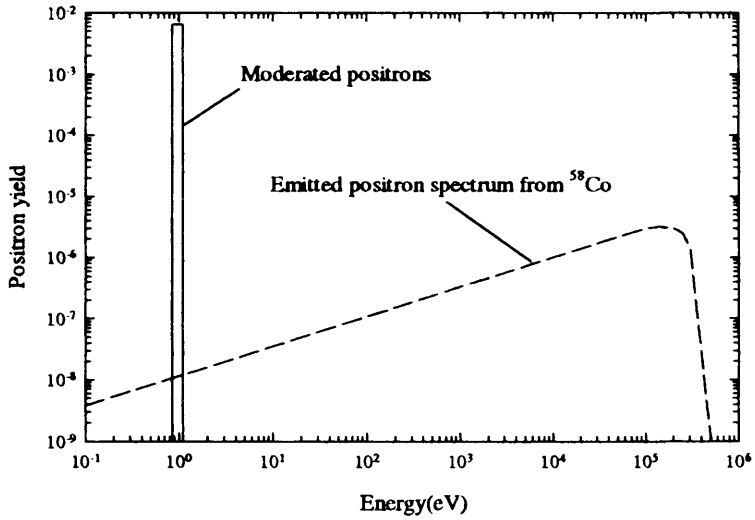

Fig. 1.3: Energy spread comparison for unmoderated β^+ from a ^{58}Co source and moderated positrons.

particles enter a solid, a fraction may be back-scattered, and this fraction is dependent on the atomic number and thickness of the moderator. Those that are not back-scattered will rapidly (10^{-13} s) lose their energy (from 100's of keV to 10's of eV) via inelastic collisions, for example ionization or excitation. The final stage of energy loss is through inelastic phonon scattering which is completed after 10^{-12} s. Once the positrons are thermalised they diffuse through the material, undergoing random scattering until they either reach the surface or annihilate within the solid. If a thermalised positron reaches the surface of the metal, it may be ejected into the vacuum with an energy equal to the magnitude of the positron work function. The latter for positrons (or electrons), is given by (Tong 1972 and Lang and Kohn 1971):

$$\phi_{\pm} = \mu_{\pm} - D \tag{1.9}$$

where μ_+ is the chemical potential which contains the contribution from electrons and ion cores and D is the surface dipole which is attractive for electrons and repulsive for positrons. The surface dipole is caused by the electron distribution extending into the vacuum for a distance of $\sim 10^{-10}$ m before becoming negligible. In practice, a number of single crystal metals in various orientations have been used for positron moderation. The higher the purity of the metal and the fewer defects in the crystalline structure the more efficient the moderator; metals with larger magnitude positron work functions are also more efficient (Murry and Mills 1980). Although effective at moderating positrons, metals have a low conversion efficiency ($\sim 10^{-4}$). Gullikson and Mills (1986) first observed high moderation efficiency from a rare gas solid (RGS) moderator. Unlike metals, RGS have a positive work function which would trap positrons in a metal. However, as the energy loss rate is much slower than in metals, the positrons reach the surface with enough energy to easily overcome this barrier. For RGS moderators, the yield is higher than a metal moderator but the energy spread is larger (Gullikson and Mills 1986).

After moderation, the slow positrons can be easily controlled using electric and/or magnetic fields, and used to form a beam. Positron beams are generally divided into two types, depending on whether the field used to guide the positrons is electrostatic or magnetic.

Recently, modified Penning-Malmberg traps in conjunction with rare gas solid moderators have been used to produce pulses of 10^4 positrons, at a repetition rate of 4Hz, with sub-eV energy spreads (e.g. Marler *et al* 2005, Sullivan *et al* 2002a). In figure 1.4, a schematic illustration of a trap is shown with variation of pressure and trapping potential. Positrons from a neon RGS moderator are confined in the trap by a magnetic field (1000-1500 Gauss). Once inside the trap, positrons pass

through regions I, II and III, held at 10^{-3}, 10^{-4} and 10^{-6} torr respectively with a buffer gas of N_2. Positrons are cooled by collisions (denoted A, B and C) with the buffer gas. Once in the final region positrons are cooled to 300 K by rotational and vibrational excitation. It was found that N_2, although the most efficient gas for trapping, was inadequate for cooling so a small amount of CF_4 was introduced (Greaves and Surko 2000).

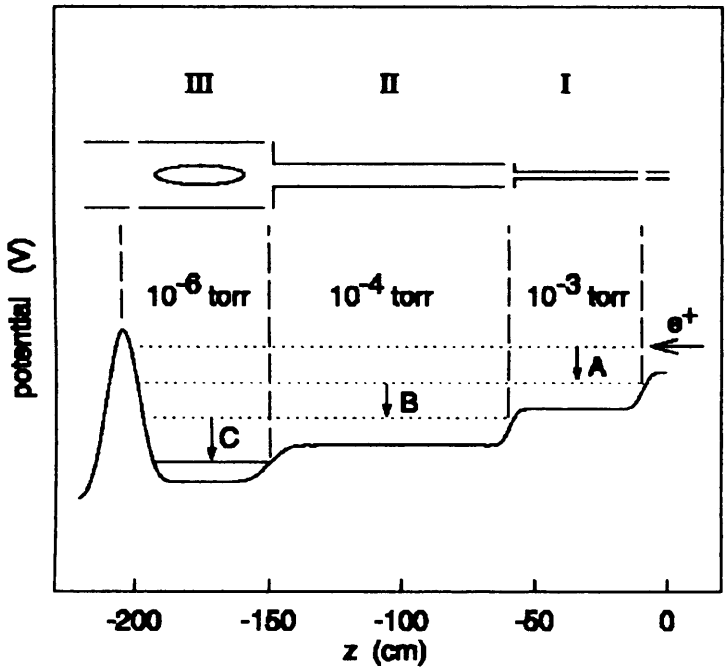

Fig. 1.4: Schematic illustration of a trap.

1.3 *Positron and positronium interactions with atoms and molecules*

Since the first positron-atom scattering experiments by Costello *et al* (1972), there has been a great deal of interest in low energy positron scattering from atomic and molecular targets. Initially measurements were concerned with measuring the total cross-section (Q^T). Developments of higher intensity positron beams in the

past few decades lead to measurements of inelastic cross-sections such as the total ionization cross-section (Q_i^t). Table 1.2 shows the main available scattering channels for positrons.

Process	Reaction
Total	$e^+ + A \rightarrow All$
Annihilation	$e^+ + A \rightarrow A^+ + 2\gamma$
Elastic Scattering	$e^+ + A \rightarrow e^+ + A$
Positronium Formation	$e^+ + A \rightarrow A^+ + Ps$
Target Excitation	$e^+ + A \rightarrow e^+ + A^*$
Direct Ionization	$e^+ + A \rightarrow e^+ + e^- + A^+$
Compound Formation	$e^+ + CD \rightarrow PsC + D^+$

Tab. 1.2: Main low energy positron scattering processes.

1.3.1 Total scattering cross-sections (Q^t)

Total scattering cross-sections exist for a number of targets, including the inert gases, hydrogen, alkali metals and some diatomic, triatomic and polyatomic molecules (for reviews see Kauppila and Stein 1990, Stein and Kauppila 1982, Charlton and Humberston 2001). It is interesting to compare electron and positron total scattering cross-sections; in figure 1.5, a schematic illustration of the behaviour of the total scattering cross-sections for electrons and positrons impact on a He target is shown. In general for the inert atoms, $Q^T(e^-)$ has very little structure, varying smoothly as the inelastic scattering channels open. $Q^T(e^+)$ on the other hand has a minimum at low energy; this is due to the Ramsauer-Townsend effect where the s-wave phase shift goes through zero. The sharp increase at the positronium

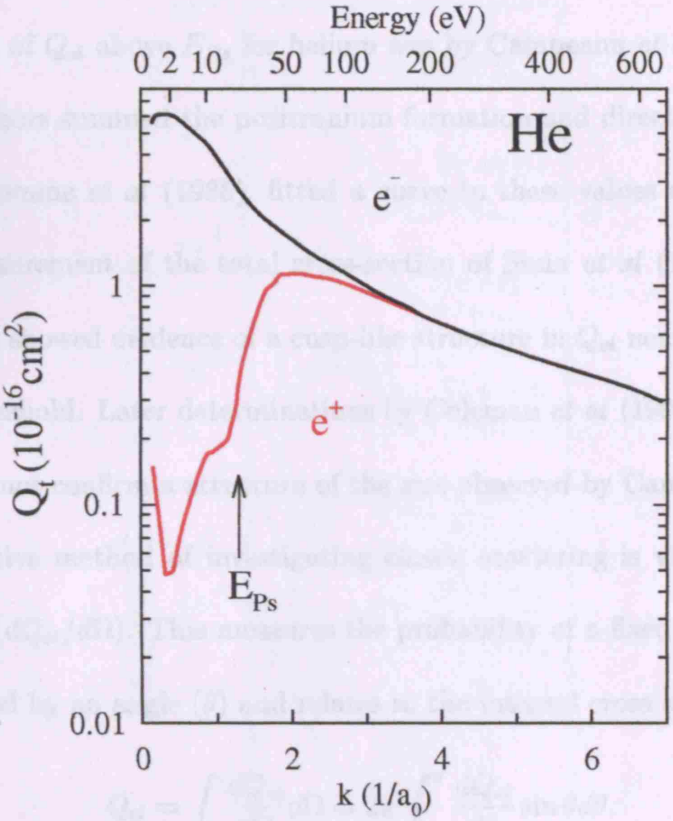

Fig. 1.5: Schematic illustration the behaviour of Q^T comparing e^- and e^+ impact on He. Lower x-axis shown in wavenumber (k) ($1/a_0$) with equivalent energies (eV) shown on the upper x-axis

formation threshold (E_{Ps}) reveals that this channel is significant when considering positron noble-gas scattering. Due to the eventual dominance of the static interaction at high energy, $Q^T(e^-)$ and $Q^T(e^+)$ merge, as is observed in He at $\sim 200\ eV$. Merging of Q^T has been observed for a number of molecular targets (e.g. C_2H_2 and SiH_4) at energies as low as 50 eV (Kimura *et al* 2000).

1.3.2 Elastic scattering cross-section (Q_{el})

When the contribution from the annihilation cross-section (Q_{ann}) is small compared to other processes, the total scattering cross-section is approximately equal to the

elastic scattering cross-section (Q_{el}) below the first inelastic threshold. The first determination of Q_{el} above E_{Ps} for helium was by Campeanu *et al* (1987). In this work, the authors summed the positronium formation and direct ionization cross-sections of Fromme *et al* (1986), fitted a curve to these values and subtracted it from the measurement of the total cross-section of Stein *et al* (1978). This early determination showed evidence of a cusp-like structure in Q_{el} near the positronium formation threshold. Later determinations by Coleman *et al* (1992) and Moxom *et al* (1993) did not confirm a structure of the size observed by Campeanu *et al* .

A more sensitive method of investigating elastic scattering is via the differential cross-section ($dQ_{el}/d\Omega$). This measures the probability of a fixed energy projectile being scattered by an angle (θ) and relates to the integral cross section by.

$$Q_{el} = \int \frac{dQ_{el}}{d\Omega} d\Omega = 2\pi \int_0^{\pi} \frac{dQ_{el}}{d\theta} \sin\theta d\theta. \tag{1.10}$$

$dQ_{el}/d\Omega$ for a number of targets have been reported including the noble gases and some molecules (for review see Surko *et al* 2005, Charlton and Humberston 2001 and references there in). These investigations have revealed that the elastic scattering channel may be influenced by inelastic channels. In figure 1.6, measurements of the $dQ_{el}/d\Omega$ (Smith *et al* 1990) for 5-50 eV positrons impact on argon are shown compared with theory. At low energy there is a good agreement between the experimental data of Smith *et al* (1990) and the theory of McEachran *et al* (1979). However, as the energy is raised, structure observed at low to intermediate angles is not observed by the experiment. The polarised-orbital method used for the calculations of McEachran and Stauffer (1986) and McEachran *et al* (1979) does not include the effect of positronium formation or direct ionization on the elastic scattering channel. There is a better agreement between the the theory of Bartschat *et*

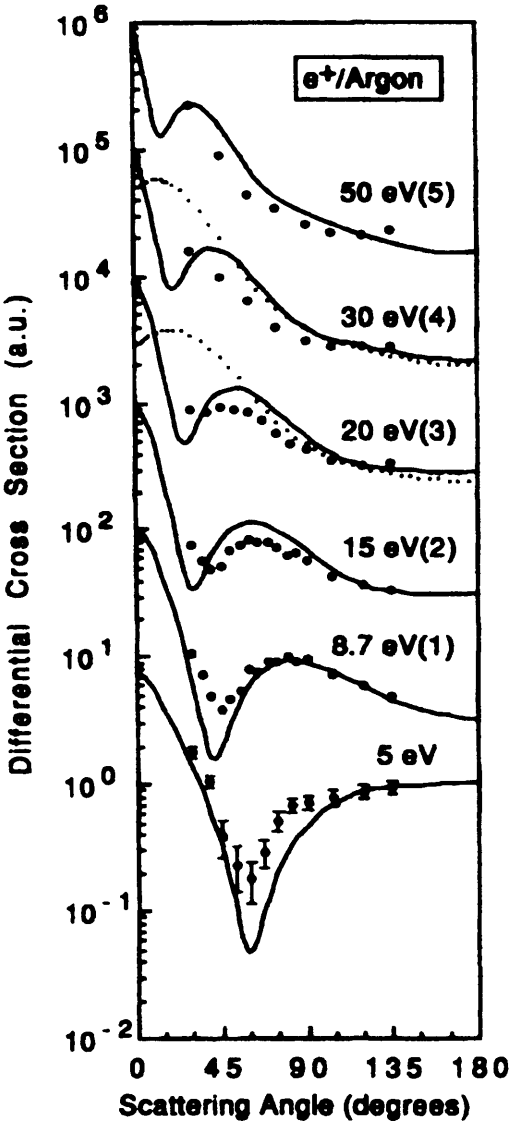

Fig. 1.6: From Smith *et al* (1990) : Experimental elastic positron-argon differential scattering cross-section in the range 5-50 eV. The theoretical data are from McEachran and Stauffer (1986) and McEachran *et al* (1979) (solid line) and from Bartschat *et al* (1988) (dotted line). The numbers in parentheses following the energy indicate the power of ten by which the cross-sections have been multiplied for clarity of display.

al (1988) and experiment at higher energy. In this case, Bartschat *et al* used an optical potential approach which included inelastic channels.

1.3.3 Positronium formation

Measurements of the positronium formation cross-section, integrated over all states, exist for all the inert gases (see figure 1.8), hydrogen (Zhou *et al* 1997 and references there in), many molecular targets, alkali metals (Zhou *et al* , 1994; Surdutovich *et al* , 1996, 2002) and magnesium (Stein *et al* 1996). In the case of atomic hydrogen, as can be seen in figure 1.7, there is a good consensus between measurements and recent theories in both energy dependence and magnitude for this target. In the case

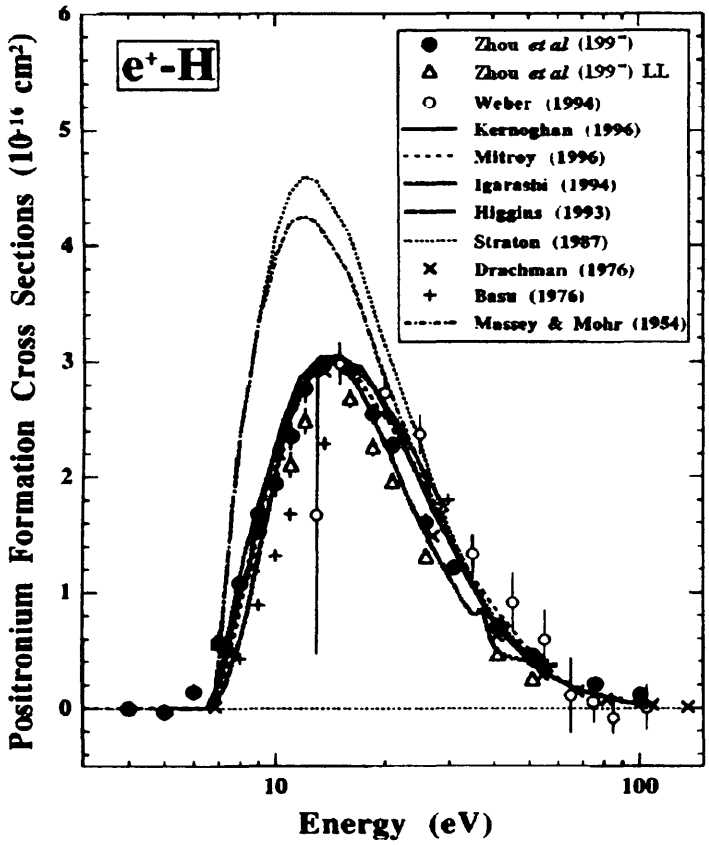

Fig. 1.7: From Zhou *et al* (1997) : Positronium formation cross-sections for hydrogen.

of the inert atoms, as can be seen in figure 1.8, there is now consensus between some measurements of Q_{Ps}. For He, the situation prior to the present work shows some disagreement over the magnitude of the peak and the energy where positronium formation becomes negligible. For Ne, Ar, Kr and Xe, there are two recent detailed

sets of measurements, those of Laricchia *et al* (2002) and those of Marler *et al* (2005). There is generally a good agreement between the measurements of Marler *et al* and Laricchia *et al* . However the Q_{Ps} of Marler *et al* does not replicate the magnitude of the structure observed in the energy region of the peak by Laricchia *et al* , as can be clearly seen in Ar, as shown in figure 1.9.

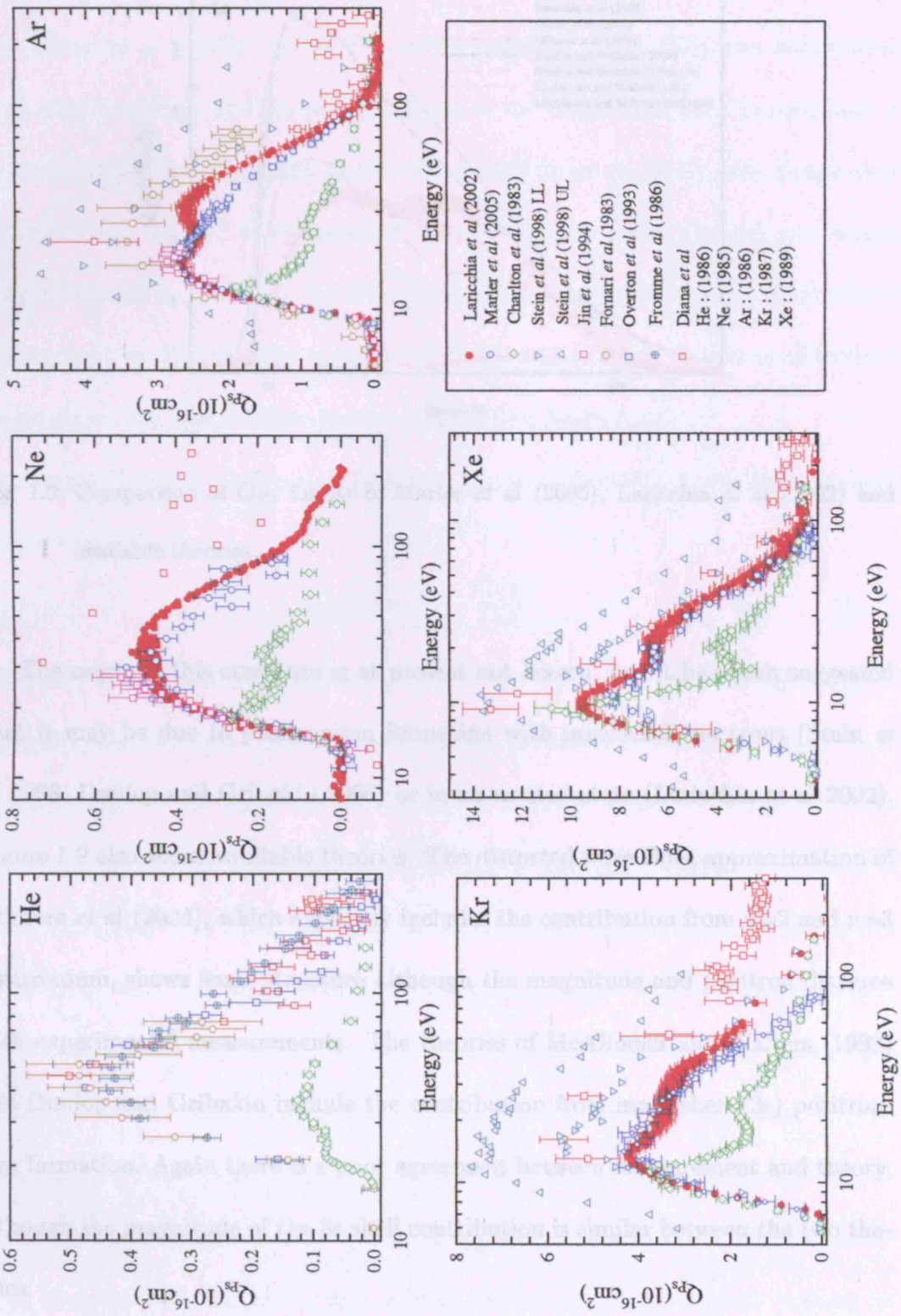

Fig. 1.8: Comparison of experimental positronium formation cross-sections (Q_{Ps}) for inert-atomic gases.

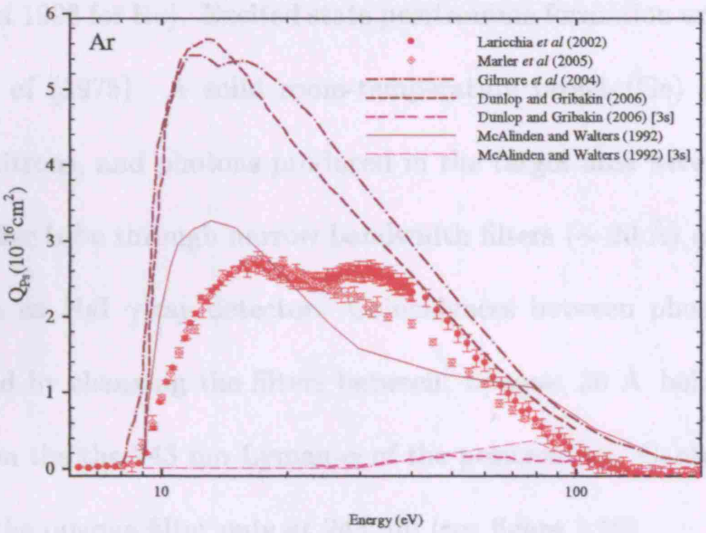

Fig. 1.9: Comparison of Q_{Ps} for Ar of Marler *et al* (2005), Laricchia *et al* (2002) and available theories.

The origin of this structure is at present not known, but it has been suggested that it may be due to positronium formation with inner-shell electrons (Stein *et al* 1998, Dunlop and Gribakin 2006) or in an excited state (Laricchia *et al* 2002). Figure 1.9 also shows available theories. The distorted wave Born approximation of Gilmore *et al* (2004), which explicitly includes the contribution from n=2 and n=3 positronium, shows some structure although the magnitude and positron disagree with experimental measurements. The theories of McAlinden and Walters (1992) and Dunlop and Gribakin include the contribution from inner-shell (3s) positronium formation. Again there is a poor agreement between measurement and theory, although the magnitude of the 3s shell contribution is similar between the two theories.

There are no published measurements of state selective positronium formation. However, there are a number of theories that explicitly calculate the contribution from excited state positronium formation to the integrated cross-section (e.g.

Campbell *et al* 1998 for He). Excited state positronium formation was first observed by Canter *et al* (1975). A solid room-temperature target (Ge) was bombarded with slow positrons, and photons produced in the target area were focused onto a photo-multiplier tube through narrow bandwidth filters ($\sim$ 20 Å) and, γ-rays were detected with an NaI γ-ray detector. Coincidences between photons and γ-rays were measured by changing the filters between: opaque, 30 Å below, 30 Å above and centred on the the 243 nm Lyman-α of the positronium. Canter *et al* found a signal above the opaque filter only at 243 nm (see figure 1.10).

In the alkali metals positronium formation is an exothermic process, the threshold for Ps formation is

$$E_{Ps} = E_i - \frac{6.8\ eV}{n^2} \tag{1.11}$$

where E_i is the ionization threshold, 6.8 eV is the ground-state binding energy of Ps and n the principle quantum number. For the alkali metals $E_i < 6.8\ eV$ (e.g. Na $E_i = 5.1\ eV$, Li $E_i = 5.3\ eV$, Rb $E_i = 4.2\ eV$). Hence it is expected that $Q_{Ps} \to \infty$ as $E \to 0$. There have been numerous theoretical studies (e.g. Ke *et al* 2004, Campbell *et al* 1998) and several experimental measurements (Surdutovich *et al* 1996, 2002 and Zhou *et al* 1994) of these systems. Interestingly, Campbell *et al* (1998) noted positronium formation in an excited state becomes increasingly dominant as alkali metal sequence is ascended from Li to Cs. Magnesium has also been studied theoretically (Cheng and Zhou 2006 and references there in) and experimentally (Surdutovich *et al* 2003). This target has a more complex structure than the alkali metals, having two active electrons in the outer shell, making its theoretical treatment challenging.

The first observation of excited state positronium formation from a gaseous target was by Laricchia *et al* (1985). Similar to the work of Canter *et al* (1975), Laricchia

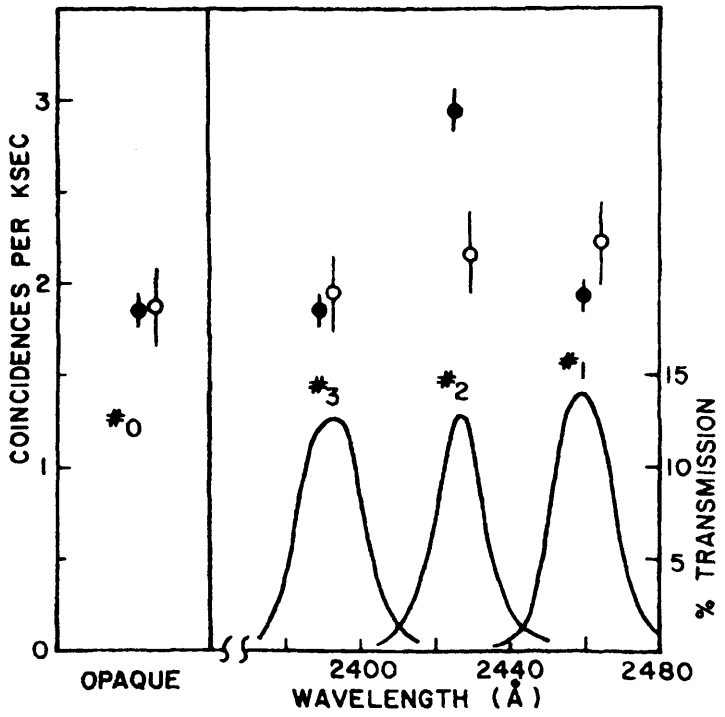

Fig. 1.10: From Canter *et al* (1975): The average coincidence (resolving time = 110nsec) counting rates obtained over a 10-day period with 25 eV positrons (solid circles) and 2.5-day period with 40 eV positrons (open circles) incident on an n-type Ge target. Also shown are transmission characteristics of the three interference filters; these transmission curves were monitored several times during the experiment.

et al used γ-ray - Lyman-α coincidences to identify the excited state positronium formation. In this experiment, a borosilicate glass filter was used to block the Lyman-α photon, and thus measure the background. In this work, excited state positronium formation was observed from Ne, Ar and H_2 targets.

Positronium formation has been investigated for a number of molecular targets ranging from simple homo-nuclear diatomics such as H_2 (e.g. Zhou *et al* 1997), which has received the most attention, or O_2 to more complex hetero-nuclear molecules such as CO (e.g. Marler and Surko 2005). Higher order poly-atomic molecules

such as H_2O and CO_2 (Murtagh *et al* 2006) have also been investigated. However, experimental and theoretical results are generally sparse for molecular targets, with the exception of H_2.

Theoretical investigations into the differential positronium formation indicated that its production is forward peaked (Brown 1985, 1986,1987). This opened up the possibility of creating a positronium beam using a positron beam and a charge exchange process. Laricchia *et al* (1987) found that approximately 4% of positrons scattered from a helium target could be detected as ortho-Ps collimated in a 6 ° cone about the incident positron beam direction. Recent investigations have shown that at low energy H_2 (Garner and Laricchia 1996) is the best positron-to-collimated-positronum convertor. At high energy ($> 90\ eV$) N_2 becomes more efficient (Leslie *et al* 2002).

1.3.4 Target excitation

The recent development of trap-based beams (discussed in section 1.2) used in conjunction with a novel scattering technique have enabled measurements of state resolved integral electronic and vibrational excitation cross-sections (Marler *et al* 2006). In figure 1.11 a schematic diagram of the apparatus used for these measurements is shown. The positrons are released from the accumulator with a well defined energy ($\Delta E \sim kT$) and pass through the scattering cell containing the target gas beyond which their final state energy E_s is analysed with a retarding potential analyser. Positrons are detected upon annihilation on a metal plate using a NaI γ-ray detector. Cross-sections are obtained by exploiting the properties of a positron orbit in a magnetic field. The total energy of a positron (E_T) in a magnetic

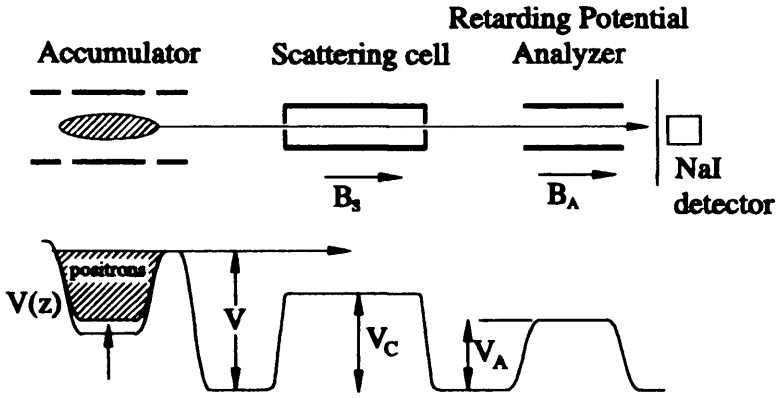

Fig. 1.11: Schematic diagram of the apparatus used in trap based scattering experiments.

field is split into two components :

$$E_T = E_{||} + E_{\perp} \tag{1.12}$$

where $E_{||}$ is the longitudinal and $E_{\perp}$ is the (cyclotron motion) transverse energy component with respect to the guiding magnetic field. If the positron interacts with the target elastically ($E_s = E_T$) or inelastically ($E_s = E_T - E_t$, where E_t is the threshold energy of a given inelastic process) energy will be redistributed such that:

$$E_{||} = E_s \cos^2\theta \tag{1.13}$$

and

$$E_{\perp} = E_s \sin^2\theta \tag{1.14}$$

Where θ is the scattering angle. In a slowly varying magnetic field, $E_{\perp}/B = eL/2m$ (where L is angular momentum and m is the mass of the e^+) is a constant, hence if the field where the positrons are analysed is much smaller than the field in the scattering region then the beam is parallelised, i.e. most of $E_{\perp}$ is converted to $E_{||}$. In this way, vibrational excitation cross-sections have been measured for a number of molecules including CF_4, CO, H_2, CH_4 and CO_2, and electronic-excitation cross-sections for Ar, H_2 and N_2. A recent study of the ν_3, asymmetric stretch mode

of CH_4 (Marler and Surko 2005) have shown the electron and positron excitation cross-sections to be virtually identical. In figure 1.12 the experimental results of

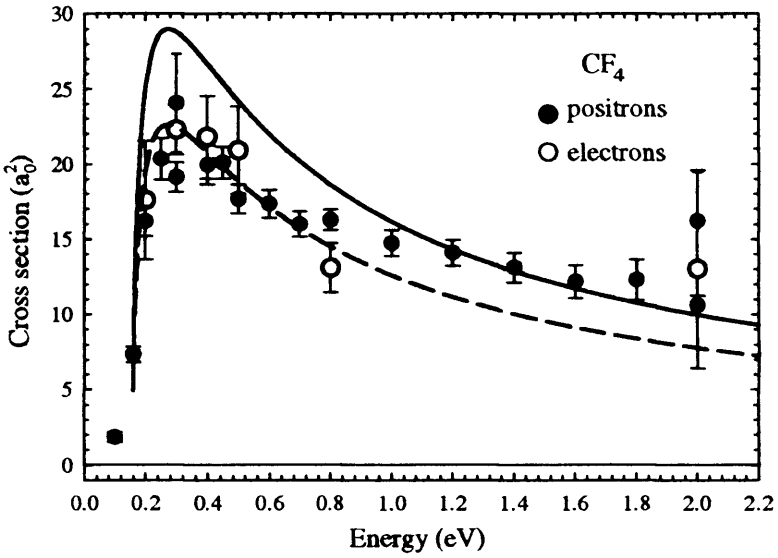

Fig. 1.12: From Marler *et al* 2006 : Comparison of the experimental results for positron-impact excitation of the ν_3 mode of CF_4 (Marler and Surko 2005) with: solid line the Born-dipole model of Mann and Linder (1992) and dashed line the Born dipole model with the magnitude adjusted to fit the data. Also shown for comparison are the electron-impact data (o) taken using the same experimental apparatus (Marler and Surko 2005).

Marler and Surko are compared with Born-dipole model calculations (see Marler *et al* 2006 and references therein), according to which cross-sections of electrons and positrons are identical. This model is applicable when long range electrostatic coupling of the charged projectile to the molecular transition dipole is the dominant excitation mechanism (Marler *et al* 2006). The results of Marler *et al* 2006 suggest dipole coupling is a significant excitation channel for molecules. In Sullivan *et al* (2002b) the first state-resolved electronic excitation cross-sections were published. In figure 1.13 their results for the $3p^5(^2P_{3/2,1/2})\ 4s(J=1)$ in argon are shown. These

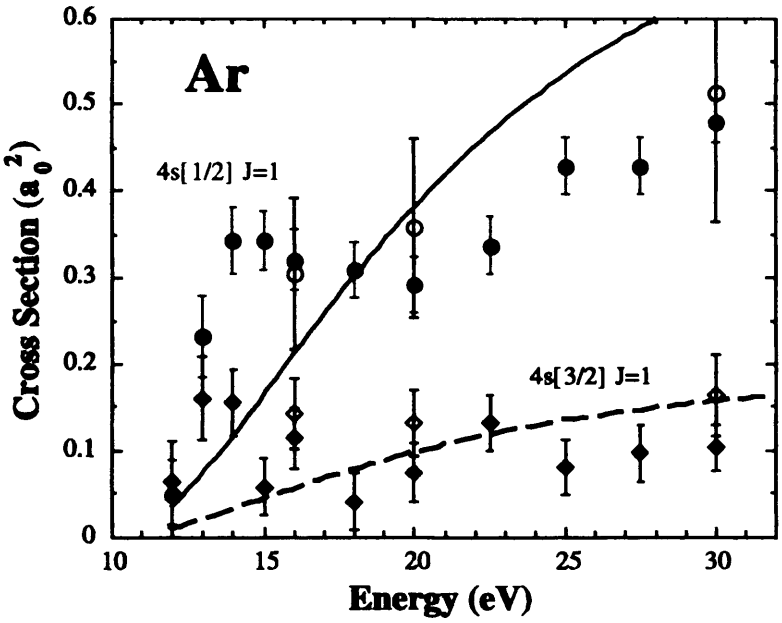

Fig. 1.13: From Sullivan *et al* (2002b): Absolute integral cross sections for the excitation of the $3p^5(^2P_{3/2;1/2})4s(J = 1)$ states of Ar from threshold to 30 eV. (black diamonds) data for the $^2P_{3/2}$ state, (dashed line) relativistic, distorted wave theory (private communication between Sullivan *et al* and R.P. McEachran), (grey circles) data for the $^2P_{1/2}$ state, (solid line) relativistic, distorted-wave theory (private communication between Sullivan *et al* and R.P. McEachran). The open symbols are electron scattering data from Chutjian and Cartwright (1981).

states are the two lowest lying 4s states that can be excited by positrons, the other two being metastable.

1.3.5 Direct ionization

Direct ionization by positron impact has been measured for many targets, both atomic and molecular (Charlton and Humberston 2001, Laricchia 2002 and Laricchia *et al* 2003). A thorough review of available measurements for helium is given in chapter 3 and available experimental cross-sections for the noble gases are shown

in figure 1.14. A brief discussion is given below.

Generally there is a good agreement between available measurements of Q_i^+, particularly for He and Ar. There is a good agreement between most measurements of Q_i^+ for Ne, although those of Knudsen *et al* (1990) exceed the others in magnitude after 40 eV. There is generally a good agreement between the recent measurements of Marler *et al* (2005) and the measurements of Kara *et al* (1997) and Moxom *et al* (1996), although some discrepancies exist at higher energies.

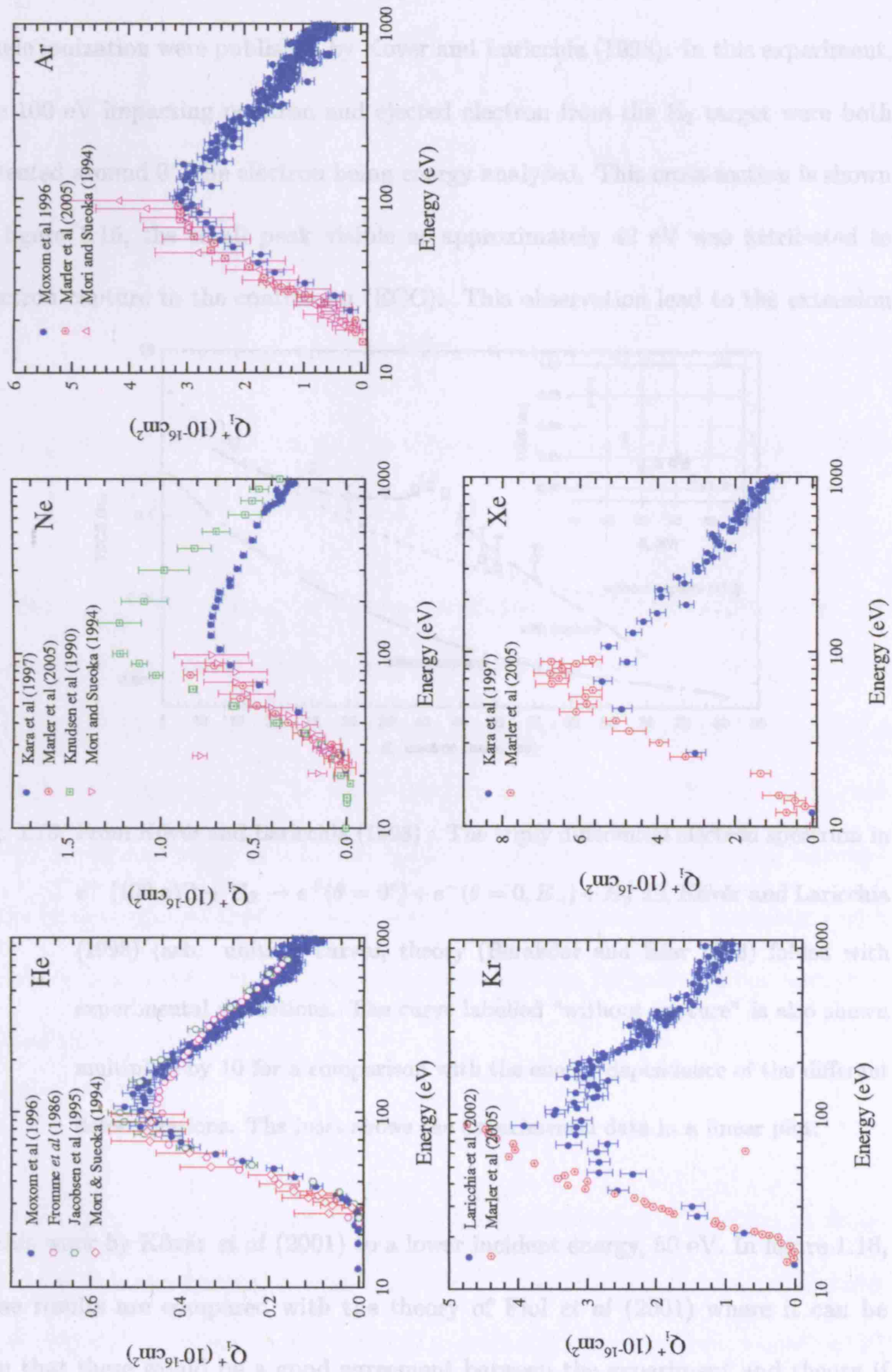

Fig. 1.14: Comparison of available measurements of Q_i^+ for He,Ne,Ar,Kr and Xe.

The first measurements of the triply-differential cross-section (TDCS) for direct single ionization were published by Kover and Laricchia (1998). In this experiment, the 100 eV impacting positron and ejected electron from the H_2 target were both detected around 0°, the electron being energy analysed. This cross-section is shown in figure 1.15, the small peak visible at approximately 42 eV was attributed to electron capture to the continuum (ECC). This observation lead to the extension

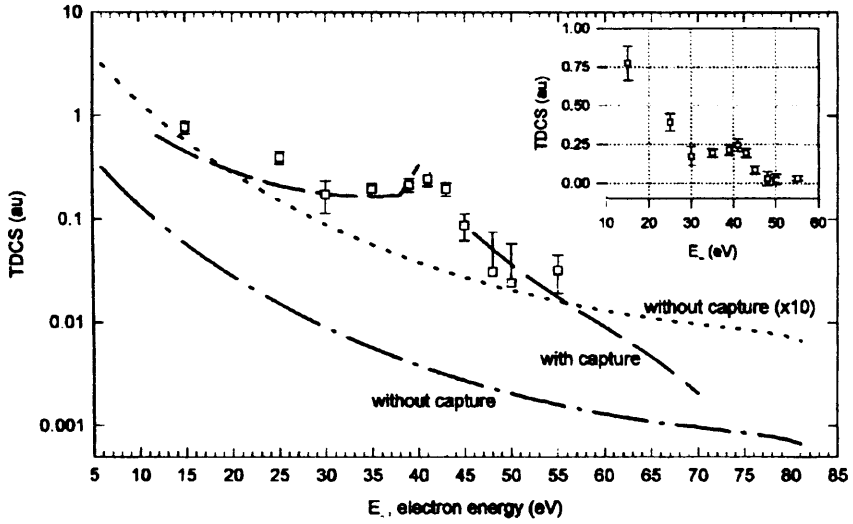

Fig. 1.15: From Kövér and Laricchia (1998) : The triply differential electron spectrum in e^+ (100 eV) + $H_2 \rightarrow e^+(\theta = 0°) + e^-(\theta = 0, E_-) + H_2^+$:□, Kövér and Laricchia (1998) (arb. units.): curves, theory (Berakdar and Klar 1993) folded with experimental resolutions. The curve labelled "without capture" is also shown multiplied by 10 for a comparison with the energy dependence of the different determinations. The inset shows the experimental data in a linear plot.

of this work by Kövér *et al* (2001) to a lower incident energy, 50 eV. In figure 1.16, these results are compared with the theory of Fiol *et al* (2001) where it can be seen that there would be a good agreement between the experiment and theory if the results of Fiol *et al* were shifted by 1.6 eV to lower energy. It was suggested by Kövér *et al* (2001) that the shift may be caused by ionization simultaneous to

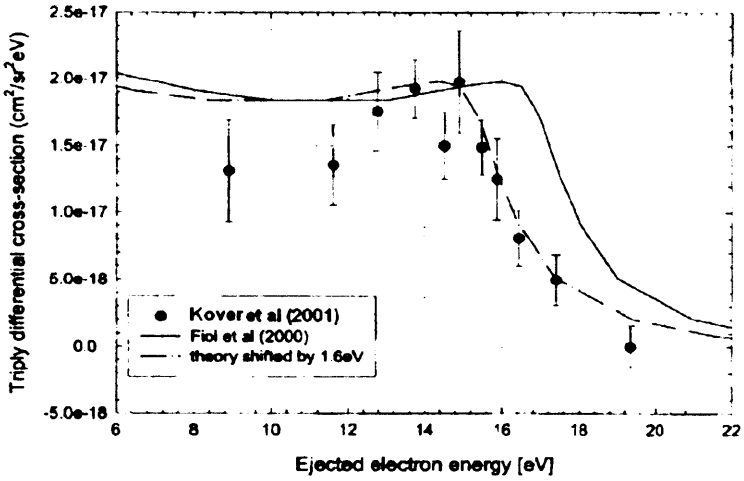

Fig. 1.16: From Kövér *et al* (2001) : The triply differential ionization cross-section of the 50 eV positrons incident on H_2.

another energy loss mechanism such as vibrational excitation or dissociation, but a number of possible systematic effects were identified which may have accounted for the shift. These systematic effects were investigated in detail by Arcidiacono *et al* (2005) and found not to be responsible for the observed shift. At the present time, the physical origin of this shift is still a matter under investigation, although it has been suggested that this shift may be due to a long range interaction with the electron and the remnant ion or competition from the positronium formation channel (Walters 2005).

1.3.6 Annihilation

Recently, there has been a great deal of theoretical interest in positron annihilation on atomic and molecular targets, especially in the vicinity of energy thresholds where, through a virtual or real process, a quasi-stationary positron would be left near a higher than average electron density of the target (Laricchia and Wilkin 1998, Van Reeth *et al* 2005). Experimentally structures have been observed near

vibrational excitation thresholds (E_{vib}) and associated with the formation of bound-states or Feshbach resonances (Gribakin and Ludlow 2003, Surko *et al* 2005).

The first energy dependent measurements of annihilation rates have been performed, using a trap based beam, with energy from 50 meV upwards, magnetically guided through a gas cell. A schematic diagram of the apparatus used in these experiments is shown in figure 1.17. A well-shielded CsI detector counts the number of γ-rays

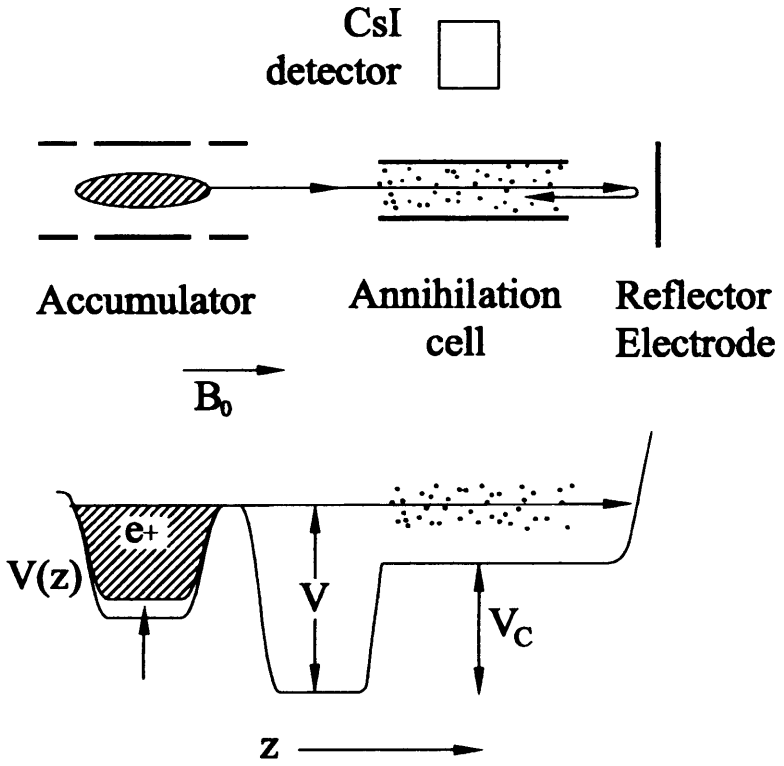

Fig. 1.17: Schematic diagram of experimental apparatus used for annihilation measurements.

produced in a 20 μs period consistently with the positron pulsing. During this time, the positrons are stopped from annihilating at the end of the beam line by being electro-statically reflected.

Figure 1.18 shows Z_{eff} measured as a function of energy for argon and xenon below the threshold for any inelastic processes. There is little structure visible with Z_{eff} decreasing with energy before becoming approximately constant. Fair agreement

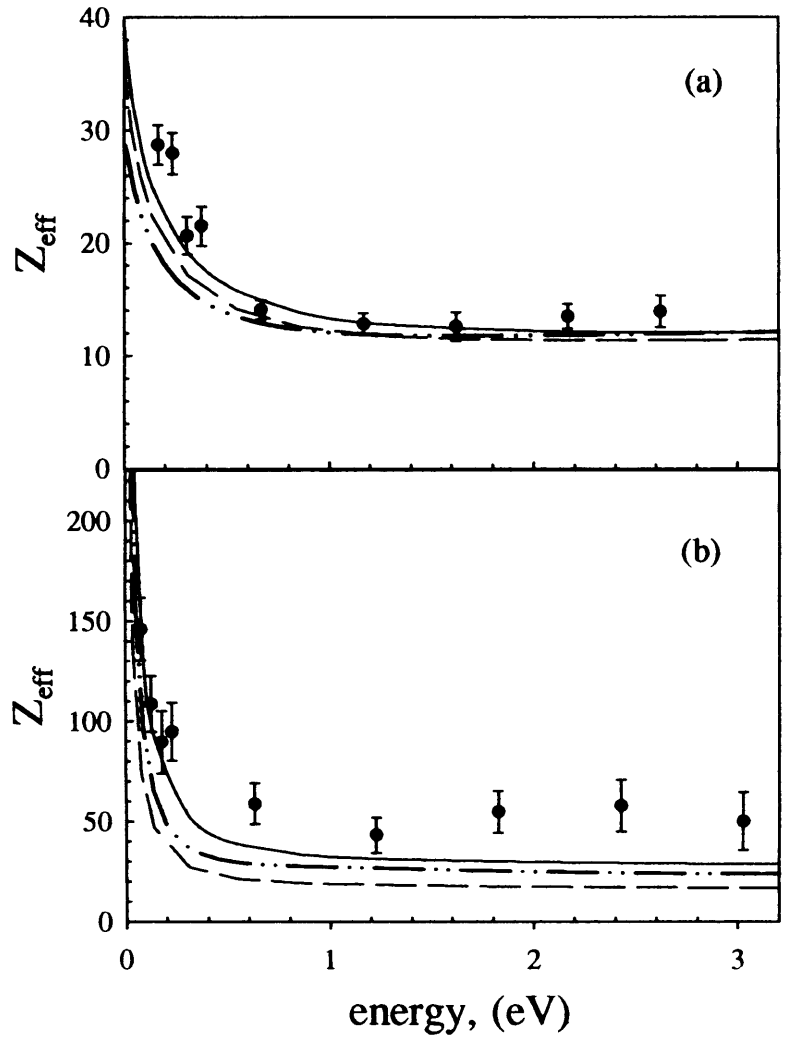

Fig. 1.18: From Surko *et al* (2005) : (•) Z_{eff} as a function of incident positron energy η, measured for argon (a) and xenon (b), using a tunable, trap-based positron beam. From Marler *et al* (2004). Also shown are Z_{eff} from the polarised-orbital theory, (dashed curve) (McEachran *et al* 1979), many-body theory, (double chain curve) (Ludlow 2003, Gribakin and Ludlow (2004)), and a model-potential calculation (solid line) (Mitroy and Ivanov 2002), tuned to reproduce the polarised-orbital scattering results and experimental room-temperature Z_{eff} values.

between measurement and theory may be seen in this energy range. In the case of molecular targets, there are many inelastic thresholds below that for positronium

formation arising from vibrational and rotational excitations. Figure 1.19 shows

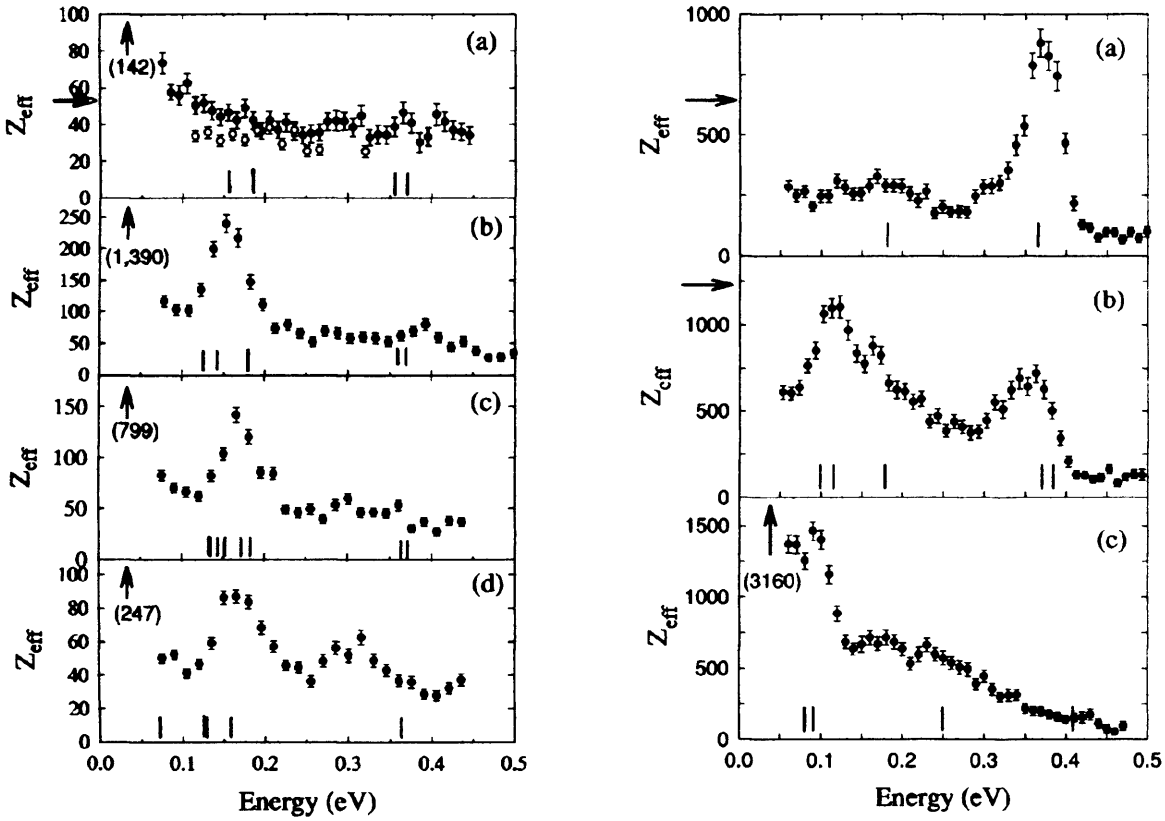

Fig. 1.19: From Barnes *et al* (2003) : Z_{eff} for left: (a) methane (CH_4) and carbon tetrafluoride (CF_4), (b) methyl fluoride (CH_3F), (c) difluoromethane (CH_2F_2), and (d) trifluoromethane (CHF_3). right: (a) ethane (C_2H_6), (b) ethylene (C_2H_4), and (c) acetylene (C_2H_2). Vertical lines indicate the energies of the vibrational modes. Arrows indicates Z_{eff} for a thermal distribution of positrons. In the left hand graph (a) the solid arrow refers to methane, the open arrow to carbon tetrafluoride.

a corresponding measurement of Z_{eff} for a number of targets (see figure caption) where enhancements of Z_{eff} are evident in the vicinity of E_{vib}. The shifts (ΔE) of some of the peaks from E_{vib} have been interpreted as signifying the presence of vibrational Feshbach resonances and the value of ΔE as the binding energy of the compound state from which the positrons annihilates (see Surko *et al* 2005 for

review). However, the presence of peaks above E_{vib} (e.g. CH_3F) is not consistent with this model.

1.3.7 Positron and positronium complexes

Of great interest are purely leptonic systems such as the positronium negative or positive ion, ($e^-e^+e^-$,Ps^-) or ($e^+e^- + e^+$,Ps^+) respectively or positronium molecules Ps_2. The observation of the positronium negative ion (Ps^-) was first reported by Mills (1981) who created Ps^- by bombarding a thin carbon film with positrons. The Ps^- was subsequently accelerated by a grid toward an γ-ray detector. This Doppler shifts the annihilation line of the Ps^- component of positron annihilation. Observation of molecular positronium Ps_2 has recently been reported by Cassidy and Mills (2007). In this experiment a high density positron pulse ($3.3 \times 10^{10}\ cm^{-1}$) was focused onto a thin film of nano-porous silica, used because of the high efficiency for forming positronium in the bulk. Cassidy *et al* (2005) observed a shortening of the ortho-positronium lifetime by $\sim 33\%$ which they attributed to both spin exchange quenching of the ortho-Ps and formation of the Ps_2 molecule. The latter has now been infered from measurements on the internal surfaces of a porous medium (Cassidy and Mills 2007).

The formation of bound states of positrons and positronium to atoms and molecules has been of interest, almost from the time of the discovery of the positron (see e.g. Ore 1951). There has been a great deal of theoretical and experimental investigation into these bound states (see Schrader 1998). Apart from the evidence discussed in section 1.3.6, there is still little experimental observation of them. There are two types of bound state considered: that of positron binding such as e^+Li or e^+Mg

and positronium binding such as PsH or LiPs. Observation of the formation of PsH was reported by Schrader *et al* (1992); according to the following reaction:

$$e^+ + CH_4 \rightarrow CH_3^+ + PsH \tag{1.15}$$

The observation of CH_3^+ ions below the threshold for $e^+ + CH_4 \rightarrow CH_3^+ + H + Ps$ (see figure 1.20) was interpreted as evidence for the formation of PsH. Schrader *et*

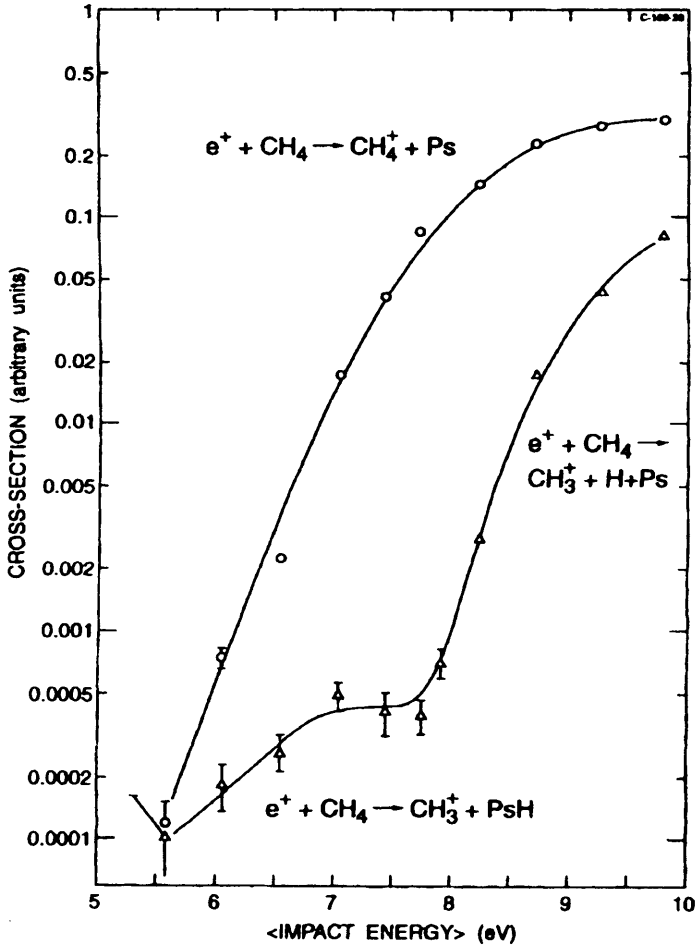

Fig. 1.20: From Schrader *et al* (1992) : Cross-sections for the production of CH_4^+ and CH_3^+ ions in positron collisions with CH_4.

al were able to estimate the binding energy of this compound to be (1.1 ± 0.2) eV in fair agreement with theoretical calculations (Mitroy *et al* 2002).

1.4 Motivation for the present work

The measurements presented in chapter 3 of the ion / γ-ray coincidence yield in helium below the Ps formation threshold (E_{Ps}) were motivated by the preliminary results of Szluinska and Laricchia (2004a), who observed a surprisingly high signal in Ne. The investigation with helium was performed in order to check the possible dependence on gas load of the contaminants back-streaming from the pumps. Additionally, as observed in section 1.3.3, considerable progress has been recently made on the convergence of the positronium formation cross-sections for the heavier noble gases. In this work, investigations have been extended to helium to address the discrepancies over the magnitude of the peak and the high energy dependence. A detailed determination of the positronium formation cross-section has thus ensued using the same method as Laricchia *et al* (2002) described in chapter 3.

For the heavier noble gases, the main area of uncertainty is the magnitude of the structure observed in the energy region of the peak. In figure 1.9, Q_{Ps} from Laricchia *et al* (2002) is shown compared with that of Marler *et al* (2005). The divergence between the two measurements is obvious after 25 eV. The hypothesis of Laricchia *et al* (2002) that the structure may be due to excited state positronium formation has motived the work in chapter 4, which has resulted in the first measurements of the excited state positronium formation cross-section for helium and argon using ion/de-excitation photon coincidences.

2. EXPERIMENTAL SET-UP

In the present work, slow positrons were produced from a ^{22}Na source and an annealed W meshes moderator. The low energy particles were confined by a weak (typically $\sim$ 80 Gauss) magnetic field, over the entire flight path from the source to the end of the beam line, via an interaction region. This consisted of a hemispherical gas cell constructed from polished Al. Various detectors were used as needed around the gas cell. Ions produced in the cell were extracted by a weak static electric field and detected with a Channel Electron Multiplier (CEM) mounted in a separate chamber. A photomultiplier tube was mounted opposite the ion extracting lens to detect low energy photons emitted in the cell during some studies. Alternatively a γ-ray detector was placed close to the cell to detect annihilation quanta. At the end of the beam line, another CEM detector was used to count the number of positrons transported from source.

In this chapter, the experimental apparatus and methods used throughout the present studies will be discussed. Methods specific to each study will be discussed in detail in the appropriate chapter.

2.1 Low Energy Positron Beam Production

^{22}Na has a branching ratio of 90 % β^+ emission to 10 % electron capture (EC). The decay scheme for this isotope is shown in figure 2.1. The source, supplied by DuPont Pharmaceutical, was contained within a capsule. The ^{22}Na material

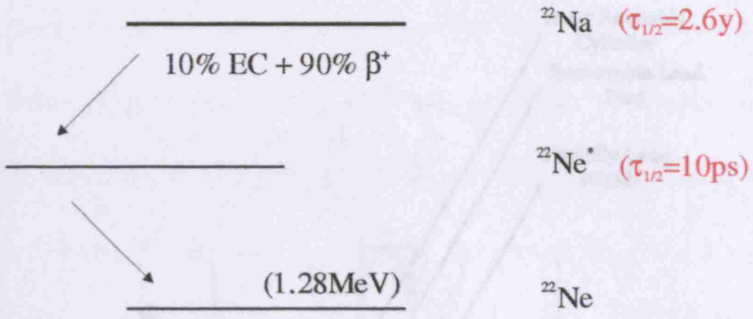

Fig. 2.1: Decay scheme for ^{22}Na.

deposited on to a spot (diameter=4mm) on a platinum disk (diameter=18mm) and sealed with a titanium window (10 μm thick). It has been estimated that 40 % of the β^+ particles are ejected forward (Massoumi *et al* 1988). The activity of the source during these studies ranged from $\sim$ 7 to 3 mCi (producing typically between $\sim$ 5000 e^+ s^{-1} and $\sim$ 1500 e^+ s^{-1} after moderation). The source was mounted on the end of a manipulator arm inside of a purpose built vacuum chamber (shown in figure 2.2). The chamber has been designed such that, once the manipulator arm with the source mounted on it is retracted, the inner cylinder can be rotated in order to shield the source. Once in this configuration, a lead plug with the moderator could be removed with minimal exposure to ionizing radiation.

The moderator assembly (shown in figure 2.3) was mounted at the end of the lead plug. The moderator consisted of typically 3-4 overlapping annealed 90 % transmission W meshes (diameter $\sim$14 mm). The annealing process was performed in a chamber with a vacuum of $< 10^{-1}$ torr. An oven is constructed from two strips of high purity (99.95 %) W foil. These strips were clamped in place between two blocks leaving a space in the centre within which the meshes were placed. The oven was then heated, whilst under vacuum, by passing a high current through the strips. As the meshes were heated, water vapour was desorbed and carbon impurities from

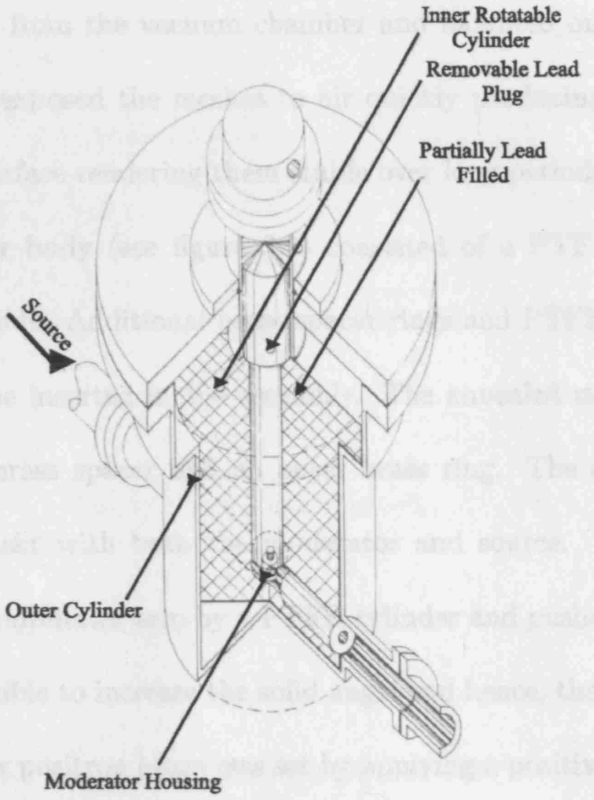

Fig. 2.2: Source end vacuum chamber.

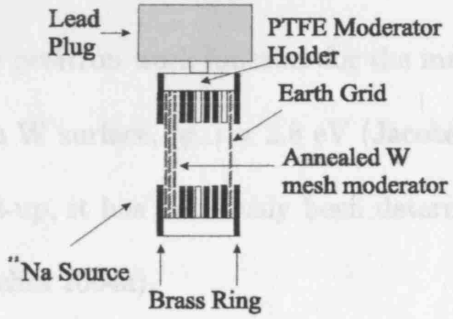

Fig. 2.3: Illustrative diagram of moderator holder.

the bulk crystalline structure were ejected. This process of removing impurities improves the moderation efficiency of the meshes. The temperature of the oven could be monitored through a pyrex window using a pyrometer, and with a typical maximum temperature reached of (2000 ± 100) °C. After annealing and cooling, the

meshes were removed from the vacuum chamber and mounted on the moderator holder. This process exposed the meshes to air quickly producing an oxide layer which forms on the surface rendering them stable over long periods of time.

The moderator holder body (see figure 2.3) consisted of a PTFE cylinder with brass rings on either side. Additional brass spacer rings and PTFE insulator rings allow extra grids to be inserted in the assembly. The annealed meshes were held between an internal brass spacer and an outer brass ring. The outer brass ring was in electrical contact with both the moderator and source. The source was insulated from the manipulator arm by a PTFE cylinder and pushed up as close to the moderator as possible to increase the solid angle and hence, the beam intensity. The energy of the slow positron beam was set by applying a positive potential (V_m) to the moderator meshes with respect to the chamber ground. The energy of the beam is given by

$$E = eV_m + |\phi_+| \tag{2.1}$$

where ϕ_+ is the negative positron work function for the material, typically of order $-(1-3)$ eV. For a clean W surface, $|\phi_+| = 2.8$ eV (Jacobsen *et al* 1990); with the present experimental set-up, it has previously been determined $|\phi_+| = (2.4 \pm 0.4)$ eV (Szluinska and Laricchia 2004a).

2.2 Beam Transport

The beam was held under high vacuum (1×10^{-6} torr) by 4 oil-vapour diffusion pumps; three Edwards E04 and an Edwards E02. These were located beneath the source (EO2), either side of the gas cell and under the ion detector chamber. These diffusion pumps were backed by 3 rotary backing pumps, which evacuated

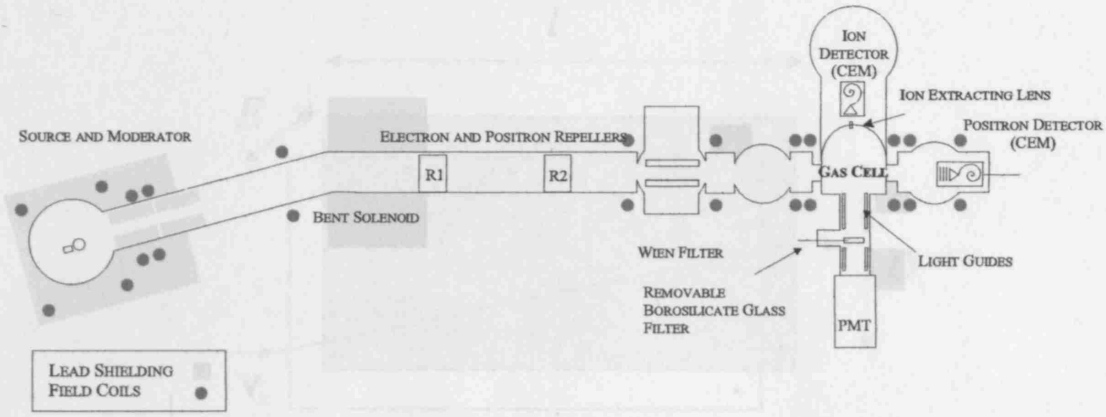

Fig. 2.4: Beam line schematic.

the system from atmospheric pressure to typically 2×10^{-2} torr (or lower) enabling the use of the diffusion pumps. The pressure was monitored in the backing lines with pirani gages. If the pressure rose above the threshold for safe operation of the diffusion pumps (1×10^{-1} torr), or the cooling water supply failed, then a protection system turned off all diffusion pumps, high voltages and closed magnetic valves over the rotary pumps.

The beam was confined along the beam line by a longitudinal magnetic field created by current carrying coils (see figure 2.4). The field varied from 40 Gauss to 120 Gauss. In the interaction region the field can be varied from 40-100 Gauss. After the source chamber, a bent solenoid reduced the number of fast particles in the line and removed a direct line of sight between the interaction region and the source. Inside the solenoid there were two electrodes (R1) and (R2). R1, held at ~-500V, was used to repel secondary electrons from, for example, the moderator holder. R2, held at typically $V_{R2} > (V_m + 3\,V)$ was used to repel the positron beam, or to bias part of it away in order to reduce the energy spread. The beam then encountered a Wien filter which further reduced the number of fast particles in the beam line. A schematic diagram of a simple Wien filter is shown in figure 2.5. The application of

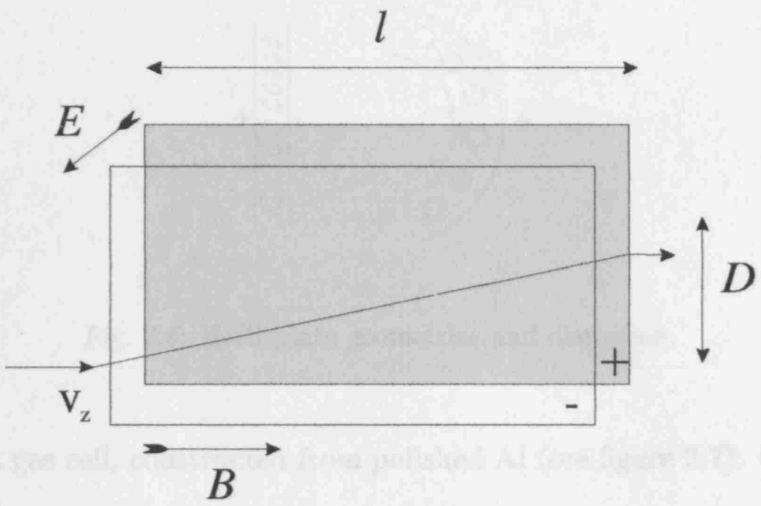

Fig. 2.5: Planar geometry of a Wien filter.

a potential difference (approximately $V_{Plate\pm} = \pm\sqrt{V_m}$) across two plates of length l generates an electric field ($\vec{E}$) which is perpendicular to the guiding magnetic field $\vec{B}$, causing the gyration centre of the positron beam to drift with velocity

$$\vec{v} = \frac{\vec{E} \times \vec{B}}{B^2}. \tag{2.2}$$

Hence the vertical displacement of the beam is given by

$$D = \frac{\left|\vec{E} \times \vec{B}\right|}{B^2} \frac{l}{v_z} \tag{2.3}$$

where v_z is the longitudinal speed of the incident positron. Hence slow particles may be easily deflected on to a new axis away from the axis of the fast particles. The actual $\vec{E} \times \vec{B}$ filter used in the present work was of a cylindrical geometry with flared ends. This geometry was used, following the work of Hutchins *et al* (1986), in order to minimize distortion to the beam profile (see figure 2.6). The $\vec{E} \times \vec{B}$ consists of two plates 120 mm in length with a separation of 10 mm, the approximate radius of the electrodes was 200 mm. At either end of the $\vec{E} \times \vec{B}$ chamber there was an aperture of diameter 8 mm.

Beyond the $\vec{E} \times \vec{B}$ chamber, the beam passes through the interaction region which

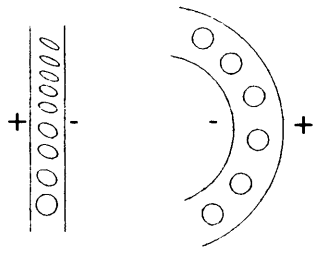

Fig. 2.6: E×B plate geometries and distortion.

consisted of a gas cell, constructed from polished Al (see figure 2.7). Gas is admitted into the cell via a fine leak valve. Two valves were used during the course of this work, firstly a manual needle valve (Edwards LV10) and latterly a computer controlled piezo-electric controlled valve (Veeco PV-10). The pressure in the gas cell was monitored using a capacitance manometer. A feedback loop between this manometer and the piezo-electric valve gave improved pressure stability over the manual needle valve. The maximum variation of target pressure tolerated before adjustment of the valve was $\sim$ 3 %, with a typical variation less than 1 %. The weak static electric field used for ion extraction within the cell had a minimal effect on the beam (Szluinska *et al* 2004a). A voltage of (-500 V) was applied to the ion extracting lens throughout this work, with ions being extracted from $\sim$ 50 % of the volume of the cell (Szluinska 2003). Once extracted from the cell, ions were detected by a CEM with a high cone voltage of $V_{cone} = -3.4$ kV to ensure similar detection efficiency for ions of different charge to mass ratios. A photomultiplier tube (PMT) could be mounted on an extension arm opposite to the ion detector. The extension arm serves to remove the PMT from the guiding magnetic field of the beam line. Light guides are inserted into the arm to improve photon collection. The light guides, consisting of glass tubes coated with a layer of Al for reflectivity then an outer layer of MgF_2 to prevent oxidization of the Al, and the polished Al

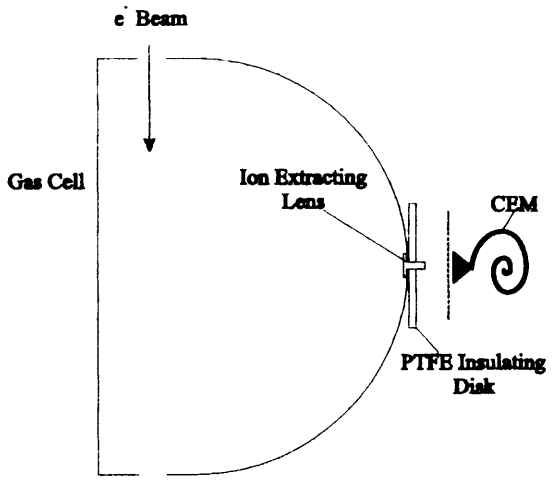

Fig. 2.7: Diagram of the gas cell and ion detection system.

surface of the scattering cell help to correct for the effect of the extension arm on the solid angle of the detector. It is also possible to mount a gamma-ray detector, a PMT and a NaI scintillator crystal, near the gas cell.

Beyond the gas cell there is a final CEM which was used to measure the beam intensity. Unless detection of the positron was essential, this detector remained grounded during measurement. This was done because, when the detector was on, a positron impacting on the cone may have caused an electron to be backscattered toward the gas cell having been accelerated by the cone voltage ($V_{cone} = -300\ V$). If these electrons were to enter the cell, they would collide with the target and produce extra ions.

An example of a typical energy spread is shown in figure 2.8. dN/dV_r is the derivative of the count rate with respect to a retarding potential (V_r) applied to a grid in front of the e^+ detector. The energy spread of the beam $\Delta E \sim 2.2\ eV$ in this example.

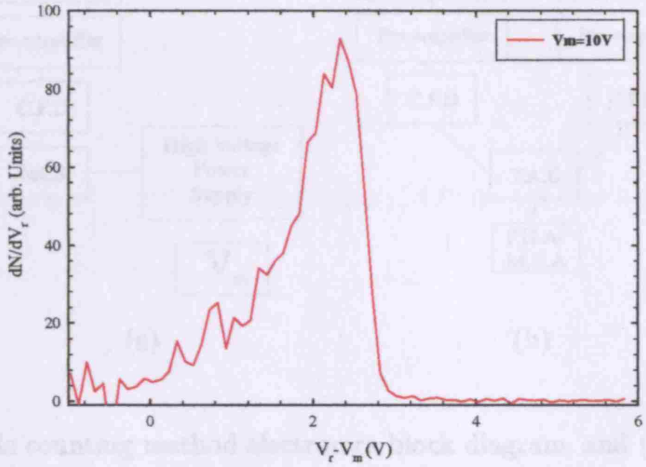

Fig. 2.8: Typical beam energy spread.

2.3 Measurement Methods

Two distinct methods of measurement were employed, namely counting single pulses from a detector and coincidences between two detectors. When counting single pulses, the count rate was recorded on a multichannel scaler, either on an Ortec MCS Plus or one written in the LabView language. The MCS counts pulses for a set dwell time for a number of channels. V_m is adjusted automatically as a function of the MCS channel number enabling measurements over a wide range of energies, thus the MCS effectively display count rate vs beam energy. An example of the electronics used is shown in figure 2.9. The coincidence method produces an ion time of flight spectrum based on the inputs from two detectors (ion detector and PMT/γ-ray detector), an example being shown in figure 2.10. The sharp peak is from helium ions produced in the cell and the secondary peak/bulge structure is from a contaminant in the vacuum system with a mass of $\sim (20 \pm 4)$ amu. The 4096 channels represent a time range of $\sim 100\ \mu s$ with $t_0 \sim channel(490)$. A start signal from one detector, in this case the positron detector, and a stop signal from the

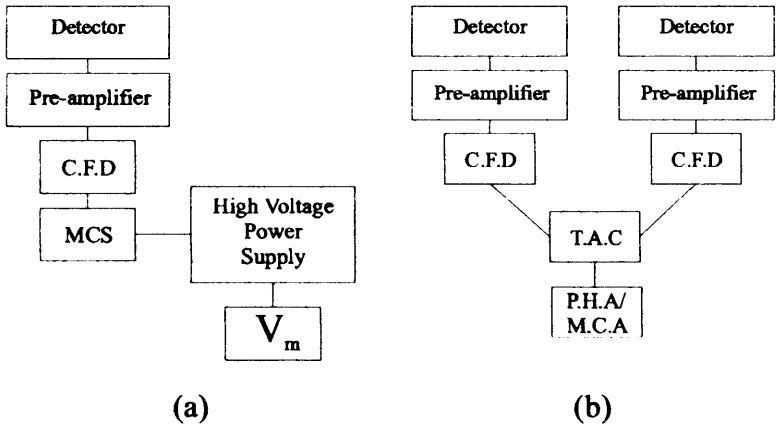

Fig. 2.9: (a) Single counting method electronics block diagram, and (b) Coincidence system electronics.

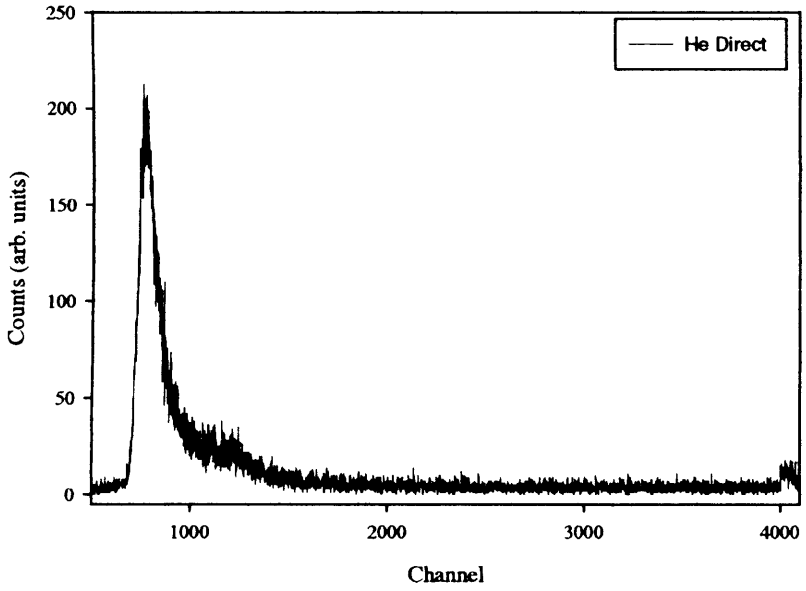

Fig. 2.10: Example of a time of flight spectra from ion-positron coincidences from an He target.

ion detector delayed by 11 μs were fed into a time to amplitude converter (TAC). The timing signal from the TAC was then fed into a pulse height/multichannel analyser (Ortec 916) which produced the TOF spectra. This method has a number of advantages over the single counting method : for example, it is possible to select

specific ionization processes e.g. single ionization where coincidences between the remnant ion and the ionizing positron are used. It also provides superior signal to noise ratio.

In the following chapters, detailed descriptions of the specific experimental system used for each study will be given.

3. LOW-ENERGY POSITRON IMPACT-IONIZATION OF HELIUM

3.1 Introduction

Because of its relative simplicity, the positron-helium scattering system has attracted considerable attention from both experimentalists and theorists (for reviews see Charlton and Humberston 2001 and Laricchia *et al* 2003). Positron impaction ionization of helium at low energy may proceed via three main channels as represented below:

$$e^+ + He \rightarrow He^+ + 2\gamma \qquad \text{annihilation.} \tag{3.1}$$

$$e^+ + He \rightarrow He^+ + Ps \qquad \text{positronium formation.} \tag{3.2}$$

$$e^+ + He \rightarrow He^+ + e^+ + e^- \qquad \text{direct ionization.} \tag{3.3}$$

The total ionization cross-section ($Q_i^t(e^+)$) is defined as :

$$Q_i^t(e^+) = Q_{Ps} + Q_i^+(e^+) + \sum Q(HO) \tag{3.4}$$

where Q_{Ps} is the positronium formation cross-section, Q_i^+ is the direct ionization cross-section and $\sum Q(HO)$ represents all other higher order processes such as : double ionization ($e^+ + A \rightarrow A^{2+} + 2e^- + e^+$) or transfer ionization ($e^+ + A \rightarrow A^{2+} + Ps + e^-$). The annihilation cross-section (Q_{ann}) is included in $\sum Q(HO)$, as it is considered to be generally negligible, although, its contribution may become

significant near inelastic thresholds. Various models have been proposed which consider this possible enhancement in terms of virtual processes, Feshbach resonances and bound states, as reviewed by e.g. Van Reeth *et al* (2005), Surko *et al* (2005). Annihilation is an ionization channel unique to positrons, and it is open at all impact energies. The measurements of ion/γ-ray coincidences below the positronium formation threshold described in this chapter were motivated by the surprisingly high corresponding signal observed from Ne in the preliminary results of Szluinska and Laricchia (2004a). This observation might have been consistent with an enhancement in Q_{ann} in the vicinity of E_{Ps}. However, these authors proposed that a possible dependence of contaminants under gas load be tested with a helium target. The availability of elaborate calculations (Van Reeth *et al* 2005 and references there in) provide an additional incentive for striving to determine experimentally Q_{ann} for this target.

Positronium formation can occur with a threshold given by :

$$E_{Ps} = E_i - \frac{6.8\ eV}{n^2} \tag{3.5}$$

where E_i (24.5 eV for He) is the single ionization threshold, 6.8 eV is the binding energy of ground-state positronium and n its the principle quantum number. Prior to the work presented within this thesis, the convergence among measurements of the positronium formation cross-section (Q_{Ps}) were unsatisfactory, noticeably at energies above its peak. There are also differences among the theoretical results obtained using various methods and furthermore differences between theory and experiment.

Experimental methods employed to study Ps formation from He have exploited a number of different signatures:

a) 3 γ-ray coincidences (Charlton *et al* 1983): this is an almost unique signal of Ps formation but the method requires no loss of ortho-Ps, e.g. to quenching on the gas cell or change in detection efficiency as the relatively long-lived ortho-Ps moves out of the detection region. Indeed both effects are believed to have played a role in the measurements of Charlton *et al* (1983) except at the lowest energies (Charlton and Laricchia, 1990);

b) the loss of the positron in the final state (Fornari *et al* , 1983; Diana *et al* , 1986; Overton *et al* , 1993). This method relies on the collection of all the scattered particles and, by assuming negligible annihilation, ascribes the loss entirely to Ps formation;

c) measurement of all the ions and of the (e^+ - ion) coincidences. Once again, by assuming negligible annihilation, ions not accompanied by a positron in the final state are attributed to Ps formation (Fromme *et al* , 1986).

Method c, was also employed by Laricchia *et al* (2002) to determine Q_{Ps} for the heavier inert atoms and is now applied in the case of He. Using this method measurements of the total ionization cross-section to sufficiently high energies so that an absolute scale may be set by normalizing to corresponding electron-impact cross-sections ($Q_i^t(e^-)$) are required. In this way, $Q_i^t(e^+)$ is independent of other positron data and can be used to set an absolute scale on the ion yield. In the present work, measurements were performed at intermediate energies to supplement the low energy measurements of Moxom *et al* (1994) and those of Laricchia (1994) (unpublished). The recent electron-impact data of Sorokin *et al* (2004) and Rejoub *et al* (2002) have been combined and used for normalization. The direct ionization cross-section, of Moxom *et al* (1994) combined with the low energy detailed study

of Ashley *et al* (1996) have also been renormalized using these detailed electron measurements and used to determine Q_{Ps}.

3.2 Experimental Set-up

The experimental set-up described in chapter 2 has been used with the addition of a γ-ray detector placed on the opposite side of the ion detector outside of the vacuum system. The method used for the total ionization cross-section $Q_i^t(e^+)$ measures the total ion yield (Y_i) as a function of incident energy (E), defined as:

$$Y_i(E) = \frac{N_i - B_i}{N_+ - B_+} \tag{3.6}$$

where N_i and N_+ refer respectively to the time normalized ion and incident beam count rates (the latter corrected for the energy dependence of the channeltron detection efficiency, amounting to a maximum of 8 % at 700 eV) and $B_{i,+}$ represent the associated backgrounds measured by biasing the slow positron beam at R2 (see figure 2.4). Measurements have been performed, from the positronium formation threshold (E_{Ps}) up to 700 eV.

Below E_{Ps} the coincidence signal between γ-rays and ions was monitored. This, stripped of all background, is directly proportional to the annihilation cross-section. Above E_{Ps} the coincidence signal is proportional to the sum of annihilation and Ps formation cross-sections (Szluinska and Laricchia 2004a and Szluinska and Laricchia 2004b).

Ions of different charge-to-mass ratios were separated by their times-of-flight and a window was set on the time-to-amplitude converter (TAC) around the coincidence peak of the ion of interest (see figure 3.1 for an example of a non-windowed TOF spectrum). Unlike the system described in chapter 2, an external voltage ramp was

used and controlled by a multichannel scaler (MCS); the signal within the MCA window was fed to the MCS simultaneously to increments in the voltage applied to the moderator. Thus, the energy dependence of the signal for a particular ion could be determined across a range of energies in a single run.

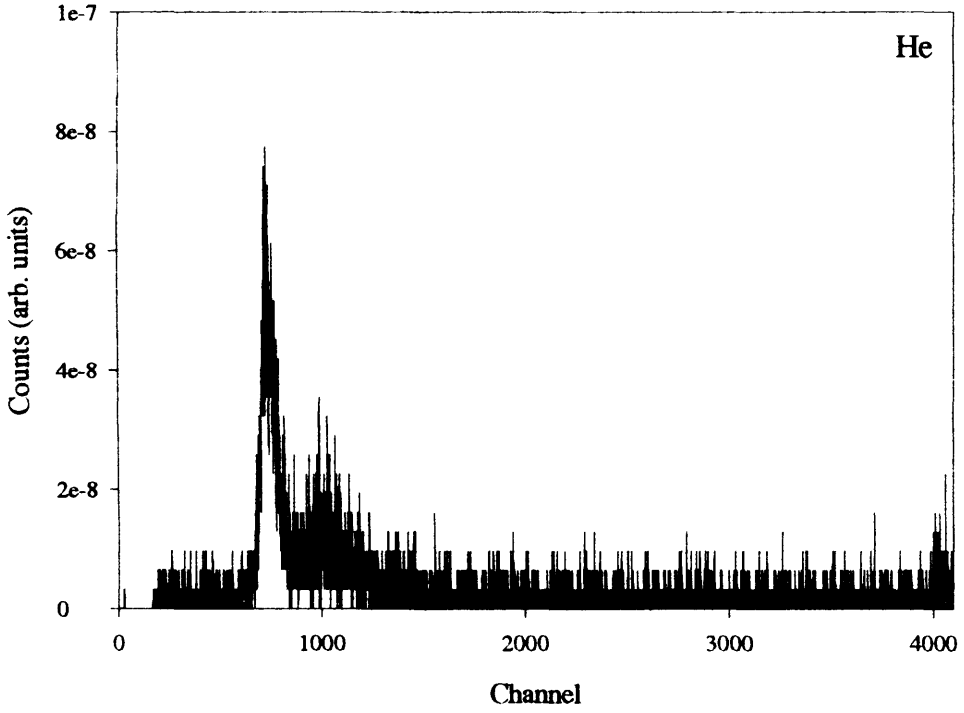

Fig. 3.1: Typical MCA spectrum from ion/γ-ray coincidences for He.

3.3 Systematic effects

As discussed by Szluinska and Laricchia (2004a), the measurement of Q_{ann} in particular poses a number of major difficulties arising from possible systematic effects. As the system was used without major modification, the findings of Szluinska and Laricchia (2004a) are still valid and their work is reviewed briefly below.

Firstly, due to the poor energy resolution of the beam ($\Delta E \sim 2\ eV$), close to E_{Ps} any signal from annihilation may be drowned out due to positronium formation. By

applying a retarding voltage to R1, the energy spread of the beam may be reduced albeit at the cost of a significant amount of beam intensity, (see figure 3.2). The

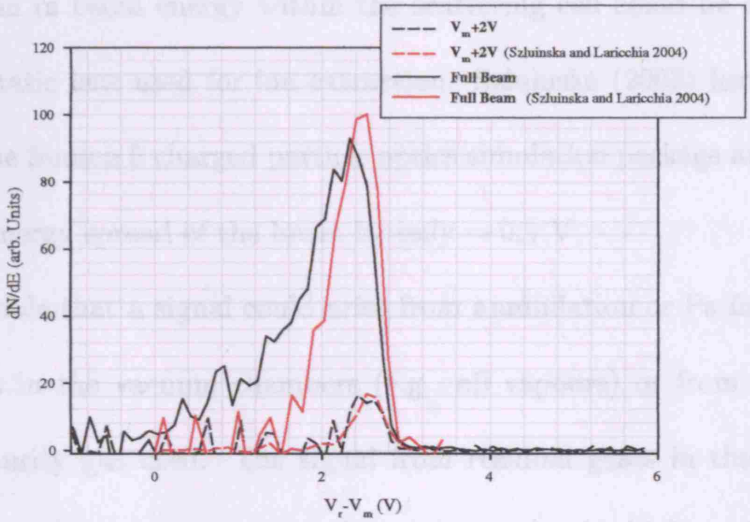

Fig. 3.2: Beam energy spreads.

energy spreads shown in figure 3.2 were measured by applying a voltage to a grid in front of the channeltron electron multiplier (CEM) used to measure the beam intensity (see figure 2.4). The energy spreads from Szluinska and Laricchia (2004a) are compared with those from the present study, as can be seen from figure 3.2 the energy spread with a full beam was somewhat larger during the present study probably due to a slight increase in spiralling. However, with a portion of the beam biased off ($V_m + 2$ V) the two energy spreads are comparable.

The absolute energy calibration of the beam was checked by Szluinska and Laricchia (2004a), using a time of flight technique. A grid in front of the moderator assembly was used to chop the beam, this was achieved by applying a voltage of $V_m + 3.5$ V to the grid. A rapid drop of 3V on the grid was triggered by a pulse generator for a period of $\sim 0.1\ \mu s$ every $7\ \mu s$. This pulse also acted as the start pulse on a TAC, the stop pulse arising from the positrons reaching the detector at the end of

the beamline. Using this timing data, the positron work function, corrected for any contact potential effects, was found to be $|\phi_+| = (2.4 \pm 0.3)$ eV.

A perturbation in beam energy within the scattering cell could be caused by the weak electrostatic lens used for ion extraction. Szluinska (2003) investigated this effect using the Simion 6 charged particle optics simulation package and found it to increase the energy spread of the beam by only ~ 0.1 V.

It is also possible that a signal could arise from annihilation or Ps formation from residual gases in the vacuum chambers (e.g. oil vapours) or from contaminants in the high purity gas used. The signal from residual gases in the vacuum was measured explicitly and subtracted. Contaminants in the high purity gases (e.g. 99.994 % Ne) have previously been estimated to be at least 2 orders of magnitude smaller than the target under consideration (Szluinska and Laricchia 2004a). However, due to the use of oil diffusion pumps, Szluinska and Laricchia (2004a) asserted the need to check the possible dependence of contaminants on the gas load. This task was undertaken in the present work.

As in Szluinska and Laricchia (2004a), the contribution from epithermal positrons was measured explicitly by applying ($V_m + 3$ V) to R1 both with a gas load and without. The net time normalized coincidence yield is given by

$$Y_{net} = Y_c^{gas} - Y_c^{vac} \tag{3.7}$$

where Y_c^{gas} and Y_c^{vac} are the measured coincidence yield in gas and vacuum respectively, and are given by :

$$Y_c^{vac}, Y_c^{gas} = \frac{N_c^{total} - N_c^{fast}}{N_{e^+}^{total} - N_{e^+}^{fast}} \tag{3.8}$$

where N_{c,e^+}^{total} refer to the time and pressure, where appropriate, normalized coincidence and positron count rate containing contributions from the slow positron beam

and epithermal positrons and N_{c,e^+}^{fast} refer to the time and pressure, again where appropriate, normalized coincidence and positron count rate containing contributions from only the epithermal positrons.

In the case of total ionization cross-section measurements, the number of systematic effects are greatly reduced. Many of the effects above still apply, for example an extra contribution from fast particles; however due to the difference in magnitude between Q_{ann} and Q_i^t they are less important but still must be considered.

One possible systematic effect could occur if the positron beam struck a wall of the gas cell creating secondary electrons which could cause further ions to be produced. If these ions were extracted then Q_i^t would be overestimated firstly due to the extra ions, and secondly due to an underestimation of the incident positron beam. The geometry of the cell combined with the ion extraction method should negate this effect; ions are only extracted from the central volume ($\sim$ 50 %) of the gas cell so that these ions should not be detected (Szluinska and Laricchia 2004a).

As hinted above, beam transport into the cell but not to the detector will lead to an overestimate of Q_i^t. This is countered by checking the configuration with a test target gas with a well known Q_i^t such as argon ($\sim$ 4 % difference between measurements) and by using a number of different beam transport optimizations.

3.4 Normalization Method

The net ion/γ-ray coincidences yield are normalized to Q_{Ps} above the positronium formation threshold. It has been shown that the energy dependence of Y_{net} for Xe and Ar agree very well with measured Q_{Ps} (Szluinska and Laricchia 2004b). The present Q_{Ps} in the case of He and in the case of Ne the Q_{Ps} of Laricchia *et al* (2002) have been used for normalization. The present results for He are $\sim$ 19 % lower than

published in Szluinska *et al* (2005) due to the renormalization of Q_i^t for He. New measurements of Q_i^t in the range (5-300 eV) have been used to combine earlier measurements taken with an alternative gas cell in sets of three overlapping energy ranges (0-40, 10-240 and 120-850 eV, see figure 3.3). The previous cell used concentric electrodes at its base to produce a radial electric field that was pulsed to extract ions with a high efficiency from all parts of the cell (Moxom *et al* 1995). Triggered by a 10kHz pulse generator, a (-180V) potential was applied to the extraction electrode for 5 μs. The positron beam was stopped, by grounding the plates of the Wien filter, in order to avoid perturbations on possible collisions during this time. Both types of measurements have been combined except in the near-threshold region where the high energy-resolution measurements of Moxom *et al* (1994) have been retained on their own.

Q_{Ps} is extracted using equation 3.4 by subtracting from the total ionization cross-

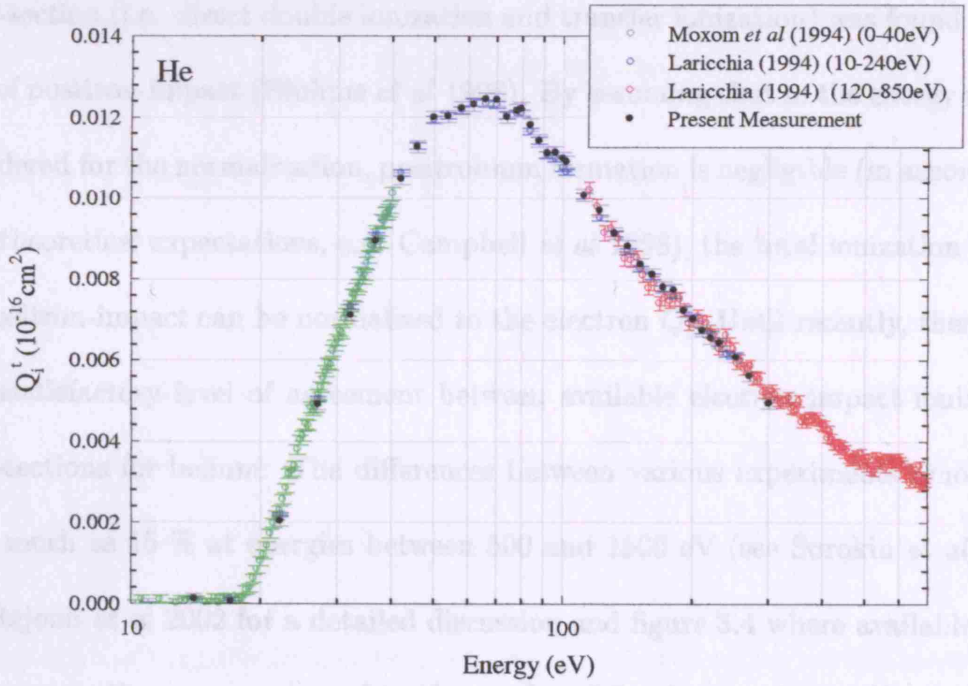

Fig. 3.3: Present results used to normalize earlier measurements of Q_i^t, shown separated.

section the direct ionization cross-section, the latter consisting of the combined data of Moxom *et al* (1996) and Ashley *et al* (1996) at low energy. Below the threshold for direct ionization (E_i) assuming Q_{ann} to be a negligible contribution, $Q_{Ps} = Q_i^t(e^+)$. Whenever no energy-matching datum were available, two neighbouring points of $Q_i^t(e^+)$ were used for interpolation. An absolute scale was set on Q_i^t and Q_i^+ by normalizing to corresponding electron data at high energies where the Born approximation predicts the merging of the direct ionization cross-sections for both projectiles. Hence by determining the region where Q_i^+ displays the same energy dependence for both projectiles, the yields may be normalized in that energy region to the absolute electron cross-sections. In the case of electron-impact ionization of helium, the main process contributing to $Q_i^t(e^-)$ is single ionization, with the double ionization process contributing less than 0.5% over the entire range (Shah *et al* 1988; Rejoub *et al* 2002). A similar contribution to the total double ionization cross-section (i.e. direct double ionization and transfer ionization) was found in the case of positron-impact (Bluhme *et al* 1998). By assuming that in the energy region considered for the normalization, positronium formation is negligible (in accordance with theoretical expectations, e.g. Campbell *et al* 1998), the total ionization yields for positron-impact can be normalized to the electron Q_i^t. Until recently, there was an unsatisfactory level of agreement between available electron impact-ionization cross-sections for helium. The differences between various experiments amounted to as much as 15 % at energies between 500 and 1500 eV (see Sorokin *et al* 2004 and Rejoub *et al* 2002 for a detailed discussion and figure 3.4 where available electron cross-sections are compared to the results of Sorokin *et al* (2004)). However, accurate and reliable experimental data are now available (Sorokin *et al* 2004 and Rejoub *et al* 2002) which are in excellent agreement (within 4%) both in energy

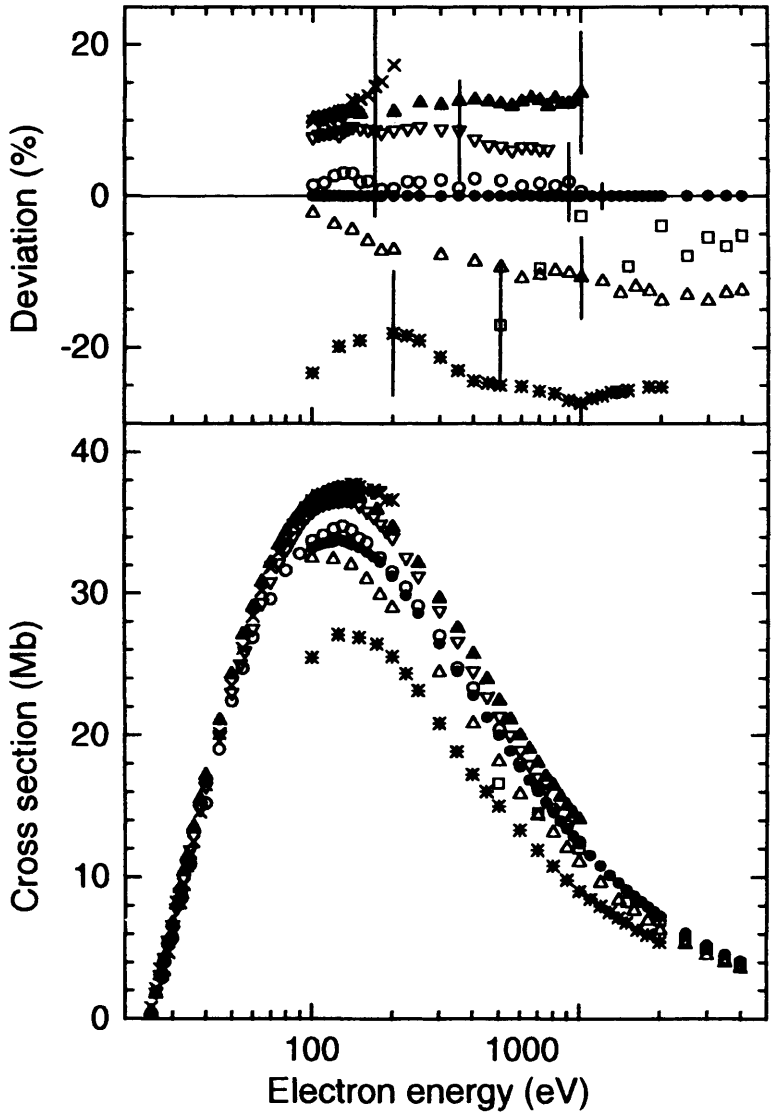

Fig. 3.4: From Sorokin *et al* (2004): Total electron-impact ionization cross-sections of He. •: Sorokin *et al* (2004), ○: Rejoub *et al* (2002), ×: Wetzel *et al* (1987), ▽: Montague *et al* (1984), □: Nagy *et al* (1980), ∗: Gaudin and Hagemann (1967), △: Schram *et al* (1965,1966), ▲: Rapp and Englander-Golden (1965). Upper plot shows the fractional deviation of experimental data from the measurements of Sorokin *et al* (2004).

dependence and magnitude over the high energy region used for normalization (see figure 3.4). In order to normalize the positron-impact data, a quadratic polynomial ($f^{-}(E)$) was fitted to the combined electron-data sets. The cross-sections for

positron-impact have then been normalized to the electron data by fitting $Q_i^t(e^+)$ and $Q_i^+(e^+)$, respectively, to $Q_i^{t,+}(e^+) = C^{t,+} f^-(E)$, where $C^{t,+}$ are normalization constants. The energy dependence of both projectiles is very similar for impact energies above 500 eV, hence the data could be normalized from 500 eV upwards. This is in agreement with the calculation of Moores (2001), which predicts the merging of $Q_i^t(e^+)$ and $Q_i^+(e^+)$ just above 400 eV. However, the normalization constants for the present data were found to be less sensitive to the form of $f^-(E)$ if the normalization is performed from 600 eV. The normalization constants, C^t and C^+, have been obtained by fitting $Q_i^t(e^+)$ from 600-850 eV and $Q_i^+(e^+)$ from 600-980 eV. In

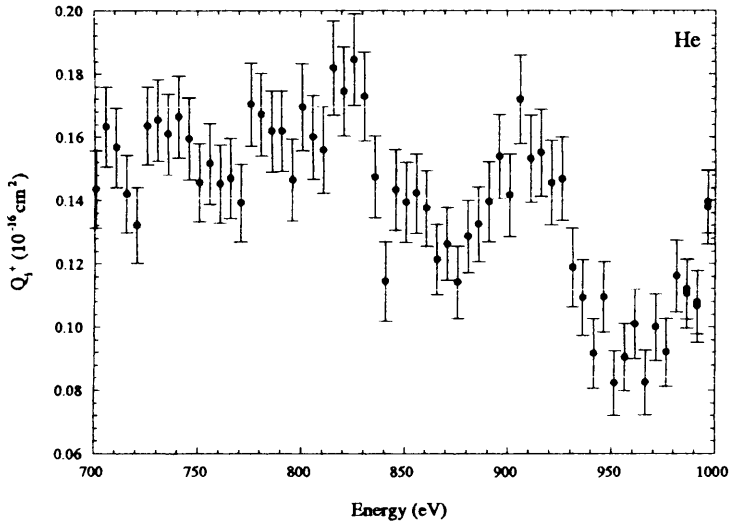

Fig. 3.5: Oscillations in Q_i^+ at high energy (700-1000 eV).

figure 3.5 $Q_i^+(e^+)$ can be seen to display a significant oscillatory behaviour, caused by the energy dependence of the beam transport (Moxom *et al* 1996) . Thus as per the method discussed in Van Reeth *et al* (2002), an integer number of oscillations were included in the normalization energy range. The uncertainties in C^t and C^+ are approximately 1 % and correspond to the range of possible values obtained by increasing the lower limit of the energy range over which the normalization is done

by 100 eV.

3.5 Results

In figure 3.6 and 3.7, the present results for Q_{ann} from He and Ne, respectively, are shown; the error bars combine the uncertainty on the weighted means of individual measurements, statistical errors and target pressure uncertainty. Figure 3.6 shows

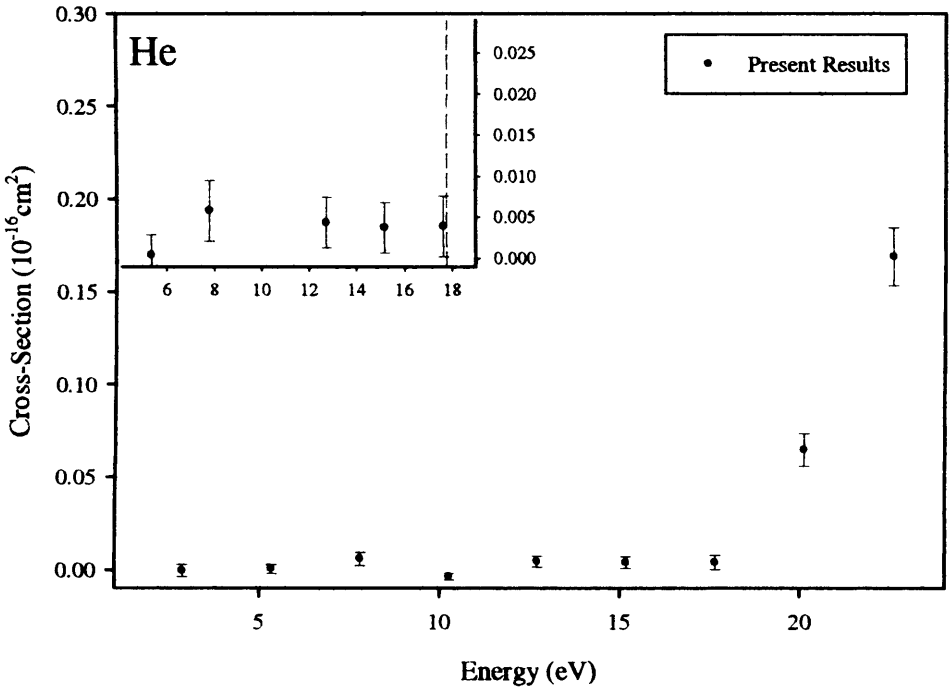

Fig. 3.6: Present results for $Q_{ann}(He)$.

the present results for Q_{ann} from He. A net positive signal is found below threshold (17.7 eV) with a maximum of $(5.77 \pm 3.66)^{-19}$ cm^2. In figure 3.7, the present measurements of Q_{ann} for Ne are shown compared with the previous results of Szluinska and Laricchia (2004a) with which there is an excellent agreement. These results peak at 12.7 eV (2 eV below E_{Ps}) with a magnitude of $(16.0 \pm 3.2) \times 10^{-19}$ cm^2.

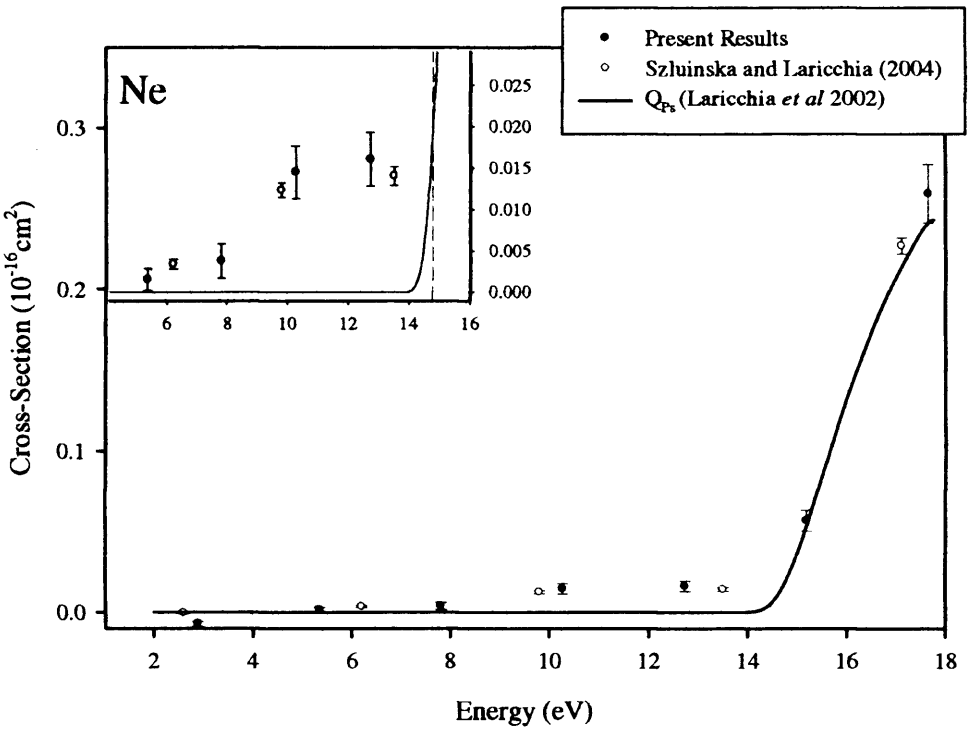

Fig. 3.7: Present results for $Q_{ann}(Ne)$.

In figure 3.8, the net coincidence signal below E_{Ps} measured in the MCA window corresponding to Ne^+ with Ne as the target gas is compared with that obtained with He as the target gas. The latter result suggests that there is a residual signal present in the region of the Ne peak in the absence of this gas. Further tests have been carried out by recording the full-range of the ion mass spectrum under a He gas load at a constant positron energy below E_{Ps} for Ne. These measurements have confirmed the presence of an unknown ion at a position which, within the mass resolution of the system (± 4 amu), cannot be distinguished from that of Ne^+. In light of this, the signal below E_{Ps} observed with Ne and reported in Szluinska and Laricchia (2004a) cannot be safely attributed to annihilation from this atom. Similarly, the non-zero average value of the signal below E_{Ps} measured in the case of He could arise from random coincidence signal from an increase of impurities from

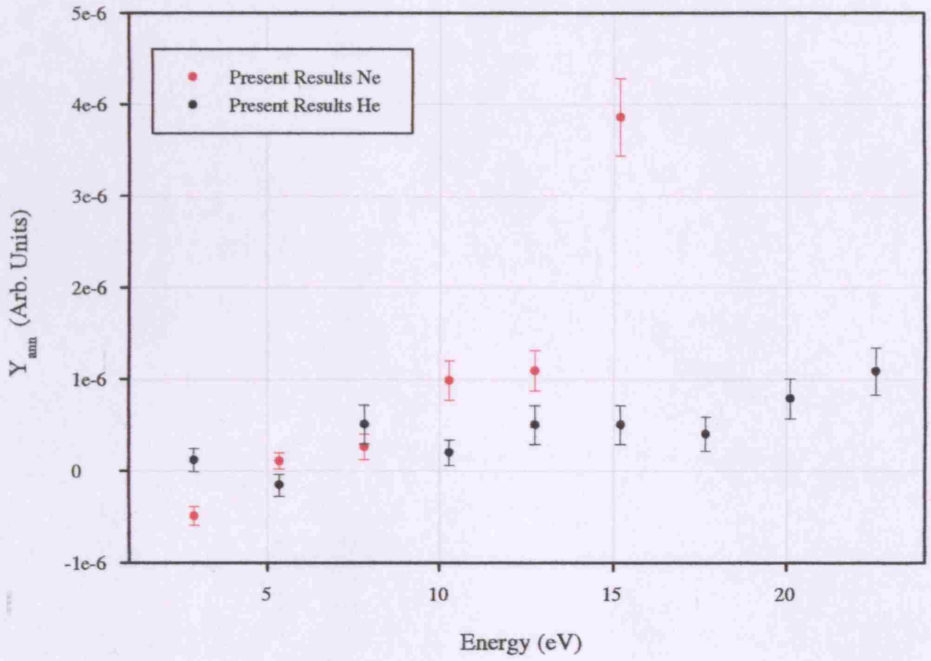

Fig. 3.8: The net coincidence yield measured in the MCA window set in the Ne^+ region with He and Ne as target gases.

the diffusion pumps under gas load. This value at $(2 \pm 1) \times 10^{-19}$ cm^2 sets a limit on the sensitivity of this experiment.

Figure 3.9 shows the present Q_i^t compared with the results of Fromme *et al* (1986). At low and very high energies there is a fair agreement. Above and in the region of the peak there are disagreements of ~ 15 %. In figure 3.10, the present results for Q_i^t are compared with the results of two close-coupling calculations. Good agreement is found at low energies with the results of Campbell *et al* (1998) that treat positronium formation explicitly but discrepancies are noted near the peak both in magnitude and shape. Compared to the convergent close coupling calculation of Wu *et al* (2004), there is a very poor agreement in shape and magnitude at low energies. This may be due to the theory of Wu *et al* not explicitly including positronium formation. However there is a good agreement on position and magnitude of

the peak.

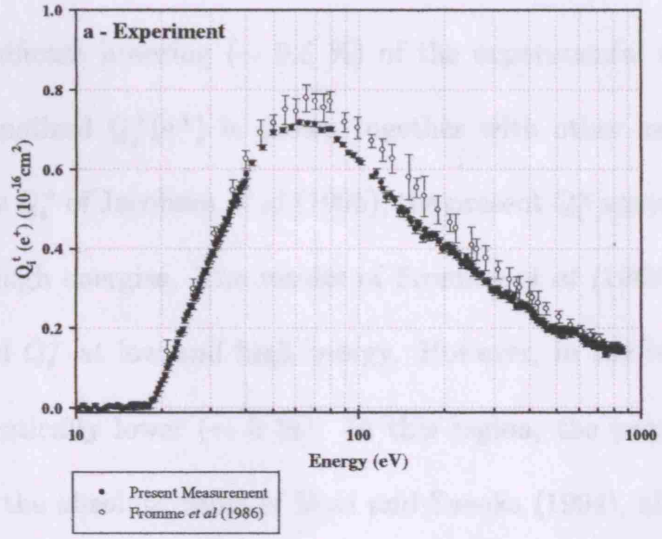

Fig. 3.9: $Q_i^t(e^+)$ for He compared with available experimental results.

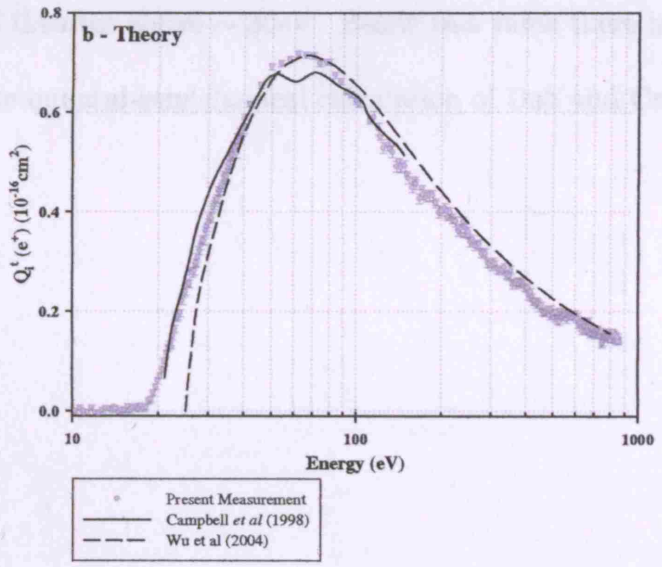

Fig. 3.10: $Q_i^t(e^+)$ for He compared with available theoretical calculations.

Renormalization of $Q_i^+(e^+)$, consisting of the combined data of Moxom *et al* (1996) and Ashley *et al* (1996) to Sorokin *et al* (2004) and Rejoub *et al* (2002), results in a significant lowering ($\sim$ 9.6 %) of the experimental results. In figure 3.11, the renormalized $Q_i^+(e^+)$ is shown together with other experimental data. Compared to the Q_i^+ of Jacobsen *et al* (1995), the present Q_i^+ agrees at low energies, but is lower at high energies. The results of Fromme *et al* (1986) are higher then the renormalized Q_i^+ at low and high energy. However, in the region of the peak they are systematically lower ($\sim$ 5 %). In this region, the present $Q_i^+(e^+)$ is in agreement with the absolute value of Mori and Sueoka (1994), although the latter has large uncertainties.

Figure 3.12 shows the renormalized Q_i^+ compared with various theoretical results. There is a good agreement with the coupled-pseudostate method of Campbell *et al* (1998) and at higher energies with the distorted Coulomb and plane-waves methods of Campeanu *et al* (1996). Near the threshold (shown in the inset), the present Q_i^+ is lower than all theories above $\sim 30eV$. Below this value there is good agreement with the absolute quantal-semiclassical calculation of Deb and Crothers (2002).

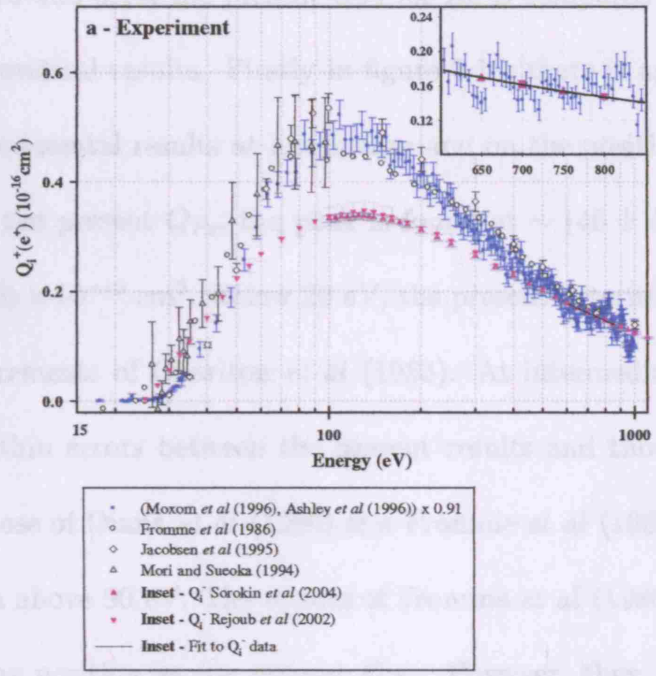

Fig. 3.11: $Q_i^+(e^+)$ for He compared with available experimental results.

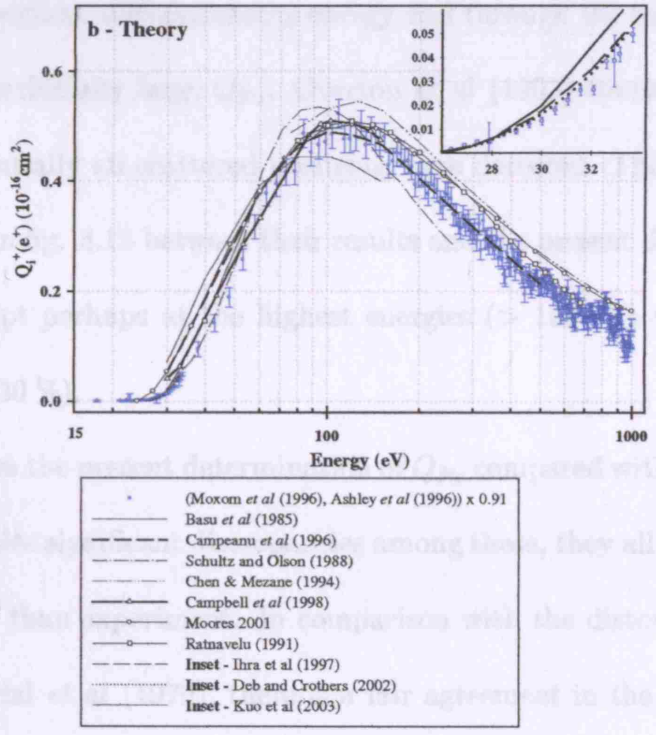

Fig. 3.12: $Q_i^+(e^+)$ for He compared with available theoretical calculations.

In figures 3.13 and 3.14, the present Q_{P_s} for He is compared with other experimental and theoretical results. Firstly in figure 3.13, there is agreement amongst most of the experimental results at low energy and on the position and magnitude of the peak. In the present Q_{P_s}, the peak is found at $\sim (46 \pm 4)$ eV with a value of $(0.484 \pm 0.020) \times 10^{-16}\ cm^2$. Below 20 eV, the present determination agrees well with the measurements of Charlton *et al* (1983). At intermediate energies, there is agreement within errors between the present results and those of Fornari *et al* (1983) whilst those of Diana *et al* (1986) and Fromme *et al* (1986) are higher than the present data above 90 eV. The results of Fromme *et al* (1986) peak in approximately the same position as the present Q_{P_s}. However, they are $\sim$ 10 % lower and decrease more slowly becoming negligable at $\sim 300\ eV$. The measurements of Overton *et al* (1993) were performed using method (b), described in section 3.1, with particular attention paid to possible loss of scattered positrons. This becomes particularly important with increasing energy and through the method used, would give rise to an artificially large Q_{P_s}. Overton *et al* (1993) concluded that in their experiment essentially all scattered positrons were detected. The very good agreement displayed in fig. 3.13 between their results and the present data supports their conclusion, except perhaps at the highest energies (> 150 eV) where the present data are lower (30 %).

Figure 3.14 shows the present determination of Q_{P_s} compared with various theoretical results. Despite significant discrepancies among these, they all peak at an energy $5 - 10$ eV lower than experiment. In comparison with the distorted wave approximation of Mandal *et al* (1979), there is a fair agreement in the magnitude of the peak. However, at energies below the peak there is a significant disagreement. The classical-trajectory-Monte-Carlo calculation of Schultz and Olson (1988) exceeds

the present data except at high energy where there is a good agreement. Below 30 eV, there is a good agreement with the close-coupling calculations of Campbell *et al* (1998) which also display a similar energy dependence to the present data above 70 eV. However, in the latter calculation the peak appears $\sim$ 5 eV earlier and is $\sim$ 10 % lower. There is a good agreement between 80 - 140 eV with the close-coupling calculation of Hewitt *et al* (1992). Below 80 eV, however, it is lower than the present result. The high-energy second-order Born results of Sarkar *et al* (1992) are higher than the present cross-section. Excellent agreement can be discerned between the present results and the high-energy target continuum distorted wave approach of Igarashi and Toshima (1992). In the inset, the present low energy Q_{Ps} is compared with the variational calculation of Van Reeth and Humberston (1999). Discrepancies of $\sim$ 20 % can be observed, however the stated uncertainty arising from the convergence of the theoretical calculations (Van Reeth and Humberston 1999) may account for up to 10 % of this deviation.

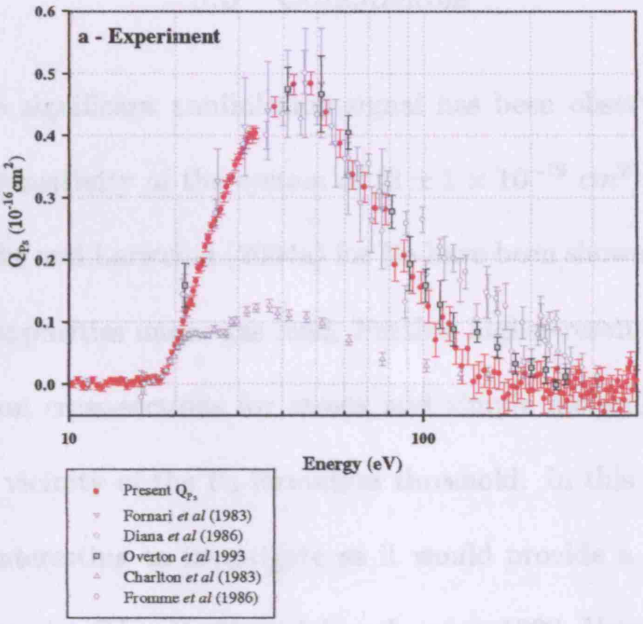

Fig. 3.13: Q_{Ps} for He compared with available experimental results.

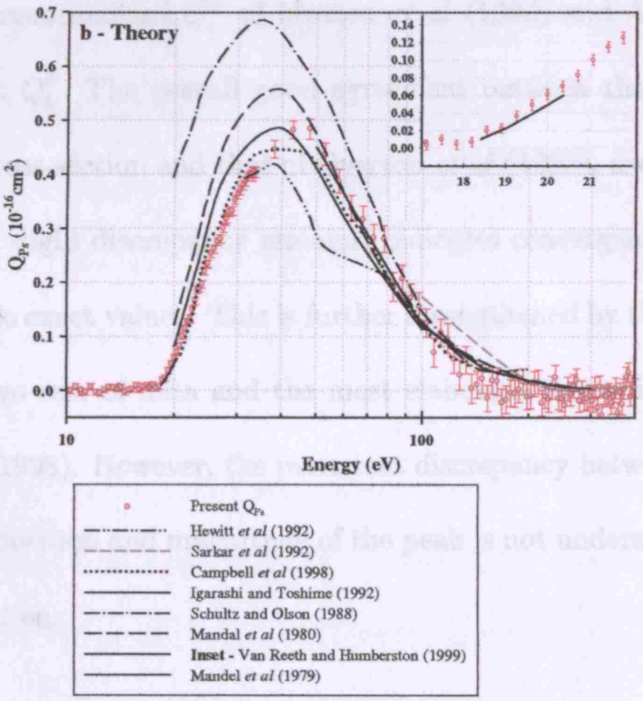

Fig. 3.14: Q_{Ps} for He compared with available theoretical calculations.

3.6 Conclusions

In conclusion, no significant annihilation signal has been observed in helium nor neon within the sensitivity of the system of ($2 \pm 1 \times 10^{-19}$ cm^2). The preliminary results of Szluinska and Laricchia (2004a) for Ne have been shown to be comparable to those due to impurities under gas load. Further higher-resolution investigations of the annihilation cross-sections for atoms and simple molecules are warranted, especially in the vicinity of the Ps formation threshold. In this respect, He would be particularly interesting to investigate as it would provide a direct comparison with available theories (Van Reeth and Humberston 1998, Varella *et al* 2001 and Biswas 2004). Detailed measurements of Q_i^t by positron impact from He have been extended to energies sufficiently high to enable an absolute scale to be obtained by normalization to new high-accuracy electron data. Q_{Ps} has been obtained by subtracting the renormalized Q_i^+ of Moxom *et al* (1996) and Ashley *et al* (1996) from the present Q_i^t. The overall good agreement between the present positronium formation cross-section and that of Overton *et al* (1993), except at the highest energies where a slight discrepancy remains, indicates convergence of experimental results toward the exact values. This is further strengthened by the good agreement between these two sets of data and the most elaborate theoretical calculations of Campbell *et al* (1998). However, the persistent discrepancy between theory and experiment in the position and magnitude of the peak is not understood and warrants further investigation.

4. EXCITED STATE POSITRONIUM FORMATION

4.1 Introduction

The search for excited state positronium (Ps*) spanned many years, as summarised in table 4.1, before the unambiguous observation by Canter *et al* (1975).

As discussed in detail in section 1.3.3, Canter *et al* (1975) bombarded a solid Ge target and monitored the 243 nm Lyman-α photon/γ-ray coincidences. The first observation of Ps* formation from a gaseous target was by Laricchia *et al* (1985), again using coincidences between Lyman-α photons and γ-rays. Laricchia *et al* were able to determine Ps* formation efficiencies for Ar, Ne and H_2 targets but unable to extract from these absolute Ps* formation cross-sections (Q_{Ps^*}).

In the present work, ion/de-excitation photon coincidences have been used to determine for the first time Q_{Ps^*} from He and Ar targets. Detecting the remnant ion, rather than the annihilation γ-ray, has a number of advantages. Firstly, the fraction of solid angle subtended by the ion detector is close to 2π as opposed to π by the NaI detector. Secondly, it avoids a number of well known systematic effects associated with the detection of γ-rays from Ps formation, for example, the positronium leaving the gas cell before annihilation (Charlton and Laricchia 1990) which would introduce an energy dependent detection efficiency as in the Q_{Ps} measurements of Charlton *et al* (1983).

As discussed in section 1.3.3 , Laricchia *et al* (2002) have hypothesised that struc-

Year	Author	Target	Result
1957	Hughes	SF_6 and freon	Estimated 1 in 30,000 e^+ captured into Ps*.
1958	Brock and Streib	gold foil	No significant signal observed.
1961	Bennett *et al*	Ne and Ar	less than 0.6 % of stopped e^+ gave Lyman-α.
1963	Duff and Heymann	inert gases	less than 1 in 100 e^+ gave Lyman-α.
1970	Fagg	SF_6	No significant signal observed.
1973	McCall *et al*	Ar, SF_6, N_2, CCL_2F_2 and Xe	Null result.
1974	Kielkoph and Ouseph	Ar	Statistically significant increase of signal with e^+ source.
1974	Dahm and Eck	Liquid He	less than 1 in 30,000 e^+ stopped yield Lyman-α.
1974	Varghese	Solid	Statistically significant signal.

Tab. 4.1: Summary of measurements before the unambiguous observation of Ps* by Canter *et al* (1975)

ture observed in the total positronium formation cross-section (all n) may be due to the formation of Ps*, deducing upper and lower limits to the possible contribution to Q_{Ps} from Ps*. The upper limit was determined by scaling the ground-state positronium-formation cross-section ($Q_{Ps}(n = 1)$) for helium of Campbell *et al*

(1998) to the first peak in the measured cross-section. This was accomplished using the scaling law reported by Szluinska *et al* (2002) which, in the case of scaling a He cross-section to another target, is given by:

$$\frac{Q_x^{He}\left(\frac{E}{E_{th}^{He}}\right)}{(Q_x^{He})_{max}} = \frac{Q_x^{B}\left(\frac{E}{E_{th}^{B}}\right)}{(Q_x^{B})_{max}} \tag{4.1}$$

Here, x refers to a particular process (e.g. positronium formation), B denotes a given atom, E is the incident projectile energy and $(Q_x^B)_{max}$ the maximum value of Q_x^B. Figure 4.1 shows the cross-sections for positronium formation into the 1S, 2S and 2P states for H and He, calculated by Kernoghan *et al* (1996) and Campbell *et al* (1998) respectively, and scaled using equation 4.1. Where data did not extend

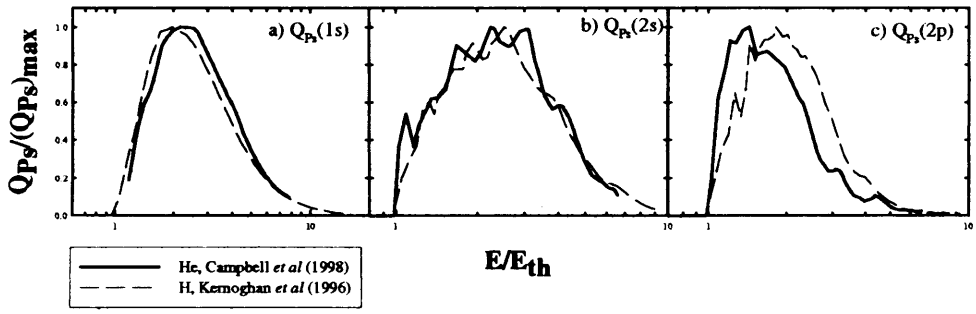

Fig. 4.1: Ps formation cross-sections for H and He as scaled by Szluinska *et al* (2002).

to high enough energies, Laricchia *et al* extrapolated the tail of the cross-section using an exponential decay curve. The rescaled $Q_{Ps}(n = 1)$ was then subtracted from the total (all n) measured Q_{Ps} giving the upper limit contribution.

Lower limits were set by extrapolating the high energy tail from the decrease in the first peak observed in the experimental data, using an exponential decay function. The extrapolated high energy tail was then reduced by 30 %, as in the case for the high energy contribution from excited state positronium formation from He, as calculated by Campbell *et al* (1998). The ensuing estimates are shown in figure

4.2. Here it may be noted that, as the sequence of noble gases is ascended from Ne to Xe the contribution to Q_{Ps} from excited state positronium was deduced to increase, similarly to the theoretical results of Campbell *et al* (1998) for the alkali metals.

Motivated by the above study, the present work set out to measure explicitly the

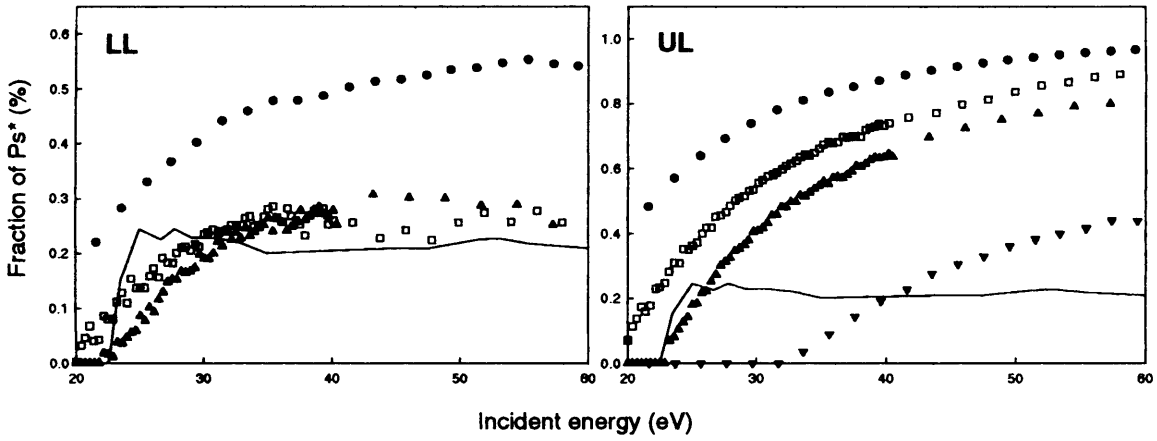

Fig. 4.2: From Laricchia *et al* (2002): Lower (LL) and upper limit (UL) estimates of the energy dependence of the relative contributions from excited state positronium (Ps*) to the total positronium formation cross-section • - Xe; □ - Kr; ▲ - Ar; ▼ - Ne; solid curve - theoretical results for He of Campbell *et al* (1998).

excited state positronium formation cross-section for He and Ar, to have a direct comparison with available theories (Campbell *et al* 1998, Gilmore *et al* 2004) and to test the hypothesis that the structure observed in Q_{Ps} could be a manifestation of excited state positronium formation.

4.2 Experimental method

The apparatus, described in chapter 2, was used with minor modifications during this study. A photomultiplier tube (PMT), Electron Tubes QB9829, was mounted on an extension arm opposite the ion detector. The PMT has a sensitivity between

200 $nm \leq \lambda \leq$ 600 nm (6.2 $eV \leq E \leq$ 2.0 eV) and figure 4.3 shows the quantum efficiency for the PMT as supplied by the manufacturers. The PMT is mounted on

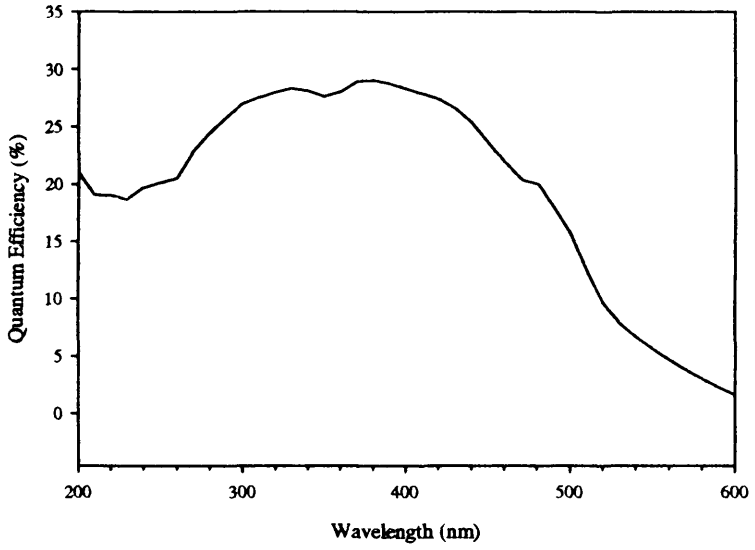

Fig. 4.3: Quantum Efficiency of the PMT.

the extension arm to remove it from the guiding magnetic field and hence, reduce the effect of the field on the gain of this detector. The extension arm is lined with UV reflectors made of glass tubes coated with Al, with an outer layer of MgF_2 to stop oxidization of the Al. The gas cell is hemispherical and constructed from polished Al to improve photon collection (at $\lambda <$ 280 nm Al has a reflectivity of $\sim$ 90 %). The PMT is chilled using a water cooled jacket in thermal contact with the PMT vacuum housing to reduce the dark counts on this detector. A borosilicate glass disk is inserted in front of the PMT to reduce its sensitivity range to 280 $nm \leq \lambda \leq$ 600 nm (4.4 $eV \leq E \leq$ 2.0 eV). In this study, the ion-photon coincidence yield (Y_{Ps^*}) has been measured with and without the borosilicate glass filter in front of the PMT. The difference between the two measurements thus arise from photons with wavelengths within an effective sensitivity range of (200 nm -

280 nm).

The structure of positronium is shown in figure 1.2, the Lyman-α photon arises from the $2P \rightarrow 1S$ transition ($\Delta l = 1$, $\Delta m = 0, \pm 1$). The transition from the 2S state to 1S state is forbidden ($\Delta l = 0$, $\Delta m = 0$) and the $2S \rightarrow 2P$ transition has a very long lifetime due to the small energy difference between the two states (Bethe and Salpeter 1957). Hence, the 2S state is metastable with a lifetime of 1ns and 1100ns against annihilation in its singlet and triplet states, respectively, although decay to the 1S state may be induced by an external perturbation e.g. an electric field. Therefore, the present measurement of the coincidence yield (Y_{Ps^*}), which should be considered as comprising of all the Ps(2P), a fraction of the Ps(2S) and some Ps formed with $n > 2$, is directly proportional to

$$Q_{Ps^*} = Q_{Ps}(2P) + xQ_{Ps}(2S) + yQ_{Ps}(n > 2) \tag{4.2}$$

where x is the fraction of perturbed $Ps(2S)$ which decays by emitting a Lyman-α photon and y the fraction of $Ps(n > 2)$ which decays (by cascade or directly) to the ground state via the emission of a photon with a wavelength within the effective range of the PMT.

Y_{Ps^*} has been measured simultaneously to the total ion yield (Y_i), in turn given by :

$$Y_i(E) = \frac{N_i - B_i}{N_+ - B_+} \tag{4.3}$$

where N_i and N_+ refer respectively to the ion and incident beam rates and $B_{i,+}$ represent the associated backgrounds measured by biasing off the slow portion of the beam. Y_i is directly proportional to Q_i^t given by :

$$Q_i^t = \frac{1}{nl_{eff}} \frac{\epsilon_+}{\epsilon_i} Y_i \tag{4.4}$$

where n is the number density of the target, l_{eff} is the effective length of the cell from which ions can be extracted, ϵ_+ is the positron detection efficiency and ϵ_i that of ions.

The yield of Ps* (Y_{Ps^*}) is hence given by :

$$Y_{Ps^*} = \frac{N_c - N_f}{N_+ - B_+} \tag{4.5}$$

where N_c is the total coincidence rate and N_f that with the borosilicate filter inserted. Figure 4.4 shows the present results for He and Ar.

The cross-section for the formation of excited state positronium, Q_{Ps^*} is then

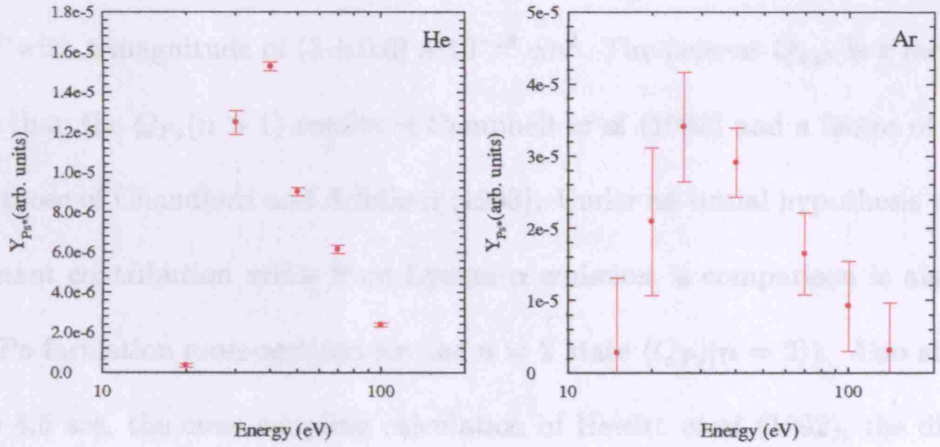

Fig. 4.4: Present measurements of Y_{Ps^*} for He and Ar.

determined from :

$$Q_{Ps^*}(E) = \left(\frac{Q_i^t}{Y_i}\right)\left(\frac{1}{C_r}\frac{4\pi}{\Delta\Omega}\right)\left(\frac{1}{\epsilon_{PMT}}\right) Y_{Ps^*}(E) \tag{4.6}$$

the first term $Q_i^t/Y_i = (1/nl_{eff})\,(\epsilon_+/\epsilon_i)$ corrects for the target areal density (nl_{eff}) and the detection efficiencies for ions (ϵ_i) and positrons (ϵ_+). $C_R = (2.12 \pm 0.58)$ is the correction applied due to the photon collection enhancement from the UV reflectors, determined by performing measurements without the light guides and with the cell coated with graphite. $\Delta\Omega/4\pi = 0.0164/4\pi$ is the fractional solid angle

subtended by the PMT, ϵ_{PMT} is the quantum efficiency of the PMT ((20 ± 2) % at $\leq$240 nm) as provided by Electron Tubes.

4.3 Results

The present results for Q_{Ps^*} from He are shown in figure 4.5 compared with the coupled state calculation of Campbell *et al* (1998) and the close coupling calculation of Chaudhuri and Adhikari (1998) for Ps formation into states with $n > 1$ (denoted by $Q_{Ps}(n > 1)$). The measurements extend from 20 eV to 100 eV peaking around 40 eV with a magnitude of $(3 \pm 0.6) \times 10^{-18}$ cm^2. The present Q_{Ps^*} is a factor of 3 lower than the $Q_{Ps}(n > 1)$ results of Campbell *et al* (1998) and a factor of 5 lower than those of Chaudhuri and Adhikari (1998). Under an initial hypothesis that the dominant contribution arises from Lyman-α emission, a comparison is also made with Ps formation cross-sections for the $n = 2$ state ($Q_{Ps}(n = 2)$). Also shown in figure 4.5 are, the close coupling calculation of Hewitt *et al* (1992), the distorted wave model of Khan *et al* (1985), and the second Born approximation of Sarkar *et al* (1992) results for $Q_{Ps}(n = 2)$. In comparison with the theoretical results for $Q_{Ps}(n = 2)$, the present Q_{Ps^*} is a factor of 1.5 to 3 times lower than theory, although there is some agreement in shape.

Figure 4.6 shows the present results for Q_{Ps^*} from Ar, where they are compared with the only available theory, namely, the distorted wave Born approximation of Gilmore *et al* (2004) for $Q_{Ps}(n > 1)$, as well as the upper and lower limit estimates of Laricchia *et al* (2002). The current results extend from threshold to 140 eV peaking at around 40 eV with a magnitude of $(2.1 \pm 0.3) \times 10^{-17}$ cm^2. Agreement between measurement and theory is poor but improves with increasing energy. The lower

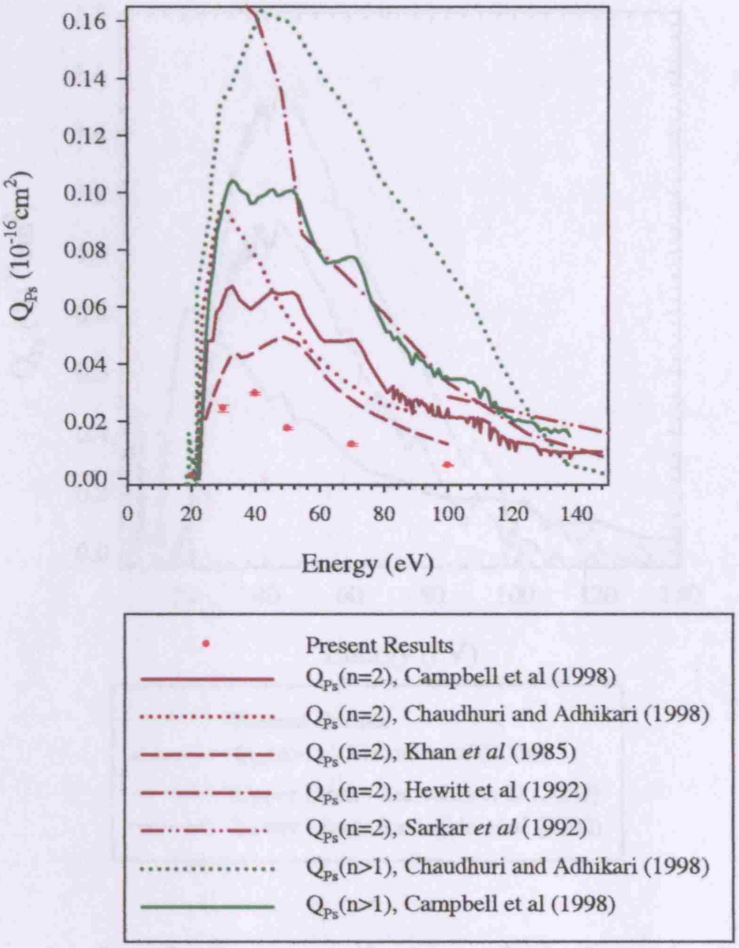

Fig. 4.5: The present Q_{Ps^*} for He compared with available theory for $Q_{Ps}(n > 1$ and $Q_{Ps}(n = 2)$

and upper limit estimates peak at approximately the same energy as the present measurements, however they are a factor of 3 and 5 times larger, respectively.

The fact that the present results for Q_{Ps^*} are lower than available theories for $Q_{Ps}(n > 1)$ and $Q_{Ps}(n = 2)$ for both Ar and He, may be due to the fraction of Ps($n > 2$) or Ps(2S) undetected in the present experiment. This is considered in the following sub-sections.

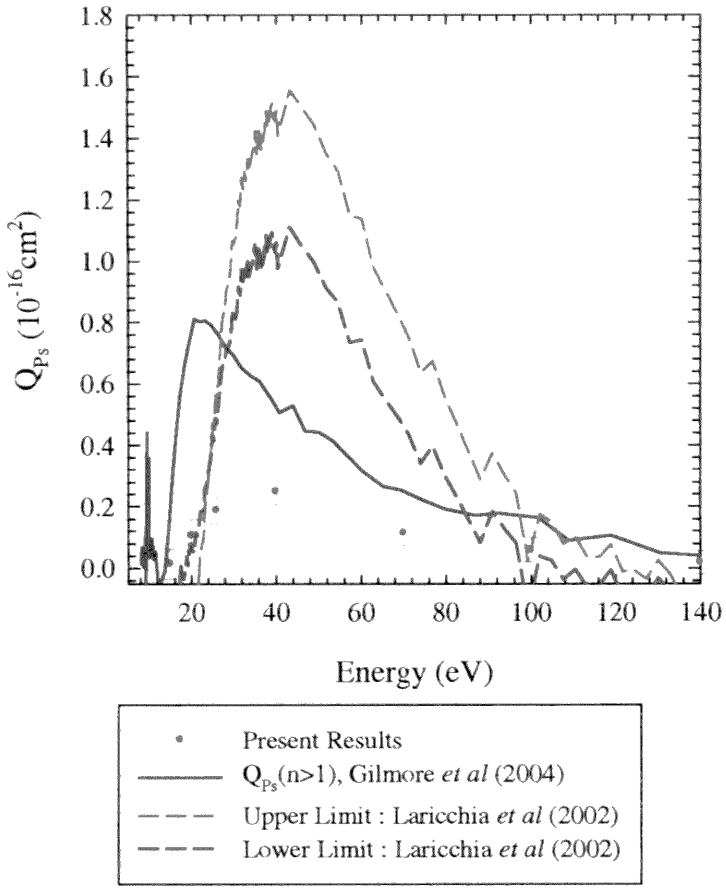

Fig. 4.6: The present Q_{Ps^*} for Ar compared with available theory for $Q_{Ps}(n > 1)$ and the lower and upper limits estimated in Laricchia *et al* (2002).

4.3.1 Detection of Ps(2S)

The channels for the decay of Ps(2S) yielding a Lyman-α photon together with their associated cross-sections are listed below:

- Spontaneous Transitions :

$$Ps(2S) \rightarrow Ps(2P) \rightarrow Ps(1S) + Ly - \alpha \tag{4.7}$$

- Collisional de-excitation ($Q_{Ps}^{2S,1S}$):

$$Ps(2S) + A \rightarrow Ps(2P) + A \rightarrow Ps(1S) + A + Ly - \alpha \tag{4.8}$$

- State mixing due to the Stark effect, motional Stark or Zeeman effects:

$$\langle Ps(2P)\,|H_S|\,Ps(2S)\rangle > 0 \tag{4.9}$$

$$\langle Ps(2^1S_0)\,|H_Z|\,Ps(2^3S_1)\rangle > 0 \tag{4.10}$$

Spontaneous Transitions

The lifetime of the $Ps(2^3S)$ state against spontaneous emission is many orders of magnitude larger than its lifetime against annihilation. Burdyuzha and Kauts (1997) calculate rates of $5.71 \times 10^{-6}s^{-1}$, $5.96 \times 10^{-6}s^{-1}$ and $2.89 \times 10^{-6}s^{-1}$ for the $2^3S \rightarrow 2^3P_0$, 2^3P_1 and 2^3P_2 transitions respectively. Therefore, the spontaneous transition from the 2^3S state to the 2^3P state may be neglected. The lifetime of the 2^1S state is only 1 ns against annihilation and has a lower energy than the 2^1P state and hence plays no role.

Collisional de-excitation

Collisional de-excitation (reaction 4.8) can occur if the Ps(2S) collides with the target after production. The cross-section for collisional de-excitation via the intermediary 2P state ($Q_{Ps}^{2S.2P}$) has recently been calculated by Starrett *et al* (2007). Using this, it has been estimated (see appendix A) that of the Ps(2S) which collides in the cell (see figure A.4) approximately 0.3 % may de-excite via the 2P state and hence be detected. Measurements of the coincidence yield as a function of target density have also been found to scale linearly, confirming that the contribution to the present yield from collisional de-excitation is small.

The Stark and Zeeman effect

The Stark effect occurs in the presence of an electric field, which mixes the 2S and 2P states ($\Delta m = \pm 1$) of positronium. This mixing leads to the 2S state acquiring a 2P like character, resulting in a reduction of its lifetime against spontaneous transition. For the present experimental set up, two sources of electric fields need to be considered, namely that from the electrostatic lens used for ion extraction and that arising from the Lorentz transformation of the guiding magnetic field, known as the motional Stark effect. This is a relativistic effect arising from the positronium velocity component transverse to the field (see appendix B).

Of the 4 sub-states of Ps(2S) ($^1S_0(m_J = 0)$, $^3S_1(m_J = 0, \pm 1)$) only the $^3S_1(m_J = \pm 1)$ states are mixed with the $^3P_2(m_J = \pm 2)$ (Curry 1973). The $^1S_0(0)$ and the $^3S_1(0)$ state are susceptible to the Zeeman effect which mixes the triplet and singlet state. As reviewed by Consolati (1996), this mixing has been the subject of many investigations. The lifetime of a mixed triplet and singlet state in a magnetic field is given by :

$$\lambda_3' = \frac{\lambda_3 + y^2\lambda_0}{1 + y^2} \tag{4.11}$$

where λ_3 and λ_0 are the intrinsic ortho-Ps and para-Ps decay rates at zero field and

$$y = \frac{\sqrt{1 + x^2} - 1}{x} \tag{4.12}$$

where x is given by :

$$x = \frac{4\mu_B B}{\Delta W} \tag{4.13}$$

where μ_B is the Bohr magneton, B the applied field and ΔW the energy separation between the triplet and singlet states (25,423 MHz in this case). Thus, in a 100 G field the lifetime of the triplet state is shortened from 1100 ns to 970 ns which is a negligible change when compared with the time Ps(2S) spends in the cell (see

appendix A).

Using the calculation of Curry (1973) for the lifetime of the $^3S_1(\pm 1)$ state in an electric field, an estimate has been made of the contribution from Ps(2S) in the present results due to Stark mixing of the 2S and 2P states and found to have an upper limit of $\sim$ 1 %.

Taking into consideration collisional de-excitation to the 2P state and the motional Stark effect, the present results may contain up to $\sim$ 1% of the Ps(2S) which is formed. The other 99 % may go on to fragment or collisionally de-excite without Lyman-α emission.

4.3.2 Detection of $Ps(n > 2)$

The lifetimes and fluorescence branching ratios for Ps($n \leq 4, l$), are shown in figure 4.7, the former obtained by scaling corresponding H data (e.g. Bozek *et al* 2006) by the Ps reduced mass. The present measurement is sensitive to the $n = 3P \rightarrow 1S$ transition as well as cascades to the ground-state via the 2P state.

Based upon experimental and theoretical results for H($n > 2$) scattering (Edwards and Thomas 1970, Bates and Walker 1966), it may be conjectured that the fragmentation probability upon collision of Ps($n > 2$) is unity. By scaling the total cross-section ($n > 2$) as outlined in appendix A, the time between collisions may be calculated for the present experimental conditions. Considering the $n = 4$ states first, the time between collisions is found to be $\sim$ 1 ns. Given the lifetime of 72 ns from the $4D \rightarrow 2P$ transition, which is expected to make the largest possible contribution to our signal, the probability of detecting a $4D \rightarrow 2P$ transition is $\sim$ 1%. Considering the Ps($n = 3$) states, the inter-collisional time is $\sim$ 3ns whilst the lifetimes are shorter than the $n = 4$ states, as indicted in figure 4.7. Thus the prob-

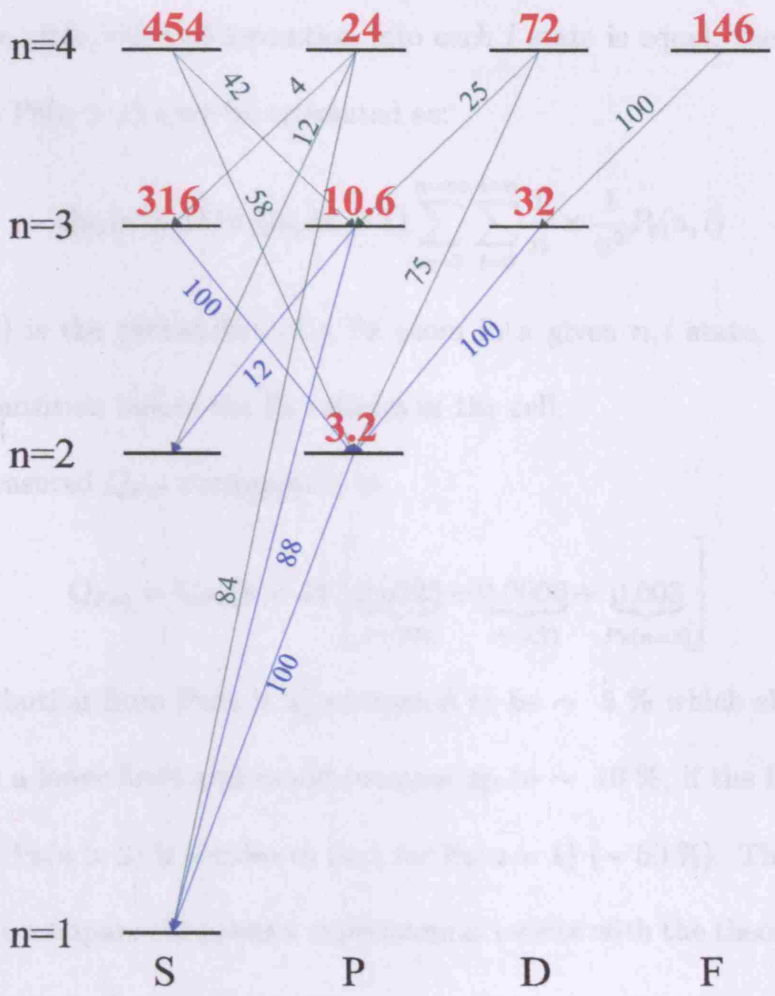

Fig. 4.7: Partial Grotarian diagram of Ps showing state lifetimes (ns) indicated in red and branching ratios (%) (Bozek *et al* 2006) for $n = 4$ transitions shown in green, and $n = 3$ transitions and Lyman-α transition shown in blue.

ability of detecting the $3P \rightarrow 1S$ and $3D \rightarrow 2P$ transitions are ~ 24 % and ~ 9 %, respectively; whereas that for $3S \rightarrow 2P$ is negligible due to the longer lifetime of Ps($3S$) (316 ns).

The formation probability of Ps into states $n > 1$, may be estimated by using the $1/n^3$ scaling for $Q_{Ps}(n > 1)$ (e.g. Campbell *et al* 1998, Kernoghan *et al* 1996):

$$Q_{Ps}(n > 1) \approx Q_{Ps}(n = 1) \sum_{n=2}^{\infty} \frac{1}{n^3} \tag{4.14}$$

Assuming the probability of formation into each l state is equal, the contribution to Q_{Ps^*} from Ps($n > 1$) may be estimated as:

$$Q_{Ps}(n > 1) \approx Q_{Ps}(n = 1) \sum_{n=2}^{n=\infty} \sum_{l=0}^{l=n} \frac{1}{n} \times \frac{1}{n^3} P_t(n, l) \tag{4.15}$$

where $P_t(n, l)$ is the probability of a Ps atom in a given n, l state, undergoing a detectable transition before the Ps collides in the cell.

Thus, the measured Q_{Ps^*} corresponds to

$$Q_{Ps^*} = Q_{Ps}(n = 1) \left[\underbrace{0.0625}_{Ps(2P)} + \underbrace{0.0006}_{Ps(2S)} + \underbrace{0.003}_{Ps(n=3)} \right] \tag{4.16}$$

with a contribution from Ps($n > 2$) estimated to be $\sim$ 5 % which should be considered to be a lower limit and would increase up to $\sim$ 10 %, if the fragmentation probabilty of Ps($n > 2$) is similar to that for Ps($n = 1$) ($\sim$ 50 %). Thus, it is more appropriate to compare the present experimental results with the theoretical results for $Q_{Ps}(2P)$ as it is done in figure 4.8.

Available theories for $Q_{Ps}(2P)$ exhibit a similar energy dependence to one another, all peaking at $\sim$ 35 eV then decreasing rapidly at high energy (> 50 eV), however there are sizeable discrepancies in absolute magnitude. It is noted here that if the results of Campbell *et al* (1998) were shifted by 5 eV, a considerably better agreement in both magnitude and energy dependence would be achieved with present results. A similar energy shift was observed in the case of the total (all n) Ps formation cross section for which a great deal of independent experimental data are available (see chapter 3 figure 3.14). The close coupling approximation calculations of Chaudhuri and Adhikari (1998) and Hewitt *et al* (1991) are respectively a factor of 2 and 3 higher in magnitude at their peak.

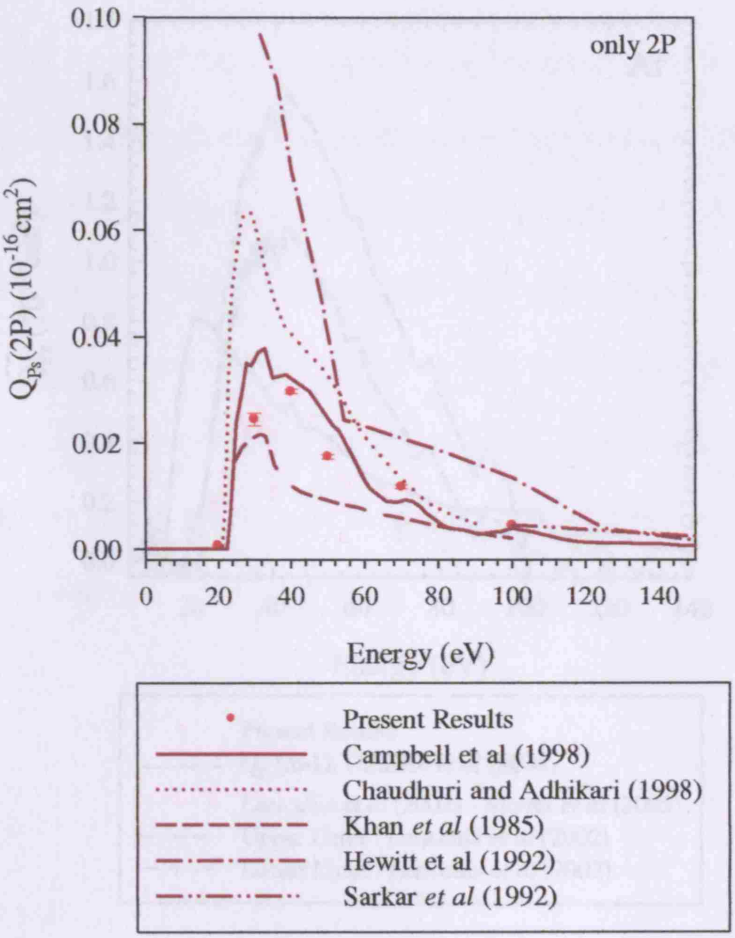

Fig. 4.8: The present $Q_{Ps}(2P)$ for He compared with available theory for 2P state Ps formation cross-sections ($Q_{Ps}(2P)$).

4.4 Conclusions

Results have been presented for the excited state positronium formation cross-section (Q_{Ps^*}) from He and Ar. In the case of He, the present Q_{Ps^*}, comprising of predominantly $Q_{Ps}(2P)$ and ~5 % of $Q_{Ps}(n > 2)$, is close to the coupled state calculation of Campbell *et al* (1998) for $Q_{Ps}(2P)$.

The magnitude and peak of the cross-sections appear to account for some of the structure observed by Laricchia *et al* (2002), as shown in figure 4.9, where the present results are compared with the upper and lower limit estimates for the excited

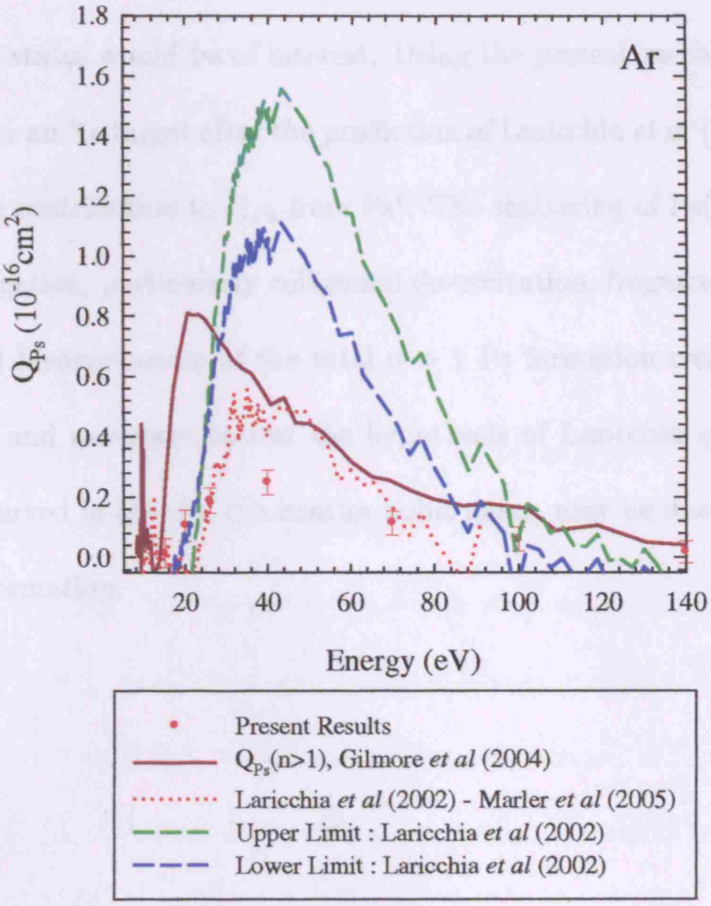

Fig. 4.9: Comparison of the present Q_{Ps^*} with the theory of Gilmore *et al* (2004), the upper and lower limits estimated in Laricchia *et al* (2002) and the difference between Q_{Ps} of Laricchia *et al* (2002) and Q_{Ps} Marler *et al* (2005).

state positronium formation cross-section. Although the lower limit has a magnitude 3 times and the upper limit 5 times higher than the present measurement, they do appear to peak at around the same energy. The origin of the discrepancy between the detailed studies of Laricchia *et al* (2002) and Marler *et al* (2005), see figure 4.9, is still open to speculation. However if Ps($n > 1$) were responsible for the observed difference, then the cross-section for fragmentation of Ps($n > 1$) could be important as this process could lead to an under-estimate of Q_{Ps} using the method of Marler *et al* (2005).

Further theoretical and experimental determinations of positronium formation into the 2S and 2P states would be of interest. Using the present method, Q_{Ps^*} should be measured for an Xe target after the prediction of Laricchia *et al* (2002) that there may be a large contribution to Q_{Ps} from Ps*. The scattering of Ps($n > 1$) warrants further investigation, particularly collisional de-excitation, fragmentation and total cross-sections. Measurements of the total $n > 1$ Ps formation cross-section would be interesting and necessary to test the hypothesis of Laricchia *et al* (2002) that structures observed in Q_{Ps} for the heavier noble gases, may be due to excited state positronium formation.

5. CONCLUSIONS AND SUGGESTIONS FOR FURTHER WORK

In this work, a mono-energetic positron beam obtained from a radioactive source (^{22}Na), in conjunction with annealed tungsten mesh moderators, and guided by a magnetic field was used to investigate a number of processes associated with ionization by low energy positron impact: annihilation, positronium formation and direct ionization. Specifically, measurements were conducted of the total ionization cross-section (Q_i^t) for He and the excited state positronium formation cross-section (Q_{Ps^*}) for He and Ar.

An attempt was made to measure the annihilation cross-section (Q_{ann}) below the positronium formation threshold (E_{Ps}) in He and Ne. This measurement, performed using ion / γ-ray coincidences, demonstrated an increase of vacuum contaminants under gas load and, within the present experimental sensitivity of the system ($2 \pm 1 \times 10^{-19}$ cm^2), no signal was observable above background. Measurements of the total ionization cross-section have been performed in He and used in conjunction with previously measured high resolution data for Q_i^t. This measurement, along with the direct ionization cross-section data of Moxom *et al* (1996) combined with the low energy measurements of Ashley *et al* (1996), has been normalized at high energy to the combined electron impact ionization data of Sorokin *et al* (2004) and Rejoub *et al* (2002). The positronium formation cross-section (Q_{Ps})

was thus determined by subtracting Q_i^+ from Q_i^t. There is now a good agreement between the present determination of Q_{Ps} and the most recent measurement by Overton *et al* (1993), except at the highest energies. There is a fair agreement with the coupled state approximation of Campbell *et al* (1998). However, the position of the peak in the latter appears shifted to lower energies, with respect to the experimental measurements, by approximately 5 eV.

Measurements of the excited-state positronium formation cross-section Q_{Ps^*} for He and Ar have been performed using ion / de-exciation photon coincidences. These measurements have been found to account predominantly for positronium formation into the 2P state. This study was motivated by the hypothesis of Laricchia *et al* (2002) that structure observed in $Q_{Ps}(all\ n)$ may be due to excited state positronium formation and for a direct comparison with available theory. In the case of He, state specific cross-sections have been calculated and there is a fair agreement between the present results and the $Q_{Ps}(2P)$ calculated by Campbell *et al* (1998). Interestingly, it appears that a better agreement is found if the cross-section of Campbell *et al* is shifted to higher energies as was observed for the total Q_{Ps} for this target. The present results are lower than theoretical cross-section for formation into any n=2 state (this includes 2S and 2P), by a factor of at least 2.

The hypothesis of Laricchia *et al* (2002), that excited-state positronium formation may be responsible for the structure observed in Q_{Ps} cannot be directly verified by this study, primarily due to its relative insensitivity to 2S and $n > 2$ states. In the upper and lower limit estimates of excited state positronium formation, made by Laricchia *et al* (2002), the peak appears at the same energy as the present measurements. Additionally, the difference between the recent measurements of Q_{Ps} by Marler *et al* (2005) and Laricchia *et al* (2002) also peaks at the same energy as the

present Q_{Ps^*}. This may imply that the method used by Marler *et al* (2005) could be insensitive to positronium formation into $n > 1$ states.

It would be interesting to extend this study to other targets, specifically xenon which has been predicted (Laricchia *et al* 2002) to have a large fraction of Q_{Ps} from excited state positronium formation. Although not possible with the present experimental set-up, measurements of the total $n \geq 2$ formation cross-section would be desirable. Theoretical calculations of specific $n \geq 2$ states for Ar and the heavier noble gases would also be useful.

APPENDIX

A. COLLISIONAL QUENCHING OF 2S POSITRONIUM

Collisional de-excitation of Ps(2S) may result in the emission of a Lyman-α photon according to the following reaction :

$$Ps(2S) + He \rightarrow Ps(2P) + He \tag{A.1}$$

The collision frequency (f_c) is given by :

$$f_c = nQ^T v \tag{A.2}$$

where $n \sim 3 \times 10^{19}\ m^{-3}$ is the density of the target, Q^T is the total scattering cross-section of Ps(2S) and v is the speed of the positronium.

In the absence of explicit data for Q^T for Ps(2S) scattering estimates have been made by scaling the ground-state positronium-helium Q^T as measured by Garner *et al* (1996). Firstly, a Bohr scaling has been used i.e. $Q^T(n=2) = 2^4 Q^T(n=1)$ (see figure A.1). Secondly, Q^T has been estimated using the ratio (as shown in figure A.2) of the fragmentation cross-sections for Ps(n=1) and Ps(n=2) calculated by Starrett *et al* (2007). The result is also shown in figure A.1.

The probability of collision (P_c) is given by :

$$P_c = 1 - \exp(-t_d f_c) \tag{A.3}$$

where t_d is the time that Ps(2S) spends in the cell i.e.

$$t_d = \frac{l}{v} = \frac{0.045\ m}{v} \tag{A.4}$$

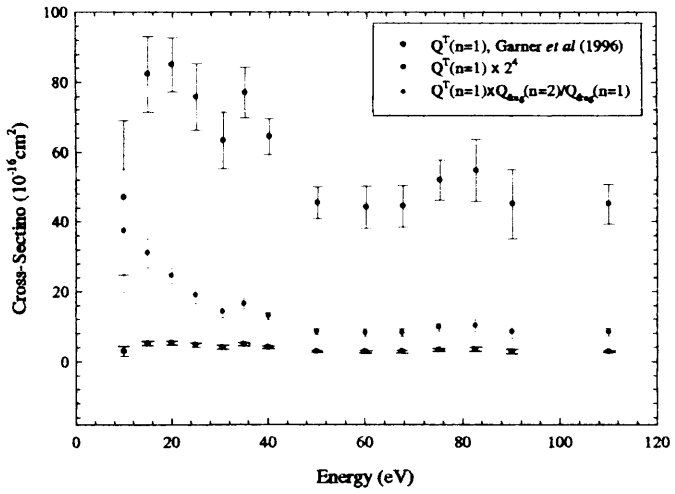

Fig. A.1: The total cross-section for ground-state Ps-helium scattering measured by Garner *et al* (1996), also shown $Q^T(2S)$ estimated using a Bohr scaling and the ratio $Q_{Ps}^{frag}(n=2)/Q_{Ps}^{frag}(n=1)$.

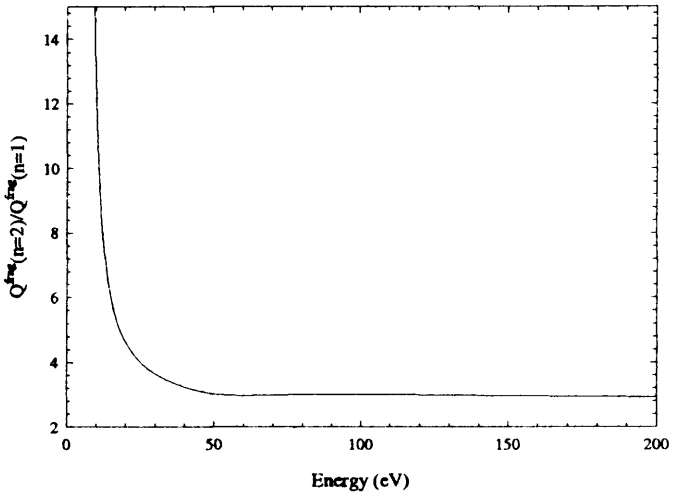

Fig. A.2: Ratio of $Q_{Ps}^{frag}(n=2)/Q_{Ps}^{frag}(n=1)$ found using cross-sections calculated by Starrett *et al* (2007).

where l is the cell radius (see figure A.3). Figure A.4 shows P_c calculated using the estimates of Q^T each energy.

There are at present no experimental measurements of the cross-section for colli-

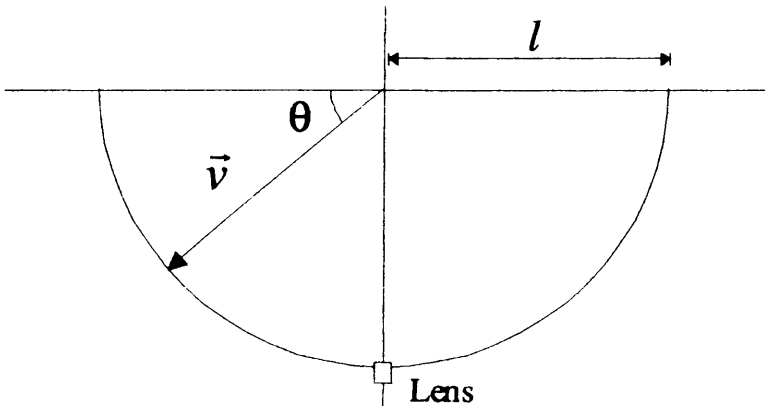

Fig. A.3: Schematic diagram of the gas cell.

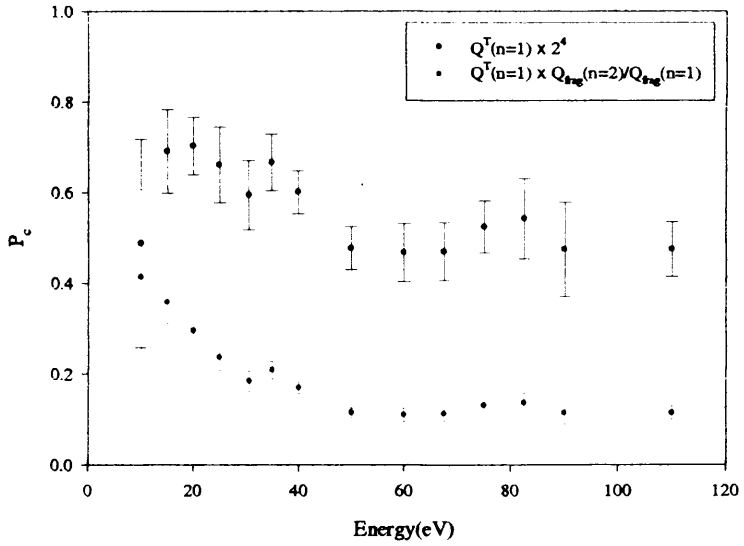

Fig. A.4: Probability of collision calculated using the ground-state Q^T scaled for Ps(n=2)-He scattering

sional quenching of Ps(2S) via the 2P state ($Q_{Ps}^{2S.2P}$). However, this cross-section has very recently been calculated by Starrett *et al* (2007) (shown in figure A.5). Hence, the probability of collisional de-excitation via the 2P state $P_{2S.2P}$ may be estimated over the energy range (10-110 eV) according to:

$$P_{2S.2P} = \frac{Q_{Ps}^{2S.2P}}{Q_{Ps}^{T}(n=2)} \tag{A.5}$$

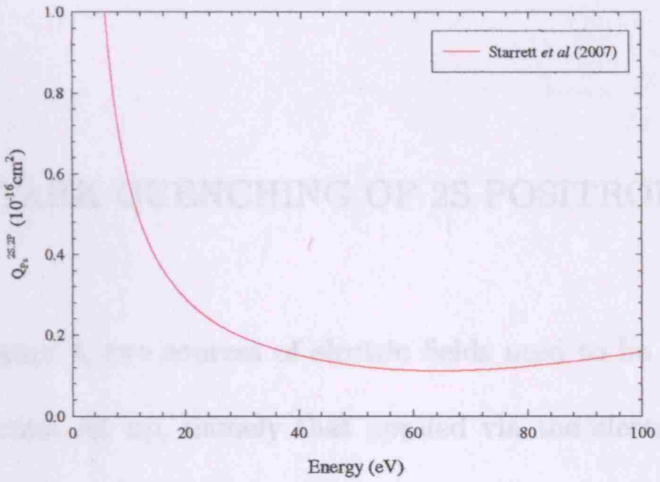

Fig. A.5: Cross-section for de-excitation of Ps(2S) via 2P state ($Q_{Ps}^{2S.2P}$) (Starrett *et al* 2007)

The probability that a collision of a Ps(2S) will result in a transition to the 2P state is shown in figure A.6 where it can be seen to be less than 1 % over the entire energy range.

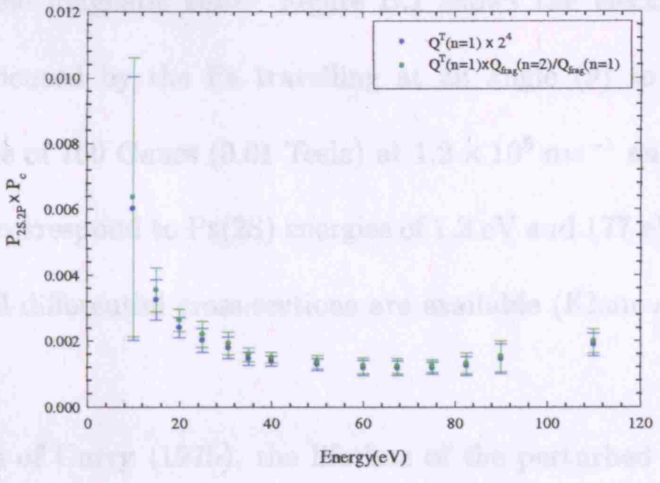

Fig. A.6: Probability of collisional de-excitation via 2P state.

B. STARK QUENCHING OF 2S POSITRONIUM

As stated in chapter 4, two sources of electric fields need to be considered in the present experimental set up, namely that applied via the electrostatic lens used for ion extraction and that arising from the Lorentz transformation of the guiding magnetic field, which is responsible for the so called the motional Stark effect.

Under Lorentz transformation of the magnetic field, the Ps(2S) will experience an electric field which is given by

$$\vec{E}_{mse} = \gamma(\vec{v} \times \vec{B}) \tag{B.1}$$

where $\gamma = 1/\sqrt{1-\beta^2}$, $\beta = v/c$ where c is the speed of light, $\vec{v}$ the velocity of the Ps and $\vec{B}$ the magnetic field. Figure B.1 shows the electric field ($E_{mse} = \gamma v B \sin\theta$) experienced by the Ps travelling at an angle (θ) to a magnetic field with a magnitude of 100 Gauss (0.01 Tesla) at $1.2 \times 10^5\ ms^{-1}$ and $5.6 \times 10^6\ ms^{-1}$. These velocities correspond to Ps(2S) energies of 1.2 eV and 177 eV respectively, for which theoretical differential cross-sections are available (Khan *et al* 1985, Sarkar *et al* 1992).

From the results of Curry (1975), the lifetime of the perturbed 2S state with an admixture of 2P character against transition to the ground state (τ_t) as a function of electric field strength (E) is computed and shown in figure B.2.

Using τ_t and $\tau_d = (1/t_d + 1/t_{3\gamma})^{-1}$ where t_d is defined in equation A.4 and $t_{3\gamma} = 1100\ ns$ is the lifetime against annihilation, the probability of Ps(2S) undergoing

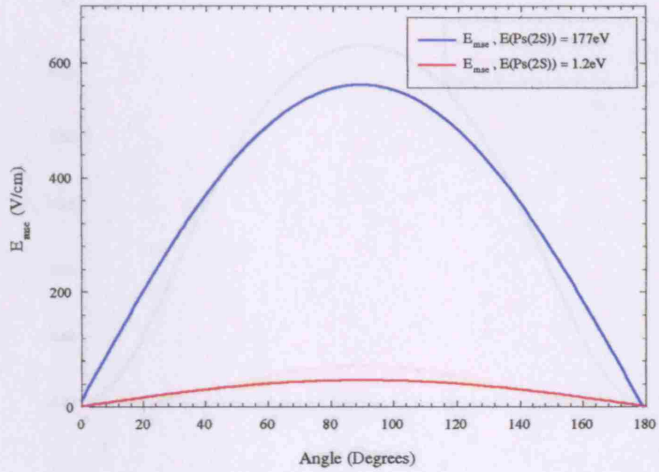

Fig. B.1: Electric field E_{mse} vs angle θ for 1.2 eV and 177 eV Ps.

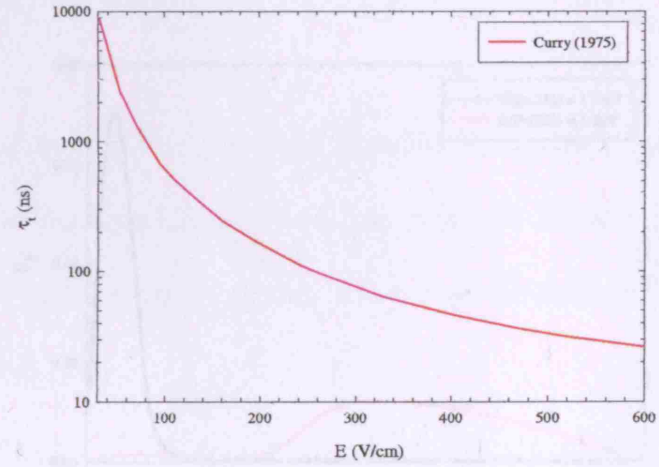

Fig. B.2: Lifetime (τ_t) of the 2S state with an admixture of 2P like character against transition as a function of electric field strength.

transition in the cell can be found using

$$P_t = 1 - \exp(-\tau_d/\tau_t) \tag{B.2}$$

where τ_d at 1.2 eV and 177 eV Ps is 90 ns and 8.93 ns respectively, P_t is shown in figure B.3.

Using the differential Ps(2S) formation cross-sections (Khan *et al* 1985, Sarkar *et*

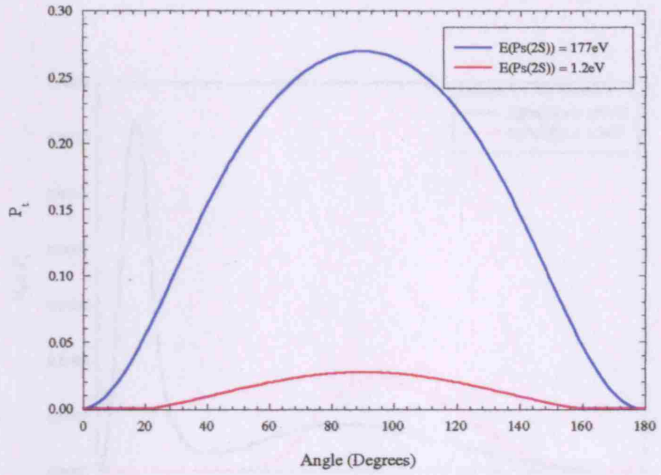

Fig. B.3: Probability of transition P_t as a function of angle at Ps(2S) energies of 177 eV and 1.2 eV.

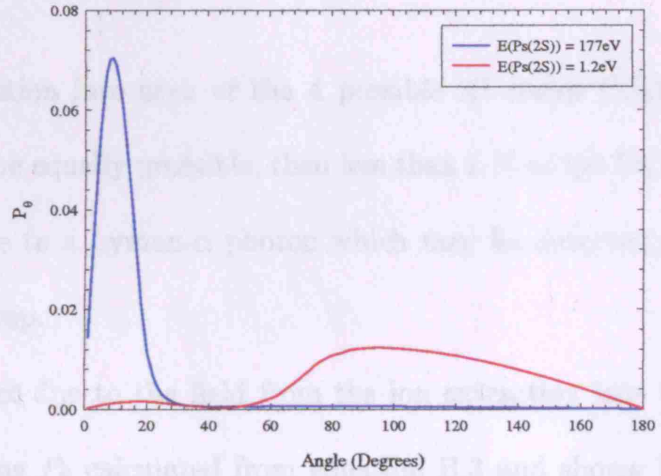

Fig. B.4: Probability of formation of Ps(2S) (P_θ) at a given angle (θ).

al 1992), the probability of formation at a given angle (θ)

$$P_\theta = \frac{2\pi \sin\theta}{Q_{Ps}(2S)} \frac{dQ_{Ps}(2S)}{d\theta} \tag{B.3}$$

is computed and shown in figure B.4. So that the total probability of transition may be obtained from

$$P_d = \sum_0^\pi P_t(\theta) P_\theta(\theta) \Delta\theta \tag{B.4}$$

and it is shown in figure B.5.

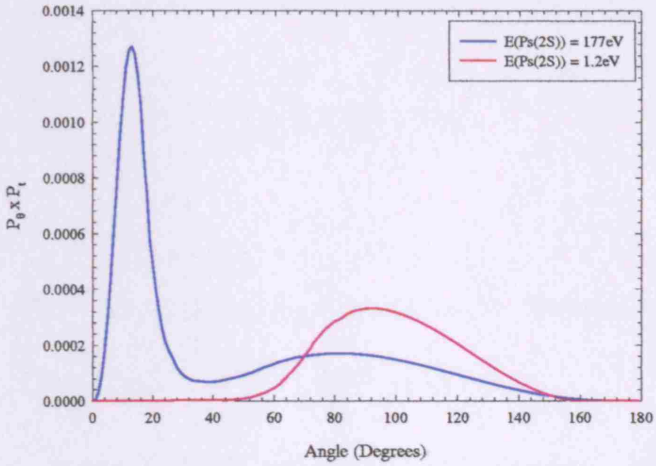

Fig. B.5: Probability of transition convoluted with the probability of production for a given angle (θ).

Assuming formation into each of the 4 possible 2S states ($^1S_0(0), ^3S_1(0, \pm 1)$) of positronium to be equally probable, then less than 1 % of the Ps(2S) formed in the cell will give rise to a Lyman-α photon which may be detected using the present experimental setup.

Finally, the effect due to the field from the ion extracting lens (see figure 2.7) is considered. Using P_θ calculated from equation B.3 and shown in figure B.4, the fraction of Ps atoms emitted within a cone of $\pm 15°$ towards the lens (i.e. at 90°) is less than 5 % at 1.2 eV. At higher energies, this fraction diminishes as the differential Ps formation becomes increasingly peaked around 0°, as shown at 177eV in figure B.4. Within this cone, the electric field experienced in the vicinity of the lens ($\geq 400\ V/cm$ Szluinska 2003) is sufficient to induce a transition with a probability of $\geq 50\%$, assuming that this field is experienced over the entire flight path. As before assuming equal population of the 2S substates, considerably less than 1 %

of the Ps(2S) will give rise to a Lyman-α photon.

REFERENCES

Adachi S., Chiba M., Hirose T., Hagayama S., Nakamitsi Y., Sato T. and Yamada T. *Phys. Rev. Lett* **65** (1990) 2634

Aharonov Y., Avignone F.T., Brodzinski R.L., Collar J.I., Garcia E., Miley H.S., Morales A., Morales J., Nussinov S., de Solorzano A.O., Puimedon J., Reeves J.H., Saenz C., Salinas A., Sarsa M.L. and Villar J.A. *Phys. Lett. B.* **353** (1995) 168

Anderson C. D. *Phys Rev* **41** (1932a) 405

Anderson C. D. *Science* **76** (1932b) 238

Anderson C. D. *Phys Rev* **43** (1933) 491

Arcidiacono C., Kövér A. and Laricchia G. *Phys. Rev. Lett* **95** (2005) 223202

Ashley P., Moxom J. and Laricchia G. *Phys. Rev. Lett* **77** (1996) 1250

Barnes L. D., Gilbert S. J. and Surko C. M. *Phys. Rev. A.* **67** (2003) 032706

Bartschat K., McEachran R. P. and Stauffer A. D. *J. Phys. B.* **21** (1988) 2789

Basu D., Banerji G. and Ghosh A. S. *Phys. Rev. A.* **13** (1976) 1381

Basu M., Mazumdar P. S. and Ghosh A. S. *J. Phys. B.* **18** (1985) 369

Bates D. R. and Walker J. C. G. *Plan. Space Sci.* **14** (1966) 1367

Beier T., Djekic S., Hffner H., Hermanspahn N., Kluge H.-J., Quint W.,Stahl S.,Valenzuela T.,Verd J. and Werth G. *Can. J. Phys./Rev. can. phys.* **80** (2002) 1241

Biswas P. K. *Eur. Phys. J. D* **29** 321 (2004)

Bennett W. R. Jr., Thomas W., Hughes V. W. and Wu C. S. *Bull. Amer. Phys. Soc.* **6** (1961) 49

Berakdar J. and Klar H. *J. Phys. B.* **26** (1993) 3891

Bethe H. A. and Salpeter E. E. *Quantum mechanics of one- and two-electron atoms* Springer-Verlag (1957)

Blackett P. M. S. and Occhilialini G. P. S *Proc. Roy. Soc A* **139** (1933) 699

Bluhme H., Knudsen H.,Merrison J. P. and Poulsen M. R. *Phys. Rev. Lett* **81** (1998) 73

Bluhme H., Frandsen N. P., Jacobsen F. M., Knudsen H., Merrison J. P., Mitchell R., Paludan K. and Poulsen M. R. *J. Phys. B.* **32** (1999) 5825

Bozek J. D., Furst J. E., Gay T. J., Gould H., Kilcoyne A. L. D., Machacek J. R., Martin F., McLaughlin K. W. and Sanz-Vicario J.J. *J. Phys. B.* **39** (2006) 4871

Brock R. L. and Streib J. F. *Phys. Rev.* **109** (1958) 399

Brown B. L. (1985) Positron Annihilation ed Jain P., Singru R. M. and Gopinathan K. P. (Singapore: World Scientific) p 328

Brown B. L. (1986) Proc. 3rd Int. Workshop on Positron (Electron) Gas Scattering ed Kauppila W. E. and Stein T. S. (Singapore: World Scientific) p 212

Brown B. L. (1987) Atomic physics with positrons ed Humberston J W and Armour E A G (New York:Plenum) p241

Burdyuzha V. V. and Kauts V. L. *Astrophys. and Space Sci.* **253** (1997) 329

Campbell C. P., McAlinden M. T., Kernoghan A. A. and Walters H. R. J. *Nim:B* **143** (1998) 41

Campeanu R. I., McEachran R. P. and Stauffer A. D. *J. Phys. B.* **20** (1987) 1635

Campeanu R. I., McEachran R. P. and Stauffer A. D. *Can. J. Phys* **74** (1996) 544

Canter K. F., Mills, Jr. A. P., and Berko S. *Phys. Rev. Lett* **34** (1975) 177

Cassidy D. B., Deng S. H., Greaves R.G., Maruo T., Nishiyama N., Snyder J.B., Tanaka H.K. and Mills A.P. Jr. *Phys. Rev. Lett* **95** (2005) 195006

Cassidy D. B. and Mills A. P. Jr *Book of abstracts ICPEAC XXV* (2007)

Chang T., Li Q., Wang Y and Li Y. in "Positron Annihilation" eds. P. G. Coleman, S. C. Sharman and L. M. Diana (North Holland: Amsterdam) (1982) p32

Charlton M., Clark G., Griffth T. C. and Heyland G. R. *J. Phys. B.* **16** (1983) L465

Charlton M. and Laricchia G. *J. Phys. B.* **23** (1990) 1045

Charlton M. and Humberston J. W., in "Positron Physics" (Cambridge University Press) (2001)

Chaudhuri P. and Adhikari S. K. *J. Phys. B.* **31** (1998) 3057

Chen Z. and Msezane A. Z. *Phys. Rev. A.* **49** (1994) 1752

Cheng C. and Zhou Y. *Phys. Rev. A.* **73** (2006) 024701

Chutjian A. and Cartwright D. C. *Phys. Rev. A.* **23** (1981) 2178

Coleman P. G., Johnston K. A., Cox A. M. G., Goodyear A. and Charlton M. *J. Phys. B.* **25** (1992) L585

Consolati G. *J. Radioanalytical Nuc. Chem. Art.* **210** (1996) 273

Costello D. G., Groce D. E., Herring D. F., McGowan J.W. *Can. J. Phys.* **50** (1972) 23

Curry S. M. *Phys. Rev. A.* **7** (1973) 447

Dahm A. J. and Eck T. G. *Phys. Lett.* **49A** (1974) 267

Deb N. C. and Crothers D. S. F. *J. Phys. B.* **35** (2002) L85

Deutsch M. *Phys. Rev.* **82** (1951) 455

Diana L. M (1985) Proc. 7th Int. Conf. on Positron Annihilation ed Jain P., Singru R. M. and Gopinathan K. P. (Singapore: World Scientific) p 428

Diana L. M., Coleman P. G., Brooks D. L., Pendleton P. K. and Norman D. M. *Phys. Rev. A.* **34** (1986) 2731

Diana L. M., Coleman P. G., Brooks D. L., Pendleton P. K., Norman D. M., Seay B. E. and Sharma S. C. (1986) Positron (Electron) Gas Scattering ed Kauppila W. E., Stein T. S. and Wadehra J. M. (Singapore: World Scientific) p 296

Diana L. M., Coleman P. G., Brooks D. L. and Chaplin R. L. (1987) Atomic Physics with Positrons ed Humberston J. W. and Armour E. A. G. (NewYork: Plenum) p 55

Diana L. M. *et al* (1989) Positron Annihilation ed Dorokins-Vanpraet L., Dorokins M. and Segers D. (Singapore: World Scientific) p 311

Dirac P. A. M. *Proc. Roy. Soc* **126** (1930a) 360

Dirac P. A. M. *Proc. Camb. Phil. Soc.* **26** (1930b) 361

Drachman R. J. and Omidvar K. *Phys. Rev. A.* **14** (1976) 100

Duff B. G. and Heymann F. F. *Proc. Roy. Soc., Ser. A* **272** (1963) 363

Dunlop L. J. M. and Gribakin G. F. *Nim:B* **247** (2006) 61

Edwards J.L. and Thomas E. W. *Phys. Rev. A.* **2** (1970) 2346

Fagg L. W. *Nucl. Instrum. Methods* **85** (1970) 53

Fiol J., Rodrguez V. D. and Barrachina R. O., *J. Phys. B.* **34** (2001) 933

Fornari L. S., Diana L. M. and Coleman P. G. *Phys. Rev. Lett* **51** (1983) 2276

Fromme D., Kruse G., Raith W. and Sinapius G. *Phys. Rev. Lett* **57** (1986) 3031

Gribakin G. F. *Phys. Rev. A.* **61** (2000) 022720

Gribakin G. F. and Ludlow J. *Phys. Rev. Lett* **88** (2002) 163202

Garner A. J. and Laricchia G. *Can. J. Phys.* **74** (1996) 518

Gaudin A. and Hagemann R. *J. Chem. Phys.* **64** (1967) 1209

Gilmore S., Blackwood J. E. and Walters H. R. J. *Nim:B* **221** (2004) 129

Greaves R. G. and Surko C. M. *Phys. Rev. Lett* **85** (2000) 1883

Gullikson E. M. and Mills A. P. *Phys. Rev. Lett* **57** (1986) 376

Hewitt. R. N., Noble. C. J. and Bransden. B. H. *J. Phys. B.* **25** (1992) 557

Higgins K. and Burke P. G. *J. Phys. B.* **26** (1993) 4269

Hill. J., Geddes. J and Gilbody. H.B. *J. Phys. B.* **12** (1979) L653

Hughes V. W. *J. App. Phys* **28** (1957) 16

Hutchins S. M., Coleman P. G., Stone R. J. and West R. N. *J. Phys. E* **19** (1986) 282

Igarashi A. and Toshima N. *Phys. Lett. A.* **164** (1992) 70

Igarashi A. and Toshima N. *Phys. Rev. A.* **50** (1994) 232

Igarashi A., Kimura M. and Shimamura I. *Phys. Rev. Lett* **89** (2002) 123201

Ihra W., Macek J. H., Mota-Furtado F. and O'Mahony P. F. *Phys. Rev. Lett* **78** (1997) 4027

Jacobsen F. M., Charlton M., Chevallier J., Deutch B.I., Laricchia G. and Poulsen M.R., *J. App. Phys.* **67** (1990) 575

Jacobsen F. M., Frandsen N. P., Knudsen H., Mikkelsen U. and Schrader D. M. *J. Phys. B.* **28** (1995) 4691

Jacobsen F. M., Frandsen N. P., Knudsen H. and Mikkelsen U. *J. Phys. B.* **28** (1995) 4675

Jin B., Miyamoto S., Sueoka O. and Hamada A. *At. Collision Res. Japan* **20** (1994) 9

Kara V., Paludan K., Moxom J., Ashley P. and Laricchia G. *J. Phys. B.* **30** (1997) 3933

Kauppila W. E. and Stein T. S. *Adv. At. Mol. opt. Phys.* **26** (1990) 1

Ke Y., Zhou Y., and Nan G. *Phys. Rev. A.* **70** (2004) 024702

Kernoghan A. A., Robinson D. J. R., McAlinden M. T. and Walters H. R. J. *J. Phys. B.* **29** (1996) 2089

Khan P., Mazumdar P. S. and Ghosh A. S. *Phys. Rev. A.* **31** (1985) 1405

Kielkopf J. F. and Ouseph P. J. *Bull. Amer. Phys. Soc.* **19** (1974) 592

Kimura M., Sueoka O., Hamada A. and Itikawa Y. *Adv. Chem. Phys.* **111** (2000) 537

Klemperer O., Proc. Camb. *Philos. Soc.* **30** (1934) 347

Knudsen H., Brun-Nielson L., Charlton M., Poulsen M. R. *J. Phys. B.* **23** (1990) 3955

Krishnakumar E and Srivastava S K *J. Phys. B.* **21** (1988) 1055

Kövér A. and Laricchia G. *Phys. Rev. Lett* **80** (1998) 5309

Kövér A., Paludan K. and Laricchia G., *J. Phys. B.* **34** (2001) L219

Kuo T. Y., Sun H. L. Huang K. N. *Phys. Rev. A.* **67** (2003) 012705

Lang N. D. and Kohn W. *Phys. Rev. B.* **3** (1971) 1215

Laricchia G., Charlton M., Clark G. and Griffith T.C. *Phys. Lett.* **109A** (1985) 97

Laricchia G., Charlton M., Davies S. A., Beling C. D. and Griffith T. C., *J. Phys. B.* **20** (1987) L99

Laricchia G., Moxom J., and Charlton M. *Phys. Rev. Lett* **70** (1993) 3229

Laricchia G. and Wilkin C. *Phys. Rev. Lett* **79** (1997) 2241, *Nim:B* **143** (1998)

Laricchia G. 2002 in "The Physics of Photonic, Electronic and Atomic Collisions" (Rinton Press, New York) p329

Laricchia G., Van Reeth P., Szluinska M. and Moxom J. *J. Phys. B.* **35** (2002) 2525

Laricchia G., Armitage S., Leslie D. E., Szluinska M. and Van Reeth, P. *Rad. Phys. and Chem.* **68** (2003) 21

Leslie D. E., Armitage S. and Laricchia G. *J. Phys. B.* **35** (2002) 4819

Ludlow J. 2003 *PhD Thesis Queens University, Belfast, unpublished*

Mandal P., Guha S. and Sil N. C. *J. Phys. B.* **12** (1979) 2913

Mann A. and Linder F. *J. Phys. B.* **25** (1992) 545

Marler J. P., Sullivan J. P. and Surko C. M. *Phys. Rev. A.* **71** (2004) 022701

Marler J., Barnes L. D., Gilbert S. J., Sullivan J. P., Young J. A. and Surko C. M. *Nim:B* **221** (2004) 84

Marler J. P. and Surko C. M. *Phys. Rev. A.* **72** (2005) 062713

Marler J. P., Sullivan J. P., and Surko C. M *Phys. Rev. A.* **71** (2005) 022701

Marler J. P., Gribakin G. F., Surko C. M. *Nim:B* **247** (2006) 87

Massey H. S. W. and Mohr C. B. O. *Proc. Phys. Soc. London, Sect. A* **67** (1954) 695

Massoumi G.R., Schultz P.J., Lennard W.N. and Ociepa A.J. *Nim:B* **30** (1988) 592

McAlinden M. T. and Walters H. R. J. *Hyperfine Int.* **73** (1992) 65

McCall S. L. *Bull. Amer. Phys. Soc.* **18** (1973) 1512

McEachran R. P., Ryman A. G. and Stauffer A. D. (1979) *J. Phys. B.* **12** (1979) 1031

McEachran R. P. and Stauffer A. D. *Positron(electron)-Gas Scattering* eds. Kauppila W. E., Stein T. S. and Wadehra J. M. (World Scientific) (1986) 122

McKee. J. D., Geddes. J. and Gilbody H.B. *J. Phys. B.* **12** (1979) 1701

Mills A. P., *Phys. Rev. Lett* **46** (1981) 717

Mitroy J. *J. Phys. B.* **29** (1996) L263

Mitroy J. and Ryzhikh G. G., *Phys. Rev. Lett* **83** (() 35701999)

Mitroy J., Bromley M. W. and Ryzhikh G. G., *J. Phys. B.* **35** (2002) R81

Mitroy J. and Ivanov I. A. *Phys. Rev. A.* **65** (2002) 042705

Mohorovicic S. *Astrn. Nachr.* **235** (1934) 94

Montague R. G., Harrison M. F. A. and Smith A. C. H. *J. Phys. B.* **17** (1984) 3295

Moores D. L. *Nim:B* **179** (2001) 316

Mori S. and Sueoka O. *J. Phys. B.* **27** (1994) 4349

Moxom J., Laricchia G. and Charlton M. *J. Phys. B.* **26** (1993) L376

Moxom J., Laricchia G. and Charlton M. Kver and Meyerhof W E *Phys. Rev. A.* **50** (1994) 3129

Moxom J., Laricchia G. and Charlton M. *J. Phys. B.* **28** (1995) 1331

Moxom J., Ashley P. and Laricchia G. *Can. J. Phys* **74** (1996) 367

Murry C. A. and Mills A. P. *Solid State Commun.* **34** (1980) 780

Murtagh D. J., Arcidiacono C., Pesic Z. D. and Laricchia G. *Nim:B* **247** (2006) 92

Nagy P., Skutlartz A. and Schmidt V. *J. Phys. B.* **13** (1980) 1249

Ore A. and Powell J. L. *Phys. Rev.* **75** (1949) 1696

Ore A. *Phys. Rev.* **83** (1951) 665

Overton N., Mills R. J. and Coleman P. G. *J. Phys. B.* **26** (1993) 3951

Palathingal J. C., Asoka-Kumar P., Lynn K. G., Posada and Wu X. Y., *Phys. Rev. Lett* **67** (1991) 3491

Rapp D. and Englander-Golden P. *J. Chem. Phys.* **43** (1965) 1464

Ratnavelu K. *Aust. J. Phys.* **44** 265 (1991)

Rejoub R., Lindsay B. G. and Stebbings R. F. *Phys. Rev. A.* **65** (2002) 042713

Rich A. *Rev. Mod. Phys.* **53** (1981) 127.

Ruark A. E. *Phys. Rev* **68** (1945) 278

Sarkar. N. K, Basu. M. and Gosh. A. S. *Phys. Rev. A.* **45** (1992) 6887

Schrader D. M., Jacobsen F. M., Frandsen N. P. Mikkelsen U. *Phys. Rev. Lett* **69** (1992) 57

Schrader D. M. *Nim:B* **143** (1998) 209

Schultz D. R. and Olson R. E. *Phys. Rev. A.* **38** (1998) 1866

Shah M. B., Elliott D. S., McCallion P. and Gilbody H. B. *J. Phys. B.* **21** (1988) 2751

Schram B. L., De Heer F. J., Van der Wiel M J and Kistemaker J. *Physica* **31** (1965) 94

Schram B. L., Boerboom A. J. H. and Kistemaker J. *Physica* **32** (1966) 185

Schram B. L., Moustafa H. R., Schutten J. and De Heer F. J. *Physica* **32** (1966) 734

Smith S. J., Hyder G. M. A., Kauppila W. E., Kwan C. K. and Stein T. S. *Phys. Rev. Lett* **64** (1990) 1227

Sorokin A. A., Beigman I. L., Bobashev S. V., Richter M. and Vainshtein L. A. *J. Phys. B.* **37** (2004) 3215

Starrett C., Walters H. R. J and McAlinden M. T. *Proceedings of XIV international conference on low energy positron and positronium physics* (2007)

Stein T. S., Kauppila W. E., Pol V., Smart J. H. and Jesion G. *Phys. Rev. A.* **17** (1978) 1600

Stein T. S. and Kauppila W. E. *Adv. At. Mol. Phys.* **18** (1982) 53

Stein T. S., Jiang J., Kauppila W. E., Kwan C. K., Li H. and Zhou S., *Can. J. Phys* **74** (1996) 313

Stein T. S., Harte M., Jiang J., Kauppila W. E., Kwan C. K., Li H. and Zhou S. *Nim:B* **143** (1998) 68

Straton J. C. *Phys. Rev. A.* **35** (1987) 3725

Straub H. C., Lindsay B. G., Smith K. A. and Stebbings R. F. *J. Chem. Phys.* **105** (1996) 4015

Sullivan J. P., Gilbert S. J., Marler J. P., Greaves R. G., Buckman S. J. and Surko C. M., *Phys. Rev. A.* **66** (2002a) 042708

Sullivan J. P., Gilbert S. J., Marler J. P., Buckman S. J. and Surko C. M. *Nim:B* **192** (2002b) 3

Surdutovich A., Jiang J., Kauppila W. E., Kwan C. K., Stein T. S. and Zhou S. *Phys. Rev. A.* **53** (1996) 2861

Surdutovich A., Johnson J. M., Kauppila W. E., Kwan C. K. and Stein T. S. *Phys. Rev. A.* **65** (2002) 032713

Surdutovich E., Harte M., Kauppila W. E., Kwan C. K., and Stein T. S. *Phys. Rev. A.* **68** (2003) 022709

Surko C. M., Gribakin G. F. and Buckman S. J. *J. Phys. B.* **38** (2005) R57

Szluinska M., Van Reeth P. and Laricchia G. *J. Phys. B.* **35** (2002) 4059

Szluinska M. *PhD Thesis* (2003)

Szluinska M. and Laricchia G. *Nim:B* **221** (2004a) 100

Szluinska M. and Laricchia G. *Nim:B* **221** (2004b) 107

Tong B. Y. *Phys. Rev. B.* **5** (1972) 1436

Van Reeth P. and Humberston J. W. *J. Phys. B.* **30** (1997) L95

Van Reeth P. and Humberston J. W. *J. Phys. B.* **31** (1998) L231

Van Reeth P. and Humberston J. W. *J. Phys. B.* **32** (1999) 3615

Van Reeth P., Szluinska M. and Laricchia G. *Nim:B* **192** (2002) 220

Van Reeth P., Laricchia G. and Humberston J. W. *Physica Scripta* **71** (2005) C9

Varella M.T.do N., de Carvalho C.R.C., Lima M.A.P. and da Silva E.P., *Phys. Rev. A.* **63** (2001) 052705

Varghese S. L., Ensberg E. S., Hughes V. W. and Lindgren I. *Phys. Lett.* **49A** (1974) 415

Walters H. R. J. *Private Communication* (2005)

Weber M., Hofmann A., Raith W., Sperber W., Jacobsen F. and Lynn K. G., *Hyperfine Interact.* **89** (1994) 221

Wetzel R. C., Baiocchi F. A., Hayes T. R. and Freund R. S. *Phys. Rev.* **35** (1987) 559

Weyl R. N. *"Grouppentheorie and Quantenmechanil"* 2^{nd} ed. (1931) p234

Wheeler J. A. *Ann. N Y. Acad. Sci.* **48** (1946) 219

Wu H., Bray I., Fursa S. V. and Stelbovics A. T. *J. Phys. B.* **37** (2004) 1164

Yang C. N., *Phys. Rev.* **77** (1950) 242

Zhou S., Li H., Kauppila W.E., Kwan C. K. and Stein T.S. *Phys. Rev. Lett* **73** (1994) 236

Zhou S., Li H., Kauppila W.E., Kwan C. K. and Stein T. S. *Phys. Rev. A.* **55** (1997) 361